IOP Publishing Reports on Progress in Physics
Rep. Prog. Phys. 79 (2016) 046601 (57pp) doi:10.1088/0034-4885/79/4/046601

Review

Fracture and adhesion of soft materials: a review

Costantino Creton[1,2] and Matteo Ciccotti[1,2]

[1] Sciences et lngénierie de la Matière Molle, CNRS UMR 7615, École Supérieure de Physique et de Chimie Industrielles de la Ville de Paris (ESPCI), ParisTech, PSL Research Univeristy, 10 rue Vauquelin, F-75231 Paris cedex 05, France
[2] SIMM, UPMC Univ Paris 06, Sorbonne-Universités, 10 rue Vauquelin, F-75231 Paris cedex 05, France

E-mail: costantino.creton@espci.fr and matteo.ciccotti@espci.fr

Received 18 September 2014, revised 21 September 2015
Accepted for publication 30 September 2015
Published 23 March 2016

Invited by Mark Geoghegan

Abstract

Soft materials are materials with a low shear modulus relative to their bulk modulus and where elastic restoring forces are mainly of entropic origin. A sparse population of strong bonds connects molecules together and prevents macroscopic flow. In this review we discuss the current state of the art on how these soft materials break and detach from solid surfaces. We focus on how stresses and strains are localized near the fracture plane and how elastic energy can flow from the bulk of the material to the crack tip. Adhesion of pressure-sensitive-adhesives, fracture of gels and rubbers are specifically addressed and the key concepts are pointed out. We define the important length scales in the problem and in particular the elasto-adhesive length Γ/E where Γ is the fracture energy and E is the elastic modulus, and how the ratio between sample size and Γ/E controls the fracture mechanisms. Theoretical concepts bridging solid mechanics and polymer physics are rationalized and illustrated by micromechanical experiments and mechanisms of fracture are described in detail. Open questions and emerging concepts are discussed at the end of the review.

Keywords: adhesion, fracture, hydrogels, elastomers, mechanical properties, adhesive

(Some figures may appear in colour only in the online journal)

Contents

List of symbols

α	reciprocal of the attenuation length of the normal stress in Kaelble's model of peeling
β	reciprocal of the attenuation length of the shear stress in Kaelble's model of peeling
γ	thermodynamic surface energy
Γ	fracture energy
Γ_0	threshold fracture energy
Γ_{app}	apparent fracture energy
δ	indentation depth
δ_D	critical crack opening displacement according to Dugdale model
ε	strain, nominal strain in a probe tack test
$\dot{\varepsilon}$	strain rate
ε_H	true strain or Hencky strain $= \ln\lambda$
ε_{max}	maximum nominal strain at failure or debonding
η	viscosity
η^+	extensional viscosity at onset of flow
θ	peel angle
λ	stretch $= L/L_0$
$\lambda_1, \lambda_2, \lambda_3$	the three principal stretches
λ_c	critical stretch at fracture in the cohesive failure of a peeled adhesive layer
λ_{hard}	critical stretch where $f^*(\lambda)$ reaches its minimum value in a uniaxial tensile test
λ_{max}	maximum extensibility of the 2nd network in a Double Network Gel
μ	shear modulus
$\mu'(\omega)$	dynamic shear storage modulus
$\mu''(\omega)$	dynamic shear loss modulus
μ_e	plateau modulus due to entanglements
μ_x	shear modulus due to permanent crosslinks
ν	Poisson's ratio
ν_e	volume density of entanglements in a network
ν_x	volume density of crosslinks in a network
ρ	crack tip radius, mass of monomer per unit volume of material
ρ_0	mass of monomer per unit volume of unswollen network
ρ^*	crack tip radius at propagation
σ	stress
σ_c	maximum normal stress at failure or debonding
σ_f	molecular fracture stress in a fibril
σ_{max}	maximum stress at the tip of an elliptical crack, maximum tensile stress measured in a probe tack test
σ_N	nominal stress
σ_p	plateau stress in a probe test
σ_T	true stress
σ_Y	yield stress
Σ	areal density of chains crossing the interface
τ_c	maximum shear stress at debonding
$\phi(a_T v)$	dissipative factor in peel or fracture tests
ϕ_p	polymer volume fraction
χ	Flory interaction parameter
ω	pulsation (rad/s)
a	radius of the contact area in a probe test, size of the monomer
a_i	width of the interface between two polymers
a_T	shift factors of time-temperature superposition
A	area of the crack
A_{max}	maximum contact area in a probe tack test
b	width of a peeled strip, size of half the small axis of an elliptical crack
c	crack length, size of half the large axis of an elliptical crack
$C_{hard}(\dot{\lambda})$	minimum of $f^*(\lambda)$ as a function of $1/\lambda$. Represents the permanent component of the shear modulus at the stretch rate $\dot{\lambda}$
$C_{soft}(\dot{\lambda})$	μ- $C_{hard}(\dot{\lambda})$. Represents the relaxing component of the shear modulus at the stretch rate $\dot{\lambda}$
$\frac{dc}{dn}$	crack growth per cycle in a fatigue test
DIC	digital image correlation
D	diffusion coefficient
E	Young's modulus
E^*	threshold Young's modulus for spontaneous adhesion on a rough surface
E_B	Young's modulus of the backing of an adhesive tape
E_{eff}	effective Young's modulus of the material in the damaged zone
F	force
ΔF_{exc}	excess free energy
$f^*(\lambda)$	reduced stress or Mooney stress $= \sigma_N/(\lambda - 1/\lambda^2)$
$\mathcal{G}$	energy release rate
$\mathcal{G}_{max}$	maximum applied energy release rate in a cyclic fatigue test
g_{local}	local energy release rate near the crack tip
h	thickness of adhesive layer
h_0	undeformed thickness of an adhesive layer or sample
h_B	thickness of the backing of a tape

h_c	height of a penny-shaped interfacial defect (figure 20)
Δh	increase in thickness of the adhesive layer during debonding in a probe test
H_0	undeformed thickness of the yielded zone near the crack tip
I_1	first invariant of the Cauchy-Green tensor
J	J-integral of Rice
J_m	maximum value of $I_1 - 3$ in the Gent model
k_B	Boltzmann's constant
k_{local}	local stress intensity factor in a damaged zone near the crack tip
K	stress intensity factor, dimensionless parameter in Kaelble's model
K_c	critical stress intensity factor
l, l_0	deformed and undeformed length of tensile sample
l_{fib}	fibril diameter
ℓ_D	Dugdale length: size of the plastic region at the crack tip at crack propagation
ℓ_{EA}	elasto-adhesive length $=\Gamma/E$
ℓ_{EAD}	length scale of elasto-adhesive dissipation $= \Gamma_{app}/E$
L	length over which energy is dissipated in the Lake-Thomas model
L_0	Characteristic length over which energy is dissipated by linear viscoelasticity at the crack tip
M_0	Molar mass of the monomer
n	power law exponent in the fracture dissipation function
N_x	number of monomers between crosslinks
p	tensile hydrostatic stress on a cavity or interfacial crack
P	peel force
P_c	critical cavitation stress, contact pressure during the bond formation in probe tack tests
PSA	pressure-sensitive-adhesive
r	distance in radial coordinates from the crack tip
r_0	initial size of a spherical defect in a cavitation experiment
R	radius of the crack related dissipation zone, radius of spheres, cylinders or asperities in contact mechanics models
R_0	radius of the local damage zone
R_c	radius of curvature of a penny-shaped defect at the interface (figure 20)
R_d	radius of a penny-shaped defect at the interface (figure 20)
SSY	small scale yielding
t	time
t_C	contact time during the bond formation in the probe tack test, characteristic loading time in the Kaelble's model
$\tan\delta(\omega)$	viscoelastic loss factor $= \mu''(\omega)/\mu'(\omega)$
T	temperature
T_0	reference temperature, threshold tearing energy (see Γ_0)
T_g	glass transition temperature
u	displacement
u_{11}	displacement in the direction normal to the crack propagation direction
U_b	bond energy
U_w	external work
U_{el}	stored elastic energy
v	crack or peel front velocity
V, V_{deb}	velocity of the probe in a probe tack test
w	thermodynamic (reversible) energy cost per unit fracture area
$W(\lambda)$	strain energy density as a function of stretch
W_{2nd}	strain energy density of the second network in a double network gel
W_c	strain energy density at debonding in Kaelble's model
W_{deb}	work of debonding in a probe test (in J/m^2)

1. Introduction

For most people, soft materials are materials where the deformation can be felt by hand or seen with the naked eye without applying an excessive force. In this category are clearly many synthetic, polymer made materials, such as rubbers, gels and self-adhesive materials, but also many more materials made from naturally occurring molecules such as food or living tissues. In particular because of the need to replace sick or damaged living tissue with artificial counterparts, the biomedical field is an avid user of soft materials. The materials described above remain solids, in the sense that they can sustain static loads and store elastic energy in the long term, but their elastic modulus can vary from typically 10^3 to 10^7 Pascals. A sparse population of percolating strong bonds inside the material prevents flow at the macroscopic scale without preventing (some) molecular motion at the microscopic scale. Soft materials are used in real life for their ability to accommodate large deformations without or with little permanent damage. This makes them attractive for seals and joints but also for adhesives, for tires and implants inside the body. Adhesion and fracture, which imply either the failure of interfacial bonds or of primary bonds, are particularly complex due to this dual nature of interactions inside the material. Understanding the failure of soft materials requires knowledge of mechanics at large strain, and viscoelasticity, but also polymer physics, statistical physics and thermodynamics.

There are several important general aspects that should be pointed out at the onset. First, soft dense polymer materials present a large difference between bulk modulus (usually around 10^9 Pa) and shear modulus. This implies that they can be generally modeled as incompressible and that failure mechanisms are very sensitive to the presence of hydrostatic stress. Second, the importance of large deformations requires the use of finite strain mechanics to model the process. Third, deformations in soft materials are related to the molecular structure and elastic restoring forces are mostly of entropic origin.

As a result, a description of the deformation, adhesion and fracture of soft materials requires a discussion of relevant length scales (molecular, microscopic mechanisms,

sample size), characteristic time scales (due to viscoelastic behavior) and evaluation of the amounts of dissipated or stored energy.

Theory and experiments will be addressed, but rather than presenting an exhaustive list of experimental or theoretical investigations we have favored a more detailed presentation of selected studies chosen for their insight.

Section 2 reviews the basic concepts of linear elastic fracture mechanics and discusses differences between conventional (hard) materials and soft materials. Section 3 describes the main experimental methods used for the characterization of adhesion and fracture of soft materials, which are presented as materials in section 4. Sections 5 and 6 discuss more specifically the debonding mechanisms and fracture mechanisms of soft materials in light of the concepts presented before. Section 7 discusses emerging materials, designed to better control or enhance fracture resistance. Finally, section 8 presents the sketch of a unified picture for the fracture and adhesion of soft materials and section 9 discusses some open questions.

2. Physical concepts and scales in the fracture of soft materials

2.1. Basics of linear elastic fracture mechanics

In order to understand the paradigms and pitfalls induced (separately or jointly) by both the soft nature of materials and their viscoelasticity, it is worth opening this review with some scaling concepts in fracture mechanics. We will deliberately start with linear elastic fracture mechanics (LEFM) concepts in order to bridge this review with the most widely established knowledge base of materials scientists. Although most of these tools will be inadequate for soft materials, they remain a useful guide. We will omit all numerical prefactors in this introduction and limit ourselves to scaling laws and order of magnitude estimations (indicated by the ~ symbol instead of =).

LEFM is established on the hypothesis that the bulk material behavior remains linearly elastic everywhere except in a very small region around the crack tip that is schematically collapsed into a linear crack front spanning an interface. The original argument by Griffith (Griffith 1920) associated the creation of a new crack to the conversion of mechanical energy (external work U_w and variations of the elastic energy U_{el}) into a thermodynamic (reversible) energy cost per unit area $\Gamma = w = 2\gamma$ to create new surfaces, named the Dupré work of adhesion, according to the equilibrium relation:

$$\mathcal{G} = \frac{\partial U_w}{\partial A} - \frac{\partial U_{el}}{\partial A} = \Gamma \tag{1}$$

where $\mathcal{G}$ is called the strain energy release rate, with unit J m^{-2}, and it represents the relevant part of the loading condition and structural response of the sample for the purpose of crack propagation. The stable nature of this equilibrium condition is determined by the positive sign of the derivative of $\mathcal{G}$ upon the crack area A, which is a property of the studied structure (sample). We deliberately neglect all dynamic effects, since this review is mainly devoted to quasi-static debonding.

An equivalent description of LEFM can be expressed in terms of a singular stress field in the neighborhood of the crack tip in the form of an inverse square root dependence of the stress on the distance r from the crack tip:

$$\sigma(r) \sim \frac{K}{\sqrt{r}} \tag{2}$$

The equilibrium/propagation condition can thus be expressed as $K \geqslant K_C$, where the loading parameter $K \sim \sqrt{E\mathcal{G}}$ is called the stress intensity factor (SIF). $K_C \sim \sqrt{E\Gamma}$ is called the fracture toughness and is a material property (with unit Pa $\cdot$ m$^{1/2}$), E being the elastic modulus of the material.

The elastic displacement field $u(r)$ close to the crack tip can be derived as:

$$\begin{aligned} \varepsilon(r) &\sim \frac{\sigma}{E} \sim \frac{K}{E\sqrt{r}} \\ u(r) &\sim \int \varepsilon \, \mathrm{d}r \sim \frac{K\sqrt{r}}{E} \end{aligned} \tag{3}$$

The elastic crack opening profile $u(x)$ of an initially sharp slit can be shown to have locally a parabolic shape with radius of curvature ρ given by:

$$\begin{aligned} u(x) &\sim \frac{K\sqrt{x}}{E} \\ \rho &\sim 1/\frac{\partial^2 x}{\partial u^2} \sim \frac{K^2}{E^2} \sim \frac{\mathcal{G}}{E} \end{aligned} \tag{4}$$

Since K and $\mathcal{G}$ assume a maximum value at (quasistatic) stable crack propagation, we observe here the emergence of a first physical length scale of fracture which is the crack tip radius at propagation ρ^*:

$$\rho^* \sim \frac{K_C^2}{E^2} \sim \frac{\Gamma}{E} \tag{5}$$

We remark that ρ^* is a material property, and that it can be related to a more general physical length scale $\ell_{EA} = \Gamma/E$, that we can name the elasto-adhesive length[3], naturally emerging from the units of the related constitutive material properties. ℓ_{EA} represents the length scale where the cost of creating new surfaces and the bulk elastic energy density for a large deformation have a comparable value, and thus where they can couple. Saying it differently, ℓ_{EA} is the scale below which surface energy effects become dominant and where they can cause bulk deformations larger than $\varepsilon = 1$ (100%).

We remark that when limiting to orders of magnitude, all these arguments are equally valid for interfacial fracture, taking care to use the Dupré interfacial work of adhesion $w = \gamma_1 + \gamma_2 - \gamma_{12}$ (which reduces to 2γ for cohesive fracture), and considering the substrate as infinitely stiff for simplicity.

In order to conclude this introduction on LEFM, we should comment further on the conditions of validity of this theory and formalism. LEFM is valid provided that all inelastic or nonlinear processes are limited to a small size (generally known as small scale yield condition, SSY (Williams 1984)). If this condition is met, the present formalism can be extended to more

[3] For simplicity this term will be used for both adhesion and fracture.

general materials constitutive laws, such as plasticity, viscoelasticity, and nonlinear elasticity of soft materials. However, we should never forget that the validity of the SSY approximation should be checked for all the sources of inelasticity and nonlinearity by considering the comparison with both the geometrical dimensions of the sample (in particular the smallest distance between the crack tip and one of the boundaries), and the length c of the crack (even if we are referring to a model defect microcrack). Moreover, the plane strain condition should be verified. Under these circumstances, all the LEFM formalism can be extended by simply substituting the (reversible) thermodynamic fracture energy w with an irreversible *fracture energy* Γ, intended as an effective surface energy, which can possibly depend on crack propagation velocity $\Gamma(v)$. We remark that in any case we should have $\Gamma(v) > w$ since the thermodynamic surface energy is the minimum required energy cost for propagating a crack, and in polymers Γ can indeed become several orders of magnitude larger than w under appropriate temperature and crack velocity combinations.

A classical well established example is the case of hard elasto-plastic materials, which under small deformations can be simply characterized by adding to the elastic modulus a second material parameter that is the yield stress σ_Y. By comparing the yield stress with the singular stress field in equation (2) we can directly identify a physical length scale, named after Dugdale (Dugdale 1960):

$$\ell_D \sim \frac{K_C^2}{\sigma_y^2} \sim \frac{E\Gamma}{\sigma_y^2} \tag{6}$$

which defines the size of the plastic region at the crack tip at crack propagation, and which is also the region where all energy is dissipated under SSY conditions. A second physical length scale can be obtained by substituting ℓ_D into equation (4) and thus obtaining the critical crack opening displacement:

$$\delta_D \sim \frac{K_C^2}{E\sigma_Y} \sim \frac{\Gamma}{\sigma_Y} \tag{7}$$

The fracture energy can be written as $\Gamma = \sigma_Y \delta_D$, i.e. the plastic work done at stress σ_Y to separate the crack lips up to a critical distance δ_D. We remark that the surface energy w is neglected here because it is small relative the dissipated plastic work. However Γ still characterizes properly the energy to propagate a crack into a specific material. As a few examples, silicate glasses have typical values of $E \sim 70$ GPa, $\sigma_Y \sim 10$ GPa and $\Gamma \sim 10$ J m^{-2}, so that $\ell_D \sim 7$ nm and $\delta_D \sim 1$ nm; glassy polymers, such as PMMA, have typical values of $E \sim 3$ GPa, $\sigma_Y \sim 100$ MPa and $\Gamma = 300$ J m^{-2}, so that $\ell_D \sim 10$ μm and $\delta_D \sim 1$ μm; metals, such as steel, have typical values of $E \sim 210$ GPa, $\sigma_Y \sim 1$ GPa and $\Gamma = 40$ kJ m^{-2}, so that $\ell_D \sim 8$ mm and $\delta_D \sim 40$ μm (see figure 1 for the appearance of crack tips in these materials). The first conclusion is that LEFM can easily be applied to standard cm size test samples in glasses and glassy polymers, but metals require either huge samples or more advanced non linear methods (Rice 1968). The second conclusion is that the propagation of a typical micrometer size flaw in the material can be treated with LEFM on glasses, and tentatively on glassy polymers, but not on metals, where the plastic zone will be larger than the defect size, resulting in a plastic blunting of the defect instead of unstable propagation. This is the core of the brittle or ductile nature of these materials under the application of a uniform stress such as in tensile testing.

2.2. Considerations on the fracture of soft elastic materials

While we commonly refer to soft materials as having a low value of the Young's modulus, between 1 kPa and 10 MPa, for fracture problems, the definition should be based on the competition between the elastic energy and the (effective) surface energy Γ (we initially assume that all dissipation only occurs in a very small molecular region, so that Γ can be treated as w). A material can thus be qualified as 'soft' at length scales comparable or smaller than the elasto-adhesive length $\ell_{EA} = \Gamma/E$.

When considering again equations (3) and (5), we remark that the elastic radius of curvature at crack propagation ρ^* is also the distance from the crack tip below which any material would experience large strain (the transformation from a sharp crack to a round tip implies infinite local deformation). LEFM is thus intrinsically limited by this length scale, but remains essentially valid at larger scales (if the sample is large enough to see them), independently of the value of E. ℓ_{EA}can thus be seen as the elastic blunting size, due to both dimensional arguments and to the fact that the singular field in equation (2) is preserved at larger scales.

This argument would also apply to nominally stiff solids. However, for most stiff enthalpic solids ℓ_{EA} is smaller than molecular dimensions, and is therefore masked by plastic deformation occurring at larger scales. The relevant scale for SSY plastic deformation in stiff solids is given by the Dugdale length ($\ell_D \sim K_C^2/\sigma_y^2 \sim E\Gamma/\sigma_y^2$) which is significantly larger than the molecular size (see previous section). For soft materials on the other hand, with a lower estimate for the fracture energy provided by Van der Waals interactions at $w \sim 40$ mJ m^{-2}, we obtain a lower estimate for ℓ_{EA} which ranges from 40 μm to 4 nm depending on the value of E, and this value can increase significantly when dissipation comes into play by increasing $\Gamma$by several orders of magnitude. Figure 2 presents the images of crack tips in two soft materials such as a rubber or a hydrogel, to be compared with the images in figure 1 for stiff elastoplastic materials.

When considering the fracture or adhesive debonding of a soft layer, the crack tip stress singularity of LEFM is no longer applicable when the thickness h of the layer becomes comparable to the elasto-adhesive length ℓ_{EA} and the square root stress singularity is progressively modified and suppressed for even thinner layers. For the same reason, if we consider an inner (or interfacial) small and sharp penny crack of radius $c < \ell_{EA}$, LEFM can no longer be applied at the crack front and the crack will grow in a 'soft' manner, i.e. by developing into a round cavity and expanding in the bulk of the soft material (Lin and Hui 2004, Shull and Creton 2004, Shull 2006). We remark that while in these conditions it is no longer possible to define a stress intensity factor K, and a related value of the toughness K_c, the energy based Griffith formalism described by equation (1) remains valid as long as the bulk deformation

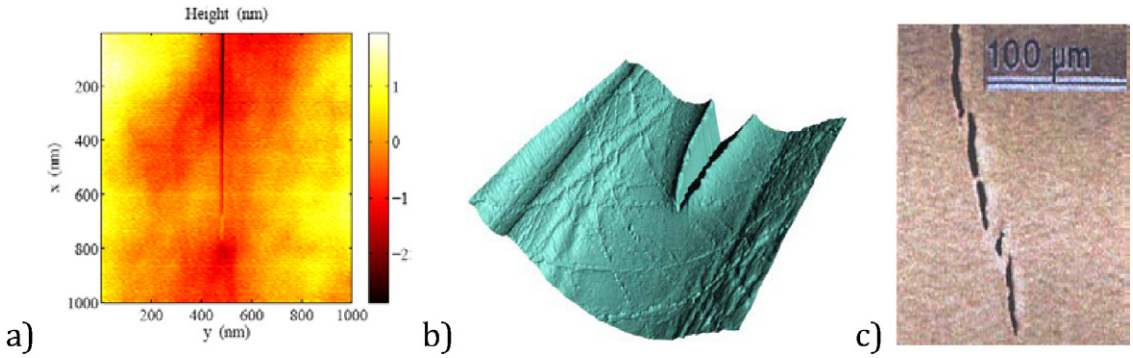

Figure 1. Images of crack tips in elasto-plastic materials (a) AFM image of the crack tip in an inorganic glass (size = 1 μm), image reproduced with permission from Han *et al* (2010; copyright IOP Publishing); (b) AFM image of a crack in a glassy polymer (size = 40 μm) image from Nziakou (2015); (c) crack tip in a metal alloy (titanium aluminium) (size = 200 μm), image reproduced from Bouchaud and Paun (1999; copyright 1999 IEEE).

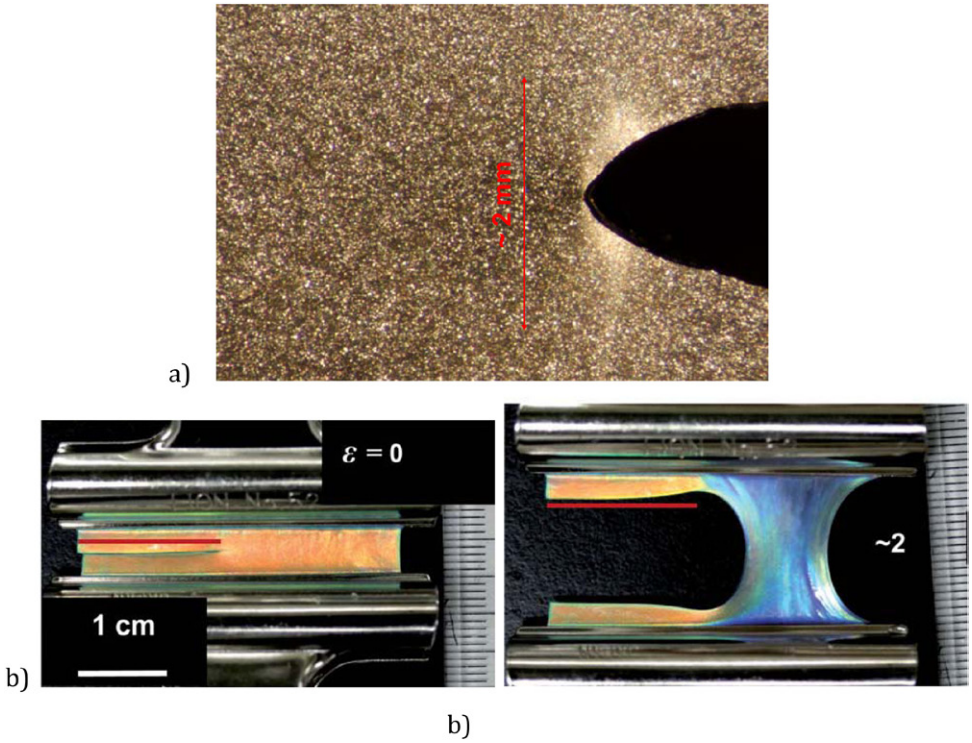

Figure 2. Images of crack tips in soft materials (a) a typical rubber (size = 2 mm), data from Mzabi *et al* (2011) (b) a soft hydrogel at $\lambda = 1$ and $\lambda = 3$ (size = 1 cm), images reproduced from Haque *et al* (2012; copyright 2012 Royal Society of Chemistry).

remains elastic, or if the region where energy is dissipated close to the crack tip remains smaller than $\ell_{EA}$and than any geometrical feature such as h and c. The validity of these energetic arguments in soft materials have been very clearly demonstrated experimentally by the seminal work of Rivlin and Thomas (Rivlin and Thomas 1953), and have subsequently been the focus of important theoretical developments to determine the J integral for nonlinear elastic materials (Rice 1968).

As discussed in the introduction, an important property of soft dense materials, such as polymers and hydrogels, is to be virtually incompressible, meaning that their Poisson ratio is close to 0.5, or equivalently, that their elastic compression modulus (~10^9 Pa) is several orders of magnitude larger than the shear modulus. This implies that the elastic strain fields are essentially constituted by a (deviatoric) shear strain tensor. On the other hand, the stress tensor field can be separated into a shear field and an additional hydrostatic stress field that plays a major role in the overall deformation. This becomes particularly important when a soft material is geometrically confined between rigid interfaces, as in the case of most adhesives, and it results in the build-up of very strong hydrostatic tensile stresses that play a major role on the growth of cavities from small defects (and on the inelastic response of the materials).

2.3. *Considerations on the fracture of soft dissipative materials*

When the energy dissipation in a soft (or hard) material can no longer be considered as limited to a very small region close to the crack tip, most of the theoretical foundations of

fracture mechanics (even non-linear) are lost, and even the existence of a well defined fracture energy becomes questionable, where we mean a material (or interfacial) quantity that can be separated from the structural response. Unfortunately, this is the case in most realistic soft materials, where the large deformations taking place in extended regions of the samples quite invariably cause energy dissipation at virtually all scales. Under these circumstances, it becomes very complex and subtle to separate the energy that is dissipated due to fracture propagation from the energy that is dissipated due to the macroscopic sample deformation. The energy required to propagate a crack thus becomes intimately related to the specific mechanical configuration of the structure, and each structure must be analyzed individually. When using samples with convenient translational invariance, this can still result in an *apparent fracture energy* $\Gamma_{\rm app}(v)$, and we can still define a length scale of elastoadhesive dissipation $\ell_{\rm EAD}(v) = \Gamma_{\rm app}(v)/E$. For example in the peeling of an adhesive strip $\ell_{\rm EAD}$ is typically larger than the thickness of the adhesive layer and is not an intrinsic property of a fracture surface or interface, but rather an *effective work of debonding* of a given structure/joint. Such a value of $\Gamma_{\rm app}(v)$ will generally change when changing some geometrical characteristic of the structure such as the thickness of the adhesive layer. In this review we will generally use the symbol $\Gamma(v)$ to characterize the intrinsic fracture energy, i.e. that part of the energy dissipation that can unambiguously be associated to crack propagation and separated from any other source of bulk dissipation occurring at larger scales which should rather be attributed to the loading history of the sample seen as a structure.

This field is a very active subject of research, and many efforts have been made to identify some special conditions where fracture mechanics can still be applied in a sound way, and where the measured $\Gamma(v)$ can still be associated with an effective surface/interface process. We will limit our introductory discussion here to viscoelastic materials, having in mind mainly polymer based materials, and consider a hypothetic condition where either the material is stiff enough, or the (effective) surface energy is low enough, that the elasto-adhesive length $\ell_{\rm EA} = \Gamma/E$ is small in front of all other structural (and defect) length, so that linear viscoelasticity applies over all of the sample at length scales $> \ell_{\rm EA}$. Under these circumstances all the bulk material response is defined by a stress relaxation function (or any other complete linear rheological characterization), and the structural response of the sample can be derived by applying the Boltzmann superposition principle on each element of the structure.

In the particular case where the structure is a fracture test sample with a well defined precrack of constant length c (non propagating, or with a very slow crack propagation velocity non appreciable on a macroscopic scale), the response of the material to any loading history can be obtained by applying the Boltzmann superposition principle to the elastic solution of the structure (this is called the correspondence principle and it is the base of interpretation of all DMA measurements). The strain energy release rate is thus simply derivable by applying the same material's relaxation functions to the elastic strain energy release rate. For example, after loading the sample to some fixed displacement, the energy release rate will decrease in the same way as the relaxation of the measured applied load, and if the fracture propagation is well described by a fracture energy $\Gamma(v)$, the crack propagation velocity will be observed to progressively slow down in time.

A second notable case is when the material relaxation is fast enough that a relaxed soft elastic condition is reached over all of the scales of the sample, except for some small scales around the slowly moving crack tip, where the crack propagation induces a continuous evolution of the local boundary condition and thus determines the continuous setup of a new viscoelastic relaxation that persists over some time after the crack has passed by some point. Or equivalently over some limited distance from the crack tip, if we use the steady state crack propagation velocity to map time into traveled distance. This assumption is the foundation of the de Gennes trumpet scaling arguments for the energy dissipated by a moving crack into a linearly viscoelastic material (de Gennes 1988, 1989, 1996), and has been the core of virtually all other important works in this domain (Schapery 1975a, 1975b, 1975c, Hui *et al* 1992b, Xu *et al* 1992, Haiat *et al* 2002, Persson *et al* 2005, Barthel and Fretigny 2009).

According to these theories it is possible to relate the fracture energy $\Gamma(v)$ to the linear viscoelastic properties of the material (Saulnier *et al* 2004) (defined for example by the knowledge of $\mu'(\omega)$ and $\mu''(\omega)$ over a very broad frequency range). However, most attempts to check these predictions experimentally on a sound quantitative base for rubbers have up to now invariably failed to the best of our knowledge (Gent 1996a, Barthel and Fretigny 2009, Cristiano *et al* 2011). Even a very important protagonist of this domain such as Gent, has pointed out the intrinsic failure of these theories to describe the real data (Gent 1996a), and called for an extension of these models to cope with more realistic conditions occurring during fracture propagation in soft materials.

The main factors that should be taken into account are clearly the non-linear finite deformations of soft materials and the non trivial modifications of the viscoelastic dissipation under finite deformations. Moreover, the effects of geometric confinement on both the material response and deformation mechanisms should be adequately taken into account. More subtle problems require the distinction between (non-linear) viscoelastic dissipation and damage mechanisms occurring in the polymer networks under large strains. At last, the thermomechanical energy balance should also be carefully taken into account, because the strong energy dissipation affecting these materials can cause significant changes in the local temperature field, and the mechanical response of these materials is particularly sensitive to even weak changes in temperature due to changes in both the molecular mobility and the entropic nature of elasticity. Some of these issues have been tackled by more recent models (Persson *et al* 2005, Persson and Brener 2005), but the large strain zone close to the crack tip has still been treated as a black box. This approach gives reasonable predictions if the energy dissipation is dominated by viscoelastic dissipation far from the crack tip (Plazek *et al* 1983, Plazek *et al* 1988), but typically fails for more elastic materials and low strain rates (Cristiano *et al* 2011).

All these issues will be a major focus of our present review, where well defined experiments will be selected to clarify at least some of these points up to the present level of knowledge.

3. Experimental methods

We describe here the main experimental tests that are generally used to characterize the failure of soft materials and discuss their advantages and limitations. Typical tests based on linear elastic fracture mechanics are not adapted to these highly deformable non-linear elastic and often viscoelastic materials. The calculation of detailed stress fields is very difficult and global energetic approaches are usually preferred for nearly elastic materials. However, such energetic approaches are not yet clearly established for markedly viscoelastic materials.

3.1. Adhesion tests: peeling, tack tests

Soft adhesives, also called pressure-sensitive-adhesives (PSA), are soft polymer layers that are used to bond two stiffer structures together (Creton 2003). Since the lateral dimension of the adhesive joints are generally much larger than the thickness h of the polymer layer, the geometrical confinement is quite strong and deeply affects the mechanics. The debonding of the adhesive from the substrate can occur by different mechanisms, implying either the propagation of a crack along one of the two interfaces and/or extensive deformation in the bulk of the adhesive layer. Even when failure is localized at a specific interface, it can involve or not strong dissipative mechanisms acting in the whole PSA layer.

Most experimental methods for testing an adhesive joint, such as the peel test or the probe tack test, are based on the measurement of the structural response of the whole joint during debonding and they provide a global result (a peel force or debonding energy) that does not reveal anything about the detailed mechanisms of debonding. In this section we will review the basics of these techniques as applied to a generic joint, while the interpretation of these measurements in light of the specific mechanisms occurring in soft polymer adhesives will be presented in section 5 after the materials have been introduced in more detail in section 4.

The case of weak adhesion of elastic soft materials (where Γ/E is small related to all geometric dimensions of the polymer layer) has been extensively studied and reviewed (Shull 2002) and is typically based on the analysis of the contact between a sphere and a flat or two crossed cylinders (figure 3).

Because in this type of analysis the elastically deformed volume in the bulk can be clearly separated from the typical length scale of dissipative interfacial processes, the problem can be treated as a classic interfacial fracture propagation problem according to the so called JKR analysis (Maugis and Barquins 1978a). Such experiments typically yield curves where the energy release rate is imposed and the crack velocity v is measured and it is found that a unique effective adhesion energy curve $\Gamma(v)$ can be obtained from a set of measurements done in different loading conditions and it constitutes a good characterization of the adhesive properties of the interface between the two solids (Maugis and Barquins 1978a, Deruelle *et al* 1998, Ahn and Shull 1998b).

However, if the adhesion is stronger or if the material is more viscoelastic in the bulk during the time scales of the test, then the strain energy release rate $\mathcal{G}$ becomes dependent on loading history and the adhesion energy is no longer easily separable from the energy dissipated in the bulk. In extreme cases, the elastic energy released by the deformed material may not be sufficient to propagate a crack and external work must be continuously applied. Under these circumstances the JKR geometry is not well suited and the two tests that have been used most extensively to investigate adhesion of soft viscoelastic material are the probe test, where a cylindrical, flat or hemispherical-ended probe is pulled at constant speed from an adhesive layer, and the peel test, where a thin adhesive strip backed with a stiff layer, is peeled at a constant velocity from the surface of a usually rigid substrate. Both tests are schematically described in figure 4. The probe test imposes a well-defined geometry of loading on the adhesive layer but does not provide information on steady-state propagation. On the contrary the peel test is ideal to study steady-state propagation but loads the adhesive film in a variable and more complex geometry. Fixed load peel tests at a zero angle of peel (called shear tests in the PSA community) are also typically carried out to study the long term adhesion at low stress levels. However the details of the catastrophic failure remain poorly understood, so we will not focus on that type of test in this review.

The peel test is typically used to test the adhesion of tapes and the peel force (per unit width of tape) is used as a measure of the adherence energy. The experiment is normally carried out at a constant peel angle and by applying either a constant peel velocity (a standard test in industry) or a constant load. Although the effect of the peel angle has been the object of several studies (Kaelble 1960, Gent and Kaang 1987, Williams 1993, Williams and Kauzlarich 2005), most materials are tested at a peel angle of 90° or 180°(PSTC 2000). Despite its apparent simplicity, the peel test applies a rather complex strain field in the region of the debonding front, resulting from a coupling between the bending stiffness of the backing and the mechanical properties of the deformable adhesive itself. It has however the advantage to focus on the steady-state propagation of a crack rather than on its nucleation. Typically in peel tests the soft adhesive material is reinforced with a backing that is much stiffer in tension than the adhesive, avoiding therefore to account for the tensile deformation of the arm. If the peel angle is not too small (a few degrees) the strain energy release rate $\mathcal{G}$ is given by:

$$\mathcal{G} = \frac{F}{b}(1 - \cos\theta) \tag{8}$$

where b is the width of the peeled strip. This reduces to $\mathcal{G} = 2F/b$ for a T-peel test (see figure 4), that is conveniently carried out in tensile testers. The typical outcome of a peel test is the steady-state peel force as a function of peel velocity, which under quasistatic steady state peeling can be directly translated into an apparent fracture energy $\Gamma_{\text{app}}(v)$ by

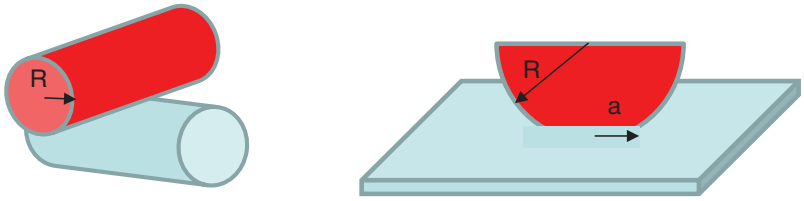

Figure 3. Simple contact geometries used in contact mechanics. Crossed cylinders and sphere on flat.

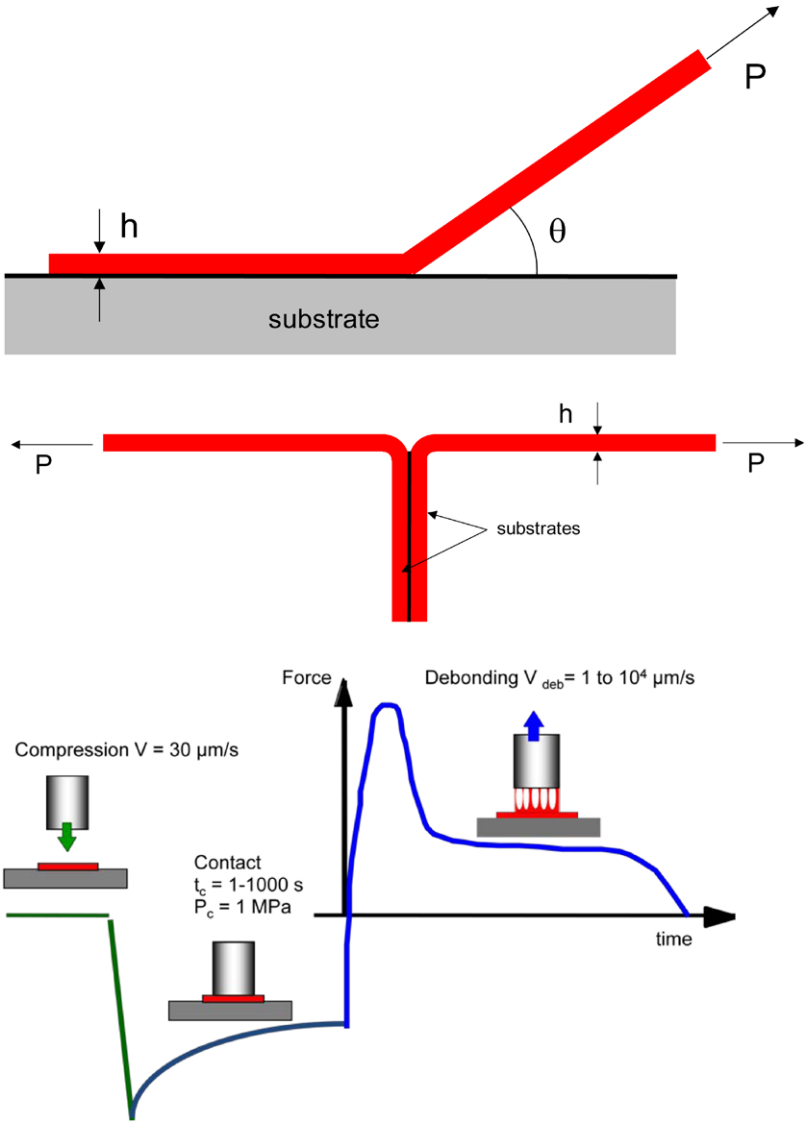

Figure 4. Schematic of a peel test and of a probe test used to test adhesion of soft materials.

normalizing the peel force by the width of the peeled strip[4]. However, in the absence of a detailed knowledge and modeling of the deformation and failure mechanisms occurring in the debonding of the soft polymer, such a single parameter, although useful for comparative purposes, does not provide a well defined property of the interface and it is generally strongly dependent on the thickness of the adhesive layer and peel angle (Gardon 1963a, Villey *et al* 2015).

[4] The work done by the force is the force multiplied by the peeled length x. The adherence energy is then this work divided by the peeled area xb, hence $\Gamma_{app}(v) = F(v)/b$.

The probe test, schematically shown on figure 4, provides very different and complementary information on the adhesive properties of soft materials. In this test an adhesive layer is first compressed between a flat ended cylindrical probe of radius a and a hard substrate. After a set contact time, the probe is removed from the surface at a constant velocity V_{deb} and the load F is measured as a function of time or distance, as illustrated in figure 4. The advantage of the probe test is the application of a well defined displacement field to the deformable adhesive, since all parts of the measuring instrument have a negligible bending stiffness. Moreover, a well defined strain history can be applied to the adhesive before debonding,

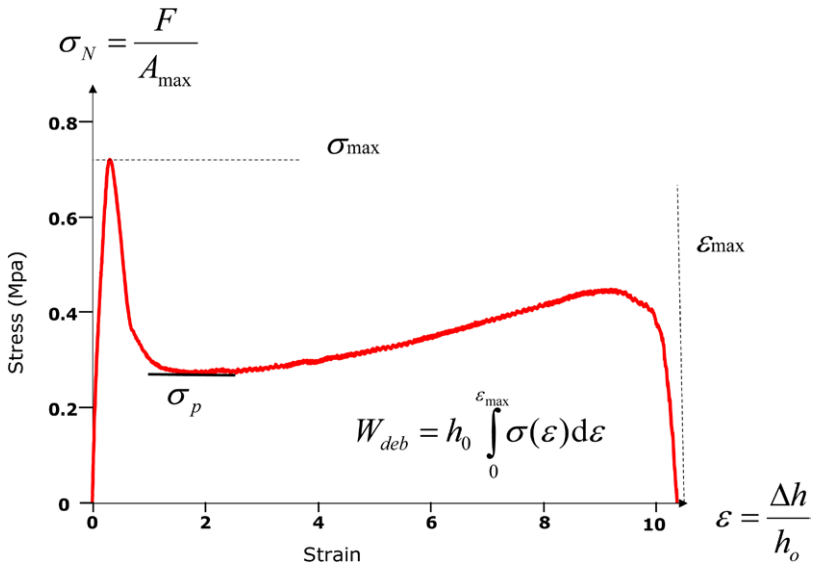

Figure 5. Normalized force displacement curve typically obtained for a probe test and definition of the main parameters that can be extracted from it.

although the effect of the compression/decompression stage is ignored in most experimental investigations on soft adhesives (Shull and Creton 2004).

The results of a probe test are a force versus displacement curve. This curve is usually transformed into a nominal stress versus nominal strain curve (figure 5), which is obtained by normalizing the force by the maximal area of contact $A_{\max}$ during the compression stage (related to the probe radius a_0) and the displacement Δh by the initial layer thickness h_0:

$$\sigma_{\mathrm{N}} = \frac{F}{A_{\max}}, \ \varepsilon = \frac{h - h_0}{h_0} \tag{9}$$

Because the debonding mechanism of a soft confined adhesive layer is usually complex and is not a simple propagation of an axisymmetric crack from the edge toward the center, data from probe tests cannot be easily compared in a quantitative way to a model or to a simulation. However, the shape of the stress-strain curve reveals details about the deformation mechanisms. In particular, four main parameters can be extracted from the curve: the peak stress $\sigma_{\max}$, the maximum extension $\varepsilon_{\max}$, the plateau stress σ_{p} and the work of debonding W_{deb} (i.e. the area under the loading curve multiplied by h_0). The nominal stress-strain curve obtained from the test can be compared for different materials and different test conditions providing significantly more information than the simple value of the peel force. However, once again, in order to derive some sound physical interpretation from these measurements, a separate investigation of the deformation and failure mechanisms during the debonding should be performed, and will be discussed in more detail in section 5.

Probe tests can be carried out both in a sphere on flat geometry or in a flat punch geometry. The sphere on flat geometry is widespread for adhesion of non fibrillating elastic rubbers where $\ell_{\mathrm{EAD}} \ll a$, due to two key advantages relative to a flat punch method: firstly, its insensitivity to small misalignments between sample and probe and secondly, the well-defined crack propagation geometry that the hemispherical probe introduces. However, for highly viscoelastic and soft adhesives where ℓ_{EAD} is comparable or larger than the radius of the probe a, these two key advantages are offset by the more complex stress field imposed by the spherical probe and by the increased difficulty of modifying chemically a curved surface (Crosby and Shull 1999b, Crosby and Shull 1999a). As a result the flat-ended probe has been used extensively for soft viscoelastic adhesives since the mid 1980's (Zosel 1985, 1989, 1992, Lakrout *et al* 1999, Creton and Fabre 2002, Poivet *et al* 2003, Shull and Creton 2004, Teisseire *et al* 2007). Initial studies focused on the adhesion energy alone (Zosel 1985, 1989, 1997, 1992), and then the combined analysis of the complete stress-strain curve and of the synchronized images obtained from a properly positioned video camera led to a much more detailed interpretation and understanding of the micromechanisms (Lakrout *et al* 1999, Creton *et al* 2001, Brown *et al* 2002, Chiche *et al* 2005a, Tanguy *et al* 2014). An example of the schematic setup built in the ESPCI laboratory and of the images obtained is shown on figure 6. It is based on a stiff sample holder, a set of three screws to adjust alignment and a 45° mirror to observe the debonding through the transparent glass substrate supporting the adhesive film.

3.2. *Fracture mechanics for rubbers: tearing, pure shear double edge notch*

As opposed to adhesion tests where the adhesive layer is confined between two stiffer surfaces, fracture tests are usually carried out on unconfined samples (films, sheets or thick samples) with materials much less viscoelastic than soft adhesives and a value of $\ell_{\mathrm{EAD}} \ll c$ and the dimensions of the sample. However fracture can occur in plane stress conditions (for thin samples) or plane strain conditions (for thick samples) giving different results for $\Gamma(v)$. Furthermore adhesion experiments involve the presence of an interface, which is typically mechanically weaker than the bulk material and constitute therefore a preferential path for the crack. Such preferential path does not exist

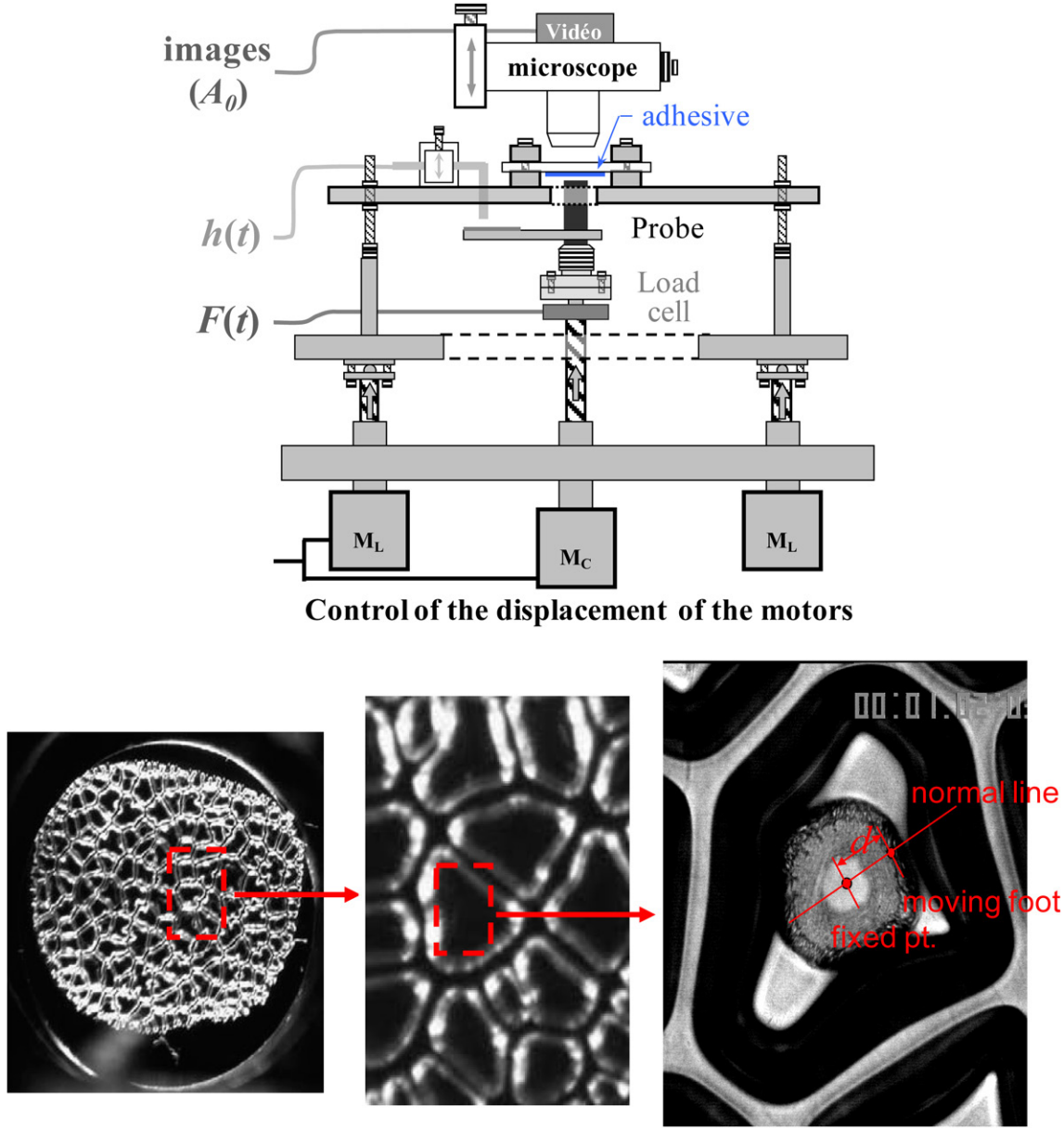

Figure 6. Schematic of an instrumented probe tack test and typical images obtained during debonding at different magnifications. The instrumentend probe test is based on a stiff sample holder, a set of three screws to adjust alignment and a 45° mirror to observe the debonding through the transparent glass substrate supporting the adhesive film.

for bulk fracture and leads sometimes to crack deviations even when the loading is in pure mode I (De and Gent 1996).

Typical test geometries that are suited for studying fracture propagation in soft viscoelastic materials such as rubber are shown in figure 7. The choice of a particular geometry for a fracture test usually depends on practical considerations. The so-called trousers test, which creates a weak propagation plane by decreasing the thickness of the sample along a side groove, is well adapted to very tough materials, but typically includes significant dissipative processes that are not related to the fracture process itself, i.e. it measures a total work of fracture $\Gamma_{\text{app}}(v)$ rather than a fracture energy $\Gamma(v)$. Two easier tests to analyze are the pure shear test and the simple or double edge notch test. The pure shear test geometry shown in figure 7 has the distinct advantage to apply an energy release rate $\mathcal{G}$ that is independent of crack length c if the material is elastic in the bulk and $c > h_0/2$ where h_0 is the height of the undeformed sample. For a purely elastic material the energy release rate can be written as:

$$\mathcal{G} = W(\lambda)h_0 \tag{10}$$

where $W(\lambda)$ is the strain energy per unit volume well ahead of the crack tip under the given fixed stretch λ. This geometry is well suited for both steady-state crack propagation and for fatigue crack propagation, i.e. crack propagation under cyclic load. It requires however a specific sample geometry and a careful grip. This is easily doable in an industrial setting where samples can be molded, but is more difficult to do in the lab with small samples and has only been rarely used for hydrogels (Seitz *et al* 2009, Baumberger *et al* 2006a, Sun *et al* 2012).

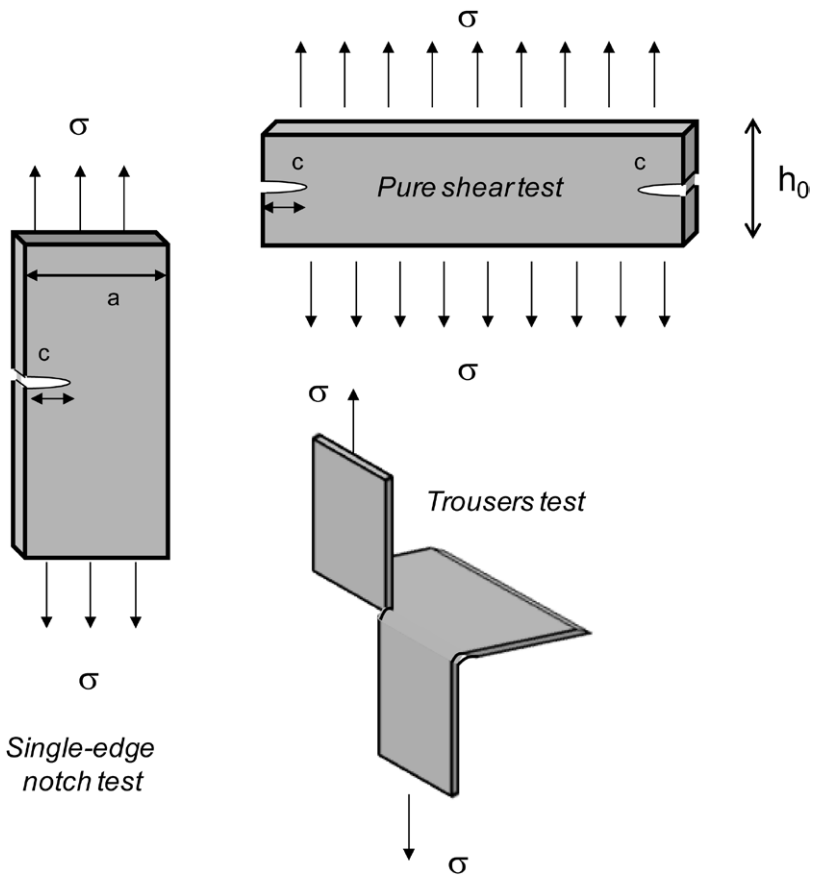

Figure 7. Schematic of the most common geometries used for fracture of rubbers: single-edge notch test (SEN), trousers tests also called tear test and pure shear test (PS).

Hence, many academic fracture studies have been published using the single or double edge notch test or the trousers test instead (Greensmith 1963, Bhowmick *et al* 1983, Gent *et al* 1994, Tanaka *et al* 2005, Lin *et al* 2010, Cristiano *et al* 2011). In the single or double edge notch test, also shown on figure 7, a prenotched strip of material is stretched in tension. For elastomers (which typically display Neo-Hookean elasticity for moderate stretch) an empirical expression was proposed by Greensmith (Greensmith 1963) based on experiments on single edge notch geometry with different crack lengths $c \ll a$, where a is the sample thickness as indicated in figure 7:

$$\mathcal{G} = \frac{6W(\lambda)c}{\sqrt{\lambda}} \tag{11}$$

where $W(\lambda)$ is the strain energy per unit volume and is typically obtained from the stress-strain curve of an unnotched sample of identical dimensions. It should be noted that in this geometry the energy release rate increases with crack length, i.e. dG/dc is positive so that the crack will accelerate once it starts to move and spontaneous uncontrolled propagation will occur.

4. Soft polymer materials: structure and deformation

Soft materials are typically defined as deformable materials with a low elastic modulus. Yet in this review we will have to make some further restrictions in terms of structure. The most important one is that we will focus on soft materials made predominantly with flexible polymers above their glass transition temperature. This definition includes three important categories of soft materials of practical and technological importance: elastomers, pressure-sensitive-adhesives and swollen gels. All three (depicted schematically in figure 8) have in common to be networks of connected polymer chains and to have an elastic behavior mostly due to a change in entropy rather than internal energy. Their Young's modulus ranges between 1 kPa and 10 MPa.

The linear viscoelastic properties of soft polymer based materials have been the focus of many studies. However, the overwhelming majority of these studies have focused on two extreme cases where the physics is better known: the ideal rubber (figure 8) where all polymer chains are attached at both ends by covalent bonds (Treloar 1973) and the case of entangled but uncrosslinked polymers, which are actually viscoelastic fluids above their T_g (de Gennes 1979, Doi and Edwards 1986, Rubinstein and Colby 2003). Briefly, the shear elastic modulus μ_x of a crosslinked but unentangled rubber can be described by the sum of the free energy of its chains, i.e.

$$\mu_x = \nu_x k_B T \tag{12}$$

where ν_x is the number of elastic chains between crosslinks per unit volume. If the rubbery material is not chemically crosslinked but simply entangled, another important physical quantity is the plateau modulus generally called by rheologists $\mathcal{G}_N^0$. In this case the modulus can be described as the sum of the

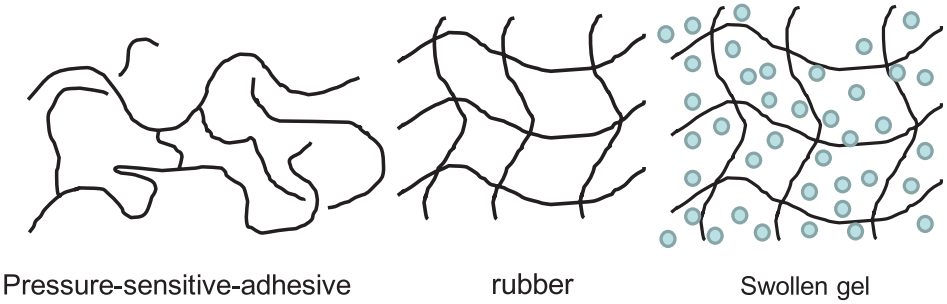

Figure 8. Schematic of a weakly crosslinked and entangled pressure-sensitive-adhesive, a crosslinked rubber and a swollen gel.

free energy of the elastic chains between entanglements. For coherence of notation we will call it here μ_e defined as:

$$\mu_e = \nu_e k_B T \tag{13}$$

where ν_e is the number of elastic chains between entanglements per unit volume. These two contributions to the modulus are additive so that when both crosslinks and entanglements are present, the elastic modulus is $\mu \sim \mu_x + \mu_e$. Soft materials can be roughly divided into two categories. When $\mu_x > \mu_e$ the soft material is typically a rubber or a swollen gel. The case of $\mu_e > \mu_x$ is more relevant for soft adhesives. It should be noted that μ_e is a characteristic of the flexibility and monomer composition of the polymer chain and does not depend on molecular weight or degree of chemical crosslinking. In the melt state, i.e. in the absence of solvent, μ_e typically ranges between 10^5 and 10^6 Pa.

To decrease further the modulus and make the material softer there are two options. The first is to reduce the concentration of elastic chains by swelling the polymer with a solvent. This situation corresponds to decreasing ν_x, and hydrogels, where the solvent is water, are a good example. Their modulus generally varies from 1 to 100 kPa depending on polymer concentration and level of crosslinking in the gel. The second option is to both reduce the level of chemical crosslinking and to broaden the molecular weight distribution to include shorter chains. In this case the elastic modulus becomes markedly frequency dependent and the material is highly viscoelastic. This case is representative of soft adhesives. The storage component of the elastic modulus μ' as a function of frequency for these different materials is shown schematically in figure 9.

While the density of entanglements and crosslinks as well as the characteristic times related to chain dynamics can be extracted from the linear viscoelastic properties of polymer networks by using suitable molecular models (Rubinstein and Colby 2003), the large strain behavior, in particular under uniaxial extension; cannot be quantitatively predicted from linear viscoelaticity. In this regime the presence of entanglements, hydrogen bonds and crosslinks couples and introduces a marked non-linearity in the behavior.

The simplest way to characterize the non-linear behavior of soft materials is in simple extension at a fixed strain rate until failure. Conventional shear rheometers can be used as well to probe large strain behavior in a cyclic test (the so-called Large Amplitude Oscillatory Shear, LAOS (Hyun *et al* 2011)) but require the material to have a steady-state behavior in a cyclic

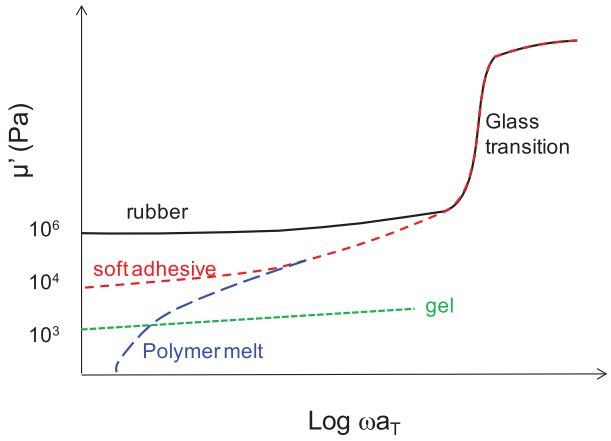

Figure 9. Schematic of the storage component of the elastic modulus $\mu'(\omega)$ at a fixed temperature T as a function of reduced frequency for representative soft materials. The a_T are the frequency-temperature shift factors according to the time-temperature superposition principle. Reproduced with permission from Williams *et al* (1955; copyright 1955 American Physical Society).

test,(i.e. no damage mechanism but only non-linear viscoelasticity) and are therefore more adapted to complex fluids than complex solids.

Uniaxial extension tests can be carried out essentially in two main ways: at a constant strain rate with an extensional rheometer or at a constant crosshead velocity with a tensile tester. Until recently the first method (in principle adapted to polymer melts) was very difficult to implement (Münstedt and Laun 1979). However, the development of the counter-rotating cylinders geometry (also called Sentmanat Extensional Rheology after (Sentmanat *et al* 2005)) to measure the extensional viscosity of polymer melts has made this method much more readily available (Wang *et al* 2007) and it turns out that its experimental design makes the measurement ideally adapted to soft and sticky solids. The constant crosshead velocity extensional test is more suitable for rubbers or gels and it gives a more accurate measurement of the initial modulus and of the extension ratio, which is typically measured locally with an optical extensometer. However, a conventional tensile test carried out in a machine by moving the crosshead at a constant velocity does not deform the sample at a constant true strain rate. Schematics of both experimental setups are shown on figure 10.

Whether tested at constant strain rate or at constant crosshead velocity, the typical stress-strain curve of a soft material

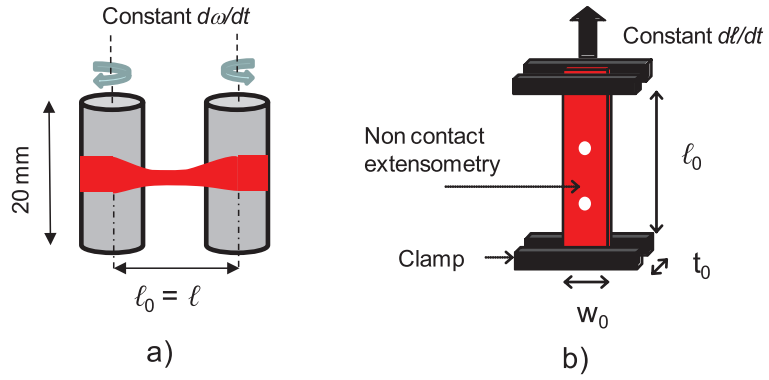

Figure 10. Schematic of: (a) the extensional rheology setup (SER version) where two cylinders counter-rotating at a constant angular velocity stretch the sample at a constant strain rate, since the gauge length is fixed and imposed by the distance between the cylinders; (b) the tensile test setup where the sample is stretched at a fixed crosshead velocity and the strain rate $d\ell/\ell$ decreases with time.

does not change qualitatively its main features but only its strain rate history. When representing a uniaxial tensile test, rheologists like to represent the extensional viscosity η^+ as a function of time in which is defined as.

$$\eta^+ = \frac{\sigma_T}{\dot{\epsilon}_H} \tag{14}$$

Where σ_T is the true stress and $\varepsilon_H = \ln \lambda$ is the Hencky strain and the stretch $\lambda = l/l_0$, where l is the deformed length and l_0 is the undeformed length. Materials scientists on the other hand prefer to represent the nominal stress σ_N as a function of λ. The two quantities are of course connected by:

$$\eta^+ = \frac{\sigma_T}{\dot{\epsilon}_H} = \frac{\sigma_N \lambda^2}{\dot{\lambda}} \tag{15}$$

For entangled and crosslinked soft materials, the large strain behavior is dominated by rubber elasticity. The simplest way to represent the strain energy density W of a crosslinked material (neglecting both entanglements and strain hardening) is the so-called neo-Hookean model (Treloar 1958). According to this model, which is based on the sum of the entropic elasticity of the elastic chains, W can be represented as a function of the three principal stretches as:

$$W = \frac{\nu_x k_B T}{2}(\lambda_1^2 + \lambda_2^2 + \lambda_3^2 - 3) = \frac{\nu_x k_B T}{2}(I_1 - 3) \tag{16}$$

where $I_1 = \lambda_1^2 + \lambda_2^2 + \lambda_3^2$ is the first invariant of the left or right Cauchy-Green tensor. For incompressible materials we must have $\lambda_1\lambda_2\lambda_3 = 1$. When considering an uniaxial extension test, the value of the nominal stress σ_N in uniaxial extension can be predicted by deriving this strain energy density function relative to the uniaxial stretch $\lambda = \lambda_1$ (with $\lambda_2 = \lambda_3 = 1/\sqrt{\lambda}$):

$$\sigma_N = \nu_x k_B T\left(\lambda - \frac{1}{\lambda^2}\right) \tag{17}$$

This prediction works well for crosslinked rubbers and hydrogels ($\mu_x \geqslant \mu_e$) at moderate strains. At large strains the main assumption of the affine network model, i.e. Gaussian elasticity of the polymer chains, does not hold anymore. In particular, the chains approach their finite extensibility limit and stiffen markedly. Several models have been used to account for that stiffening, but while the stiffening of an individual chain is well described by the Langevin function (Treloar 1958), the stiffening of an elastic material cannot be easily predicted simply from the density of crosslinks ν_x or entanglements ν_e. Hence, an additional finite extensibility parameter is used in empirical models. One of the simplest of such models is that proposed by Gent in 1996 (Gent 1996b), where W and σ_N in uniaxial extension are written as:

$$W = -\frac{\nu_x k_B T}{2} J_m \ln\left(1 - \frac{(I_1 - 3)}{J_m}\right) \tag{18}$$

$$\sigma_N = \nu_x k_B T\left(\lambda - \frac{1}{\lambda^2}\right)/1 - \left(\frac{(I_1 - 3)}{J_m}\right) \tag{19}$$

where J_m is the maximum allowable value of $I_1 - 3$ and has the meaning of the square of the maximum extensibility in uniaxial tension.

If $\mu_e \ll \mu_x$ does not hold, it is important to include in the model the effect of the topological entanglements. If the material remains elastic, meaning here non dissipative and with stresses that only depend on W, the combined presence of crosslinks and entanglements is well captured by molecularly based models combining the Doi-Edwards tube model and the affine network model. One of the most complete molecular models has been proposed by Rubinstein and Panyukov in 2002 (Rubinstein and Panyukov 2002).

The prediction of the model in uniaxial extension is a slight softening both with positive stresses (in tension) and with negative stresses (in compression). The engineering stress σ_N is then given by:

$$\sigma_N = \nu_x k_B T\left(\lambda - \frac{1}{\lambda^2}\right) + \nu_e k_B T\left(\lambda - \frac{1}{\lambda^2}\right)/(0.74\lambda + 0.61\lambda^{-0.5} - 0.35) \tag{20}$$

More complex molecularly based models have been proposed and in particular taking into account the combined effect of entanglements and finite extensibility (Edwards and Vilgis 1988), but this was done at the expense of the physical interpretability of the parameters.

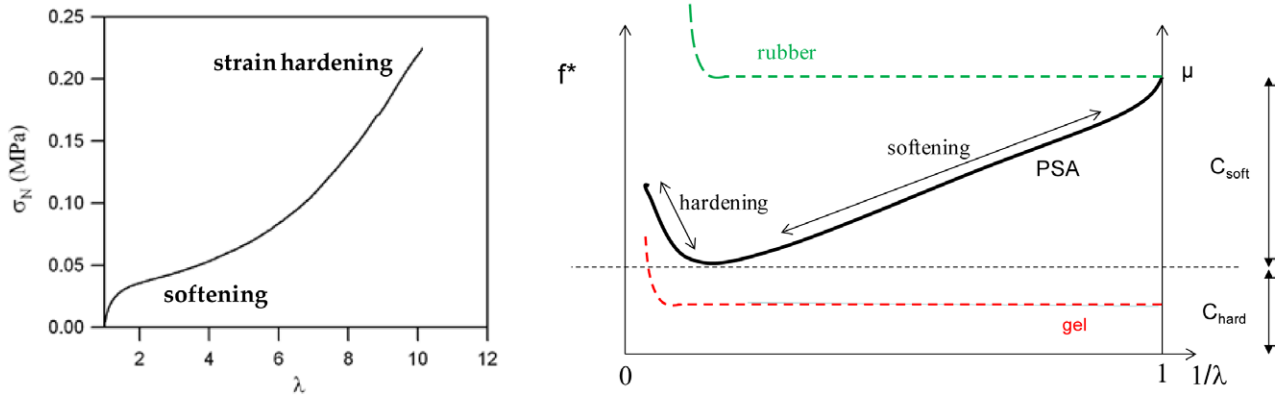

Figure 11. (a) Typical nominal stress versus uniaxial stretch plot for a PSA and (b) Mooney representation of the same data as a function of $1/\lambda$ and comparison with an elastic gel and an elastic rubber.

A convenient way to characterize experimentally the deviation from the affine network model is to represent the reduced stress also called Mooney stress defined as:

$$f^*(\lambda) = \frac{\sigma_N}{\left(\lambda - \frac{1}{\lambda^2}\right)} \tag{21}$$

For the affine network model of rubber elasticity, f^* is a constant independent of λ so that any dependence on λ can be interpreted either as the signature of the presence of entanglements, or of the onset of the finite extensibility of the chains, or of viscoelastic relaxation (discussed in more detail in section 6.2 within the context of fracture). Chain orientation between entanglements (reversible) and viscoelastic relaxation (irreversible) reduce the value of f^* with increasing strain, while the finite extensibility of the chains increases f^* at large strains.

Such a representation can in principle be used for any material with a mechanical behavior dominated by entropic elasticity. In strain-crystallizing rubbers, as for example natural rubber, and in rubbers of technological interest, which are filled with nanoparticles such as carbon black or silica, f^* varies a lot with λ due to changes of structure, and filler/polymer interactions taking place during deformation so that the unambiguous interpretation of $f^*(\lambda)$ for such complex materials is very difficult and yields limited insight. However, for unfilled rubbers, gels and soft adhesives $f^*(\lambda)$ is more directly related to the changes in stored entropic elasticity in the chains of the network and can be used for molecular insight. The analysis of $f^*(\lambda)$ is particularly useful for soft adhesives where the non linearity is marked and both softening and hardening are present. Figure 11(a) shows a typical stress-strain curve in uniaxial extension of a PSA and figure 11(b) shows f^* as a function of $1/\lambda$ for the same adhesive and for a typical elastic gel and elastic rubber in comparison.

The amplitude of non-linear softening of the stress at intermediate values of λ translates into a steady decrease in $f^*(\lambda)$ from its initial shear modulus μ (at $\lambda = 1$) to a minimum value corresponding to the onset of strain hardening. The shear modulus μ can then be conveniently separated into a relaxing component C_{soft} and a permanent component C_{hard}. The interpretation of these two quantities will be further discussed in section 5.3.3 on fibril growth in soft adhesives.

To conclude this overview of the large deformation of soft materials, we should point out that for viscoelastic fluids an equally active community has focused on characterizing strain hardening as a deviation from linear viscoelasticity (Zülle *et al* 1987). This type of strain hardening, well captured by non-linear models for viscoelastic fluids (Phan-Thien 1978, Giesekus 1982, Bird *et al* 1987), is identified in the extensional viscosity η^+ versus time curve as a deviation from the linear viscoelastic prediction. The two types of strain hardening are rather different. For a viscoelastic fluid strain hardening means that the relaxation of the stress does occur less rapidly with time than the linear relaxation would predict. On the other hand, for a viscoelastic solid strain hardening means that the stress increases faster with strain than Gaussian elasticity would predict.

This concludes the brief overview of the structure and deformation of the soft polymer materials of interest for our review. We have introduced the notion of crosslinks, entanglements, viscoelasticity and large strain behavior. We will now focus on two specific cases where large deformations occur over significant volumes and where considerations on the polymer structure become particularly important: we will address first the physics of stickyness, i.e. the adhesion of soft viscoelastic and confined layers to rigid surfaces, and then the fracture of soft materials, i.e. the case a crack tip propagates in the bulk along with a significant region of large deformations and dissipation.

5. Bonding and debonding mechanisms of soft adhesive layers

Soft adhesives are essentially thin soft and viscoelastic polymer layers that are applied between two more rigid bodies in order to hold them together. They are commonly found in a large variety of applications around us, where the adhesive bond does not need to sustain very high stresses or where reversible adhesion is required. This includes of course adhesive labels and packaging tapes, but nowadays

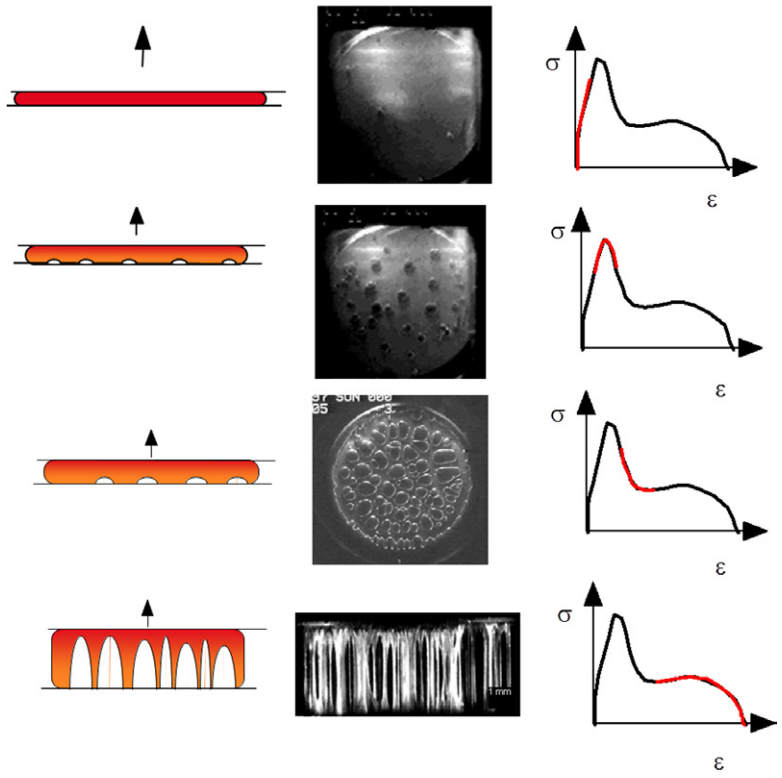

Figure 12. Schematic of the debonding mechanism of a soft adhesive from a rigid surface in a probe tack test. Reproduced with permission from Lakrout *et al* (1999; copyright 1999 Taylor & Francis).

encompasses also a lot of more technical fastening applications such as in microelectronics, automotive or biomedical where the use of a solventless solid adhesive is very attractive (Creton 2003).

Before we discuss in more detail the current understanding of the adhesion mechanisms, it is worthwhile to present a short historical prospective. Early studies on the mechanisms of adhesion are based on the peel test, which mainly provides a peel force as a function of velocity of steady state debonding, and they pointed out immediately the crucial role played by rheology and large deformation. The seminal series of papers of Dave Kaelble from 3M on the physics of peeling (Kaelble 1959, Kaelble 1960, Kaelble 1964, Kaelble 1965, Kaelble 1969) laid the foundations of the current understanding of the mechanisms already in the 60's. He first pointed out that the rheological properties of the soft adhesives were (with a few exceptions) more important than the surface properties of the adherend (Kaelble 1969), that peel adhesion master curves could be constructed by using time-temperature shift factors (Kaelble 1964) and that cavitation had to occur ahead of peel fronts (Kaelble 1965). Several much better cited studies followed focusing on the interplay between rheological properties, surface interactions and the apparent fracture energy $\Gamma_{app}(v)$(Gent and Petrich 1969, Andrews and Kinloch 1973a, Andrews and Kinloch 1973b, Gent and Schultz 1972) and confirmed indeed that the work to debond a soft viscoelastic adhesive was dependent on both the interfacial interactions and the rheological properties of the adhesives, although the details of the deformation mechanisms were undoubtedly complex and these studies did not address the effect of adhesive thickness.

The details of the deformation mechanisms were in parallel addressed by experiments using a probe method, described in section 2, which provides a more homogeneous and controlled loading condition, during both bond formation and debonding. The earliest such study to our knowledge is that of Erb and Hanson (Erb and Hanson 1960) who used a high speed camera to observe fibril formation from the side on a series of liquids and speculated that these fibrils were initiated by cavities. Cavitation itself was studied also in rubbers with poker-chip tests (Gent and Lindley 1959, Gent and Tompkins 1969), in simple liquids (Briggs 1950, 1951) and in viscoelastic liquids (Kaelble 1971), but experimental evidence was indirect or post-mortem. The first direct evidence of the nucleation and growth of cavities *during* debonding of a soft adhesive from a probe was carried out by Lakrout *et al* (1999) with a camera positioned under a transparent glass substrate and the debonding scenario that they proposed shown in figure 12, remains a good microscopic description of the debonding mechanism.

The first stage is the contact formation where the soft material makes an intimate contact with the surface. If that surface is rough, the extent of real contact and the air pockets remaining trapped at the interface depend on the interplay between the viscoelastic properties of the PSA, the strength of adhesive interactions at the interface and the topography of the surface (Creton and Leibler 1996, Fuller and Tabor 1975, Hui *et al* 2000, Persson *et al* 2004). After the contact has been established, the probe is normally maintained in contact

for a set dwell time, and subsequently removed at a constant velocity. During this stage the force first returns to zero and then becomes tensile as shown schematically on figure 5. The initial deformation of the layer is homogeneous, but around the peak stress, the video camera reveals the nucleation and growth of cavities, which grow first relatively parallel to the interface and then can grow normal to the interface and form the fibrillar structure previously observed from the side. The details of such a scenario depend strongly on the material properties of the adhesive and on the surface chemistry and topography.

It is now the purpose of the next sections to discuss the details of the bonding and debonding mechanisms. It should be noted here that the peel test is an inherently steady state test where a well defined crack front propagates involving an apparent fracture energy $\Gamma_{\text{app}}(\text{v})$, while probe tests are transient tests that separate the microscopic details of the contact formation from the debonding as a function of time (or position of the probe) while providing the measurement of a total work of debonding per unit area W_{deb}. It is therefore logical to begin with a description of the general common features involved in the bond formation. We then turn to the most interesting and complex physics occurring during debonding, where we will first address the experimentally simpler peel test that describes the more common way of debonding and then move on to the probe test for a more detailed investigation of the microscopic mechanisms of debonding.

5.1. Bond formation: spontaneous contact on rough surfaces

A crucial requirement for a PSA to stick to a surface is to form at least van der Waals bonds with the largest proportion of the macroscopic surface as possible. This process of contact formation is often described in the trade literature as 'wetting the surface'. However, most soft adhesives cannot flow and are best seen and described as soft viscoelastic solids.

Therefore it is best to start with elastic solids and to subsequently introduce viscoelasticity. For an elastic solid, the minimum criterion for the formation of an intimate contact on a rough surface is that the elastic strain energy stored in the adhesive per unit area of contact should not exceed the Dupré work of adhesion w, i.e. the energy gain in forming an interface. This simple idea can be seen already qualitatively by examining the contact of radius a between a single hemispherical rigid asperity of radius R and a soft planar surface of modulus E. The excess free energy of the contact of a single asperity is given by:

$$\Delta F_{\text{exc}} \sim -wR\delta + E\left(\frac{\delta}{a}\right)^2 a^3 \tag{22}$$

where δ/a is the elastic deformation that takes place over a volume of the order a^3, and δ is the indentation. If one uses the approximate geometric relation $a \sim \sqrt{R\delta}$ and minimizes ΔF_{exc} with respect to δ, one obtains an expression between the modulus of the material and the indentation depth δ for an asperity of radius R in order to maintain an equilibrium contact area or radius a in the absence of any applied force other than van der Waals interactions at the interface.

$$E^*\,(P=0) \sim w\left(\frac{R^{\frac{1}{2}}}{\delta^{\frac{3}{2}}}\right) \tag{23}$$

For a single asperity, the steeper the asperity (small R, large δ) the softer must the material be to create the same surface of contact a. For a fully indented asperity of 2 μm in height and a radius of 100 μm, and a work of adhesion $w = 50$ mJ m^{-2}, one finds a value of $E^* = 0.2$ MPa, which is very close to what is the practical limit for good contact.

Of course real surfaces are rough and have a random distribution of asperities. Two modeling strategies have been mainly used for random surfaces: a strategy modeling a population of uncorrelated asperities with identical radii, but a distribution of heights (Greenwood and Williamson 1966, Fuller and Tabor 1975, Creton and Leibler 1996, Hui *et al* 2000) and a second strategy where the roughness is described by a power spectrum, which emphasizes wavelength and correlation between asperities more than height of individual asperities (Persson and Tosatti 2001, Persson 2002, Persson *et al* 2004). The first strategy works well for a low level of contact, in other words when only the tip of the asperities come into contact. The second strategy typically calculates, as a function of wavelength, the strain energy necessary to force the contact of the soft material on a rigid rough surface. By comparing the strain energy per unit area of contact, to the work of adhesion this second approach determines the range of wavelengths where contact is energetically favorable, and from the power spectrum of the surface, it determines the fractional area in contact. This results in a wavelength dependent adhesion, because very small wavelength roughness entails significant deformation costs and will lose contact for lower elastic moduli than the long wavelength roughness.

Both types of models predict qualitatively the increase in true contact area with decreasing elastic modulus and decreasing roughness amplitude or aspect ratio. However, quantitative comparisons with experimental data are rare (Lorenz and Persson 2009, Lorenz *et al* 2013) because random rough surfaces are difficult to obtain and to characterize. Moreover extracting a truly relevant parameter from a random distribution of asperities is not straightforward despite recent progress in particular with simulations. (Pastewka and Robbins 2014).

The key physical aspect in these models is the notion that the interfacial area that is truly in molecular contact is generally incomplete. The elastic energy stored in the adhesive near the interface during the contact formation is a driving force to *spontaneously* detach the adhesive from the surface even without any macroscopic tensile force (Greenwood and Williamson 1966, Fuller and Tabor 1975, Persson *et al* 2002). In the absence of viscoelastic dissipation the contact is fully reversible and the applied pressure during the compression stage does not influence the detachment process (i.e. the tensile part of the curve). This prediction can only hold for very weakly adhesive rubbers and is counterintuitive to any person who has used soft adhesives. Yet it is the basis of equation (23) that predicts the existence a threshold modulus at long times

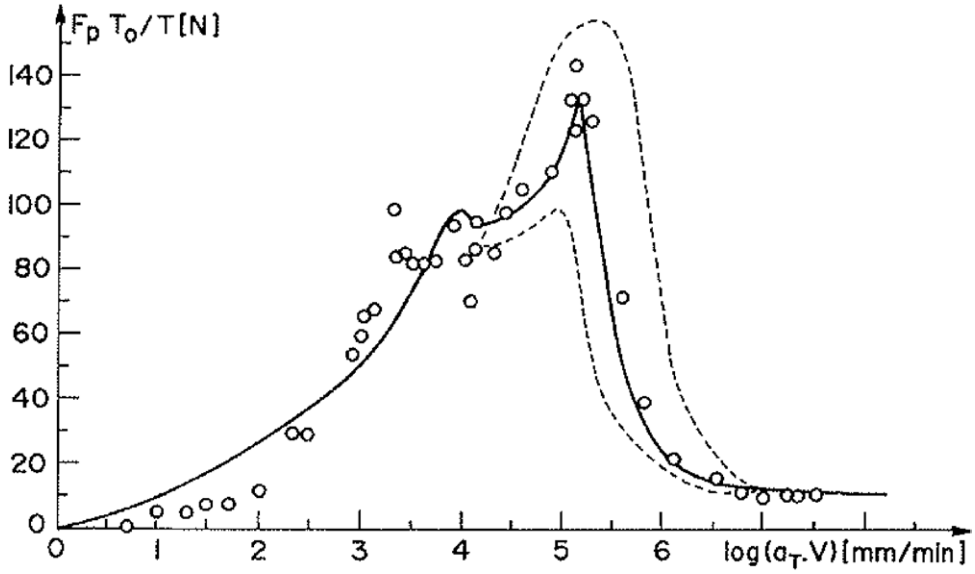

Figure 13. Peel force as a function of peel rate for a typical uncrosslinked viscoelastic polymer. Reproduced with permission from Derail *et al* (1998; copyright 1998 Taylor & Francis).

E^* above which the soft material will not spontaneously adhere to the surface under zero applied load.

While the picture presented above is true for elastic materials, pressure-sensitive adhesives are highly viscoelastic. This introduces two important differences: (1) the whole history of contact formation matters for debonding, so that the energy dissipated during debonding depends on the applied contact pressure and the contact time. This is well addressed in single asperity contacts (Lin *et al* 1999, Barthel and Haiat 2002, Haiat *et al* 2002), but is usually ignored in multi asperity contact theories (Maugis 1996, Hui *et al* 2000).

Technologists use an empirical criterion called the Dahlquist's criterion (Dahlquist 1969), which specifies a maximum value of 0.1 MPa for the storage modulus μ' at 1 Hz and hence assumes that most of the contact formation occurs over a typical time of the order of 1s. If after a one second contact and removal of the compressive force the leftover elastic stored energy per unit area near the interface exceeds the work of adhesion w, the contact will spontaneously break even under zero applied force.

5.2. *Macroscopic analysis of the steady state debonding by the peeling test*

The peel tests constitute the easiest method to test a soft adhesive, yet the interpretation of the measured peeling energy as a function of the mechanical properties of the adhesive itself remains challenging. Due to the very soft nature of the adhesive films, it is generally bonded to a flexible but weakly extensible backing and the two are peeled together from a rigid flat substrate at an angle θ as shown in figure 4. For non-vanishing peeling angles, the strain energy release rate $\mathcal{G}$ can be easily evaluated from the measured peel force by equation (8) and under steady-state propagation $\mathcal{G}$ corresponds to an apparent fracture energy $\Gamma_{\rm app}(v)$ as in figure 13. $\Gamma_{\rm app}(v)$ typically increases with velocity up to a peak that is followed by stick-slip dynamics (Barquins and Maugis 1988, Ciccotti *et al* 2004, Villey *et al* 2015) and which is out of the scope of the present review. If we limit ourselves to the steady-state propagation (slow branch with positive slope on figure 13) the apparent fracture energy $\Gamma_{\rm app}(v)$ is related to the three main ingredients of the adhesive joint: (1) the rheology of the soft adhesive, (2) the intensity of the surface interactions (discussed in section 5.3) and (3) the geometry of the adhesive layer (thickness h) and loading (peeling angle θ).

While the applied strain energy release rate $\mathcal{G}$ (given by equation (8)) is independent of the nature of the adhesive, the measured fracture energy $\Gamma_{\rm app}(v)$ is dominated by the energy dissipated during the deformation of the thin adhesive layer during debonding. A quantitative prediction of $\Gamma_{\rm app}(v)$ from the properties of the adhesive requires an adequate knowledge of the strain field in the adhesive during peeling, which turns out to be very complex due to both the elevated confinement of the adhesive and the complex deformation mechanisms that can occur at micrometer scales, such as cavitation and fibrillation (Urahama 1989, Chiche *et al* 2005b, Ito *et al* 2014, Villey *et al* 2015).

The essential point to understand when describing the peeling of a thin adhesive layer is that, due to the extremely soft nature of the adhesive used, the stress singularity at the crack tip cannot be developed within the bulk of the adhesive layer and the extremely blunt crack front can only act as a moderate local stress concentrator to some finite stress value. If we consider for example a typical viscoelastic adhesive layer of modulus E debonded from the substrate with an apparent fracture energy $\Gamma_{\rm app}(v)$, according to equation (5) the typical stress singularity of LEFM given by equation (2) can only set up at scales larger than $\Gamma_{\rm app}(v)/E$. Both the apparent fracture energy $\Gamma_{\rm app}(v)$ and the effective storage modulus E are increasing functions of the crack velocity, and their ratio can

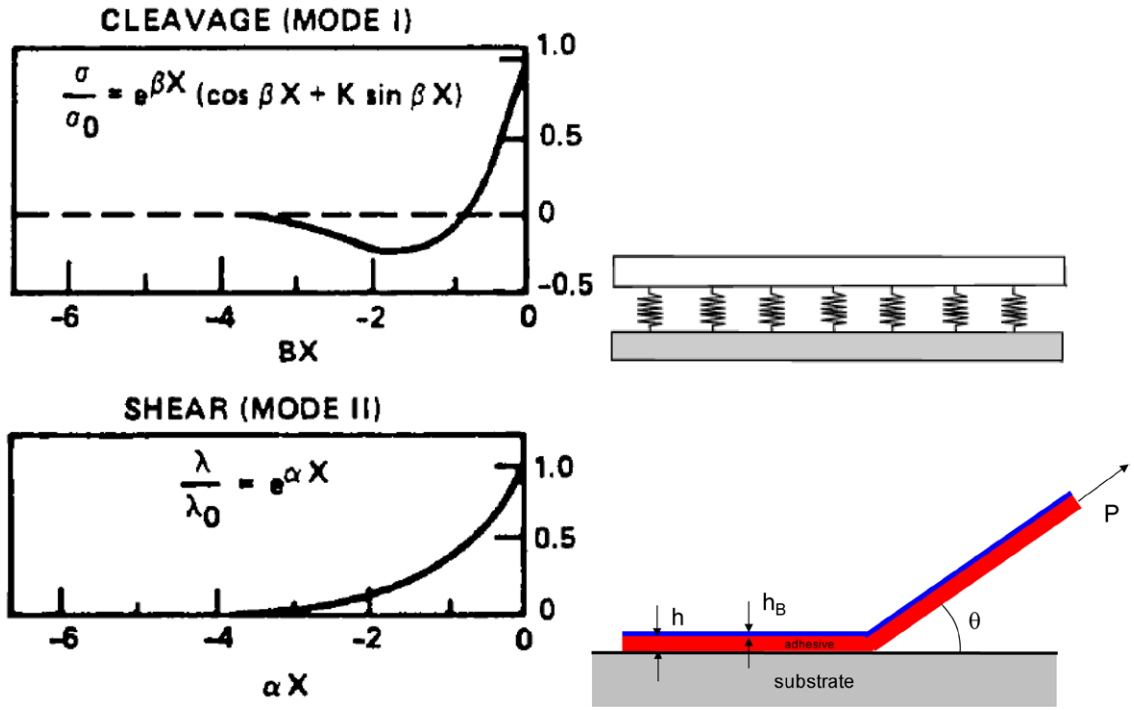

Figure 14. Left: representation of the normal (cleavage) and shear stress distributions in Kaelble's model for the peeling of a flexible elastic backing on an elastic foundation of independent springs. Right: mechanical schemes reproduced with permission from Kaelble (1992; copyright 1992 Taylor & Francis).

be estimated as larger than 1 mm for most steady state peeling conditions, which is larger than the typical thickness of the adhesive layers (Villey *et al* 2015). The stress and strain fields in the peeled adhesive can thus be assumed to be uniform through the thickness of the adhesive and to be a scalar function of the position along the tape, thus constituting a sort of cohesive zone between the backing and the substrate. This treatment assumes the adhesive to act as a series of independent strands, and it is mathematically represented by an elastic or viscoelastic foundation which is the basis of the theories for the peeling of thin adhesive layers that are described in the rest of this section.

The first such theory of peeling of soft adhesives was proposed by a 3M scientist, David H Kaelble (Kaelble 1960, 1964, 1965). The theory only aims at modeling the steady state peeling, where a coherent constant energy balance can be established through the different scales of the problem. The backing is treated as a flexible and extensible elastica, i.e. a thin linear elastic strip of typical Young's modulus E_B ~ GPa and thickness h_B (comparable to the thickness h of the adhesive), submitted to en external force F applied at an angle θ. The stress distribution in the adhesive constitutes all the remaining boundary condition for the solution of the elastic profile of the backing. The effect of confinement on the mechanical response of the adhesive is neglected and its constitutive behavior is considered as linearly viscoelastic, or more precisely as linear elastic with frequency dependent elastic moduli E and $\mu = E/3$ that depend on the peeling velocity through a local time scale t_c defined later. In a first version of the model (Kaelble 1960) cavitation is neglected and the crack front is still treated as a simple triple line (between substrate, adhesive and air). Under these assumptions the following analytical solution can be derived to express the stress distribution in the bonded part of the adhesive as a function of the distance x from the crack front:

$$\tau(x) = \tau_0 \exp(\alpha x)\ \alpha = \left[\frac{\mu}{2E_B h_B h}\right]^{\frac{1}{2}}$$

$$\sigma(x) = \sigma_0(\cos\beta x + K\sin\beta x)\exp(\beta x)\ \beta = \left[\frac{3E}{8E_B h_B^3 h}\right]^{\frac{1}{4}} \quad (24)$$

where K is a dimensionless constant depending on the peeling angle θ. This model can be interpreted as follows. Due to the linearity of the analysis, the shear and normal stress distributions can be treated as independent. Both shear and normal stress distributions present a stress concentration at the crack front and an exponential decay as a function of the distance inside the bond (as in figure 14). The attenuation lengths (or stress concentration lengths) are given respectively by $1/\alpha$ and $1/\beta$, which scale with the adhesive thickness h (close to h_B) and are strongly dependent on the ratio of the elastic moduli of the backing and adhesive. For a typical adhesive thickness of 20 μm the attenuation lengths are of the order of 1 mm for shear stress and 100 μm for normal stress and are independent of the loading condition (F, θ). Moreover, the traction part presents an additional oscillation with a wavelength identical to the attenuation length (i.e. a critically damped oscillation). The two stress distributions are found to depend on the peeling angle θ through the dimensionless constant K (ranging between 0 and 1 for non vanishing angles), which depends on the ratio between shear and normal stress.

The maximum values of the stresses are related to the peel force F through:

$$\tau_0 = \frac{\alpha}{b} F \cos\theta \ \sigma_0 = \frac{2\beta}{b(1-K)} F \sin\theta \tag{25}$$

which simply means that each force component is balanced by a stress concentrated on a length $1/\alpha$ or $1/\beta$ respectively. By imposing a debonding criterion based on a maximum traction stress σ_c for the debonding at the crack front (which is reasonable for non vanishing peeling angles), the apparent fracture energy can be derived as:

$$\Gamma_{\text{app}}(v,\theta) = hK^2 W_c(v) \tag{26}$$

where W_c is the maximum density of stored elastic energy given by σ_c^2/E according to the linear character of the model. Kaelble gave a more complete description of the contribution of shear to the fracture energy, but this can be neglected for most non-vanishing peeling angles and is not discussed here. The most important prediction of equation (26) is that $\Gamma_{\text{app}}(v)$ should be proportional to the thickness h of the adhesive layer and is not explicitly related to the Dupré work of adhesion w, although the intensity of the molecular interactions comes into play through the value of the maximum stress σ_c. Although the linear dependence of $\Gamma_{\text{app}}(v)$ on h is rarely observed experimentally, for practical adhesive layer thicknesses (10–300 μm) $\Gamma_{\text{app}}(v)$ clearly increases with h (Gardon 1963b, Kaelble 1992). This makes it clear that such apparent fracture energy should not be confused with a fundamental fracture property of the interface between the adhesive and the substrate, but it is rather the result of the deformation of the whole adhesive layer. The role of the rheology of the adhesive on $\Gamma_{\text{app}}(v)$ was investigated by Kaelble (Kaelble 1964) and others (Gent and Petrich 1969, Derail *et al* 1997, Derail *et al* 1998, Yarusso 1999) who presented extensive measurements at different peel rates and temperatures. The data of the peeling force as a function of velocity and temperature were shown to be generally collapsed into a single master curve by the same type of time-temperature equivalence used for the linear viscoelastic properties of the bulk polymer. This is strong evidence of the viscoelastic origin of the dissipation in peeling of soft adhesives, yet it does not carry exact information on the nature of the mechanisms of deformation that are involved. Kaelble's model introduces the effect of viscoelasticity by using in equation (24) the real part of the complex viscoelastic modulus associated to the characteristic local loading time t_c that is obtained by dividing the attenuation (oscillation) length of the traction stress function in 24 by the constant peeling velocity v. Since σ_c is assumed to follow the same time-temperature scaling as the elastic moduli, equation (26) justifies that also the peeling force F or the apparent fracture energy Γ_{app} follow the same scaling.

Kaelble (Kaelble 1964) presents extensive data covering a wide range of peeling velocities and temperatures, and also the effect of using eight different substrates. The data are claimed to globally support his model for the link with rheology. However, some critical (and questionable) assumptions have been made in order to fit the data. As discussed before, the critical density of elastic energy W_c in equation (26) is given by σ_c^2/E, according to linear elasticity, but the associated strain σ_c/E is well beyond the regime where linear elasticity holds. Secondly, the estimate of the velocity dependence of σ_c remains unsatisfactory. Kaelble (Kaelble 1964) simply decided to use the well established data from Smith (Smith 1958) on the true stress at break for a crosslinked elastomer as a function of temperature and strain rate. However, this is not the same physical quantity as the maximum stress sustainable at an interface before detachment, and the final experimental validation of the model is thus unsatisfactory.

As a parallel path to validate his model, Kaelble (Kaelble 1960, Kaelble 1964, Kaelble 1969, Kaelble and Ho 1974) developed a custom peeling device based on two Split Beam Transducers (SBT). The device is represented schematically in figure 15 and through clever mechanical design it can measure both the shear and the normal components of the force as a function of the position of the peeling point under steady state propagation. The data can then be used to reconstruct the spatial distribution of shear and normal stresses in the bond as shown in figure 16. The validity of the overall predictions on the shear and normal distributions have been verified on the intact part of the bond (left of the maximum tensile stress). But there is evidence of a significantly more extended region of tensile stress on the right of the peak, instead of the expected abrupt stress drop. Kaelble (Kaelble 1965) correctly attributed this extended debonding region to the occurrence of a region of cavitation and fibrillation. He also investigated the physics and conditions for cavitation in soft viscoelastic media (Kaelble 1971). However, he could not reach a sound modeling of the effective stress applied to the peeled backing by the fully fibrillated region, and he could not integrate this important element into his elaborate model for the cohesive zone and for the link with rheology. He chose instead to apply his model to the uncavitated bonded region on the left of the stress peak. While the modeling seems consistent with experiments, much of the physical interpretation becomes less clear. However, the very important picture that he proposed in (Kaelble 1965) of the debonding mechanisms (see figure 16) provides the first qualitative sound explanation of the link between the fibrillated region and the stress distribution in the bond region and of the non trivial effect of changing the peel angle on the debonding energy as demonstrated recently (Villey *et al* 2015). The shape of the tensile stress profile in the cohesive region is strongly reminiscent of the traction curves of the probe tests that were extensively studied in the 80's, 90's and 2000 (Zosel 1985, 1989, Shull and Creton 2004) (see figure 16) in order to better understand the details of the debonding mechanisms of cavitation and fibrillation and will be presented in detail in section 5.3.

A very interesting complementary investigation was presented by Gent and Petrich (Gent and Petrich 1969) who tested a set of model adhesives, mostly uncrosslinked, designed to catch the importance of the non linear behavior

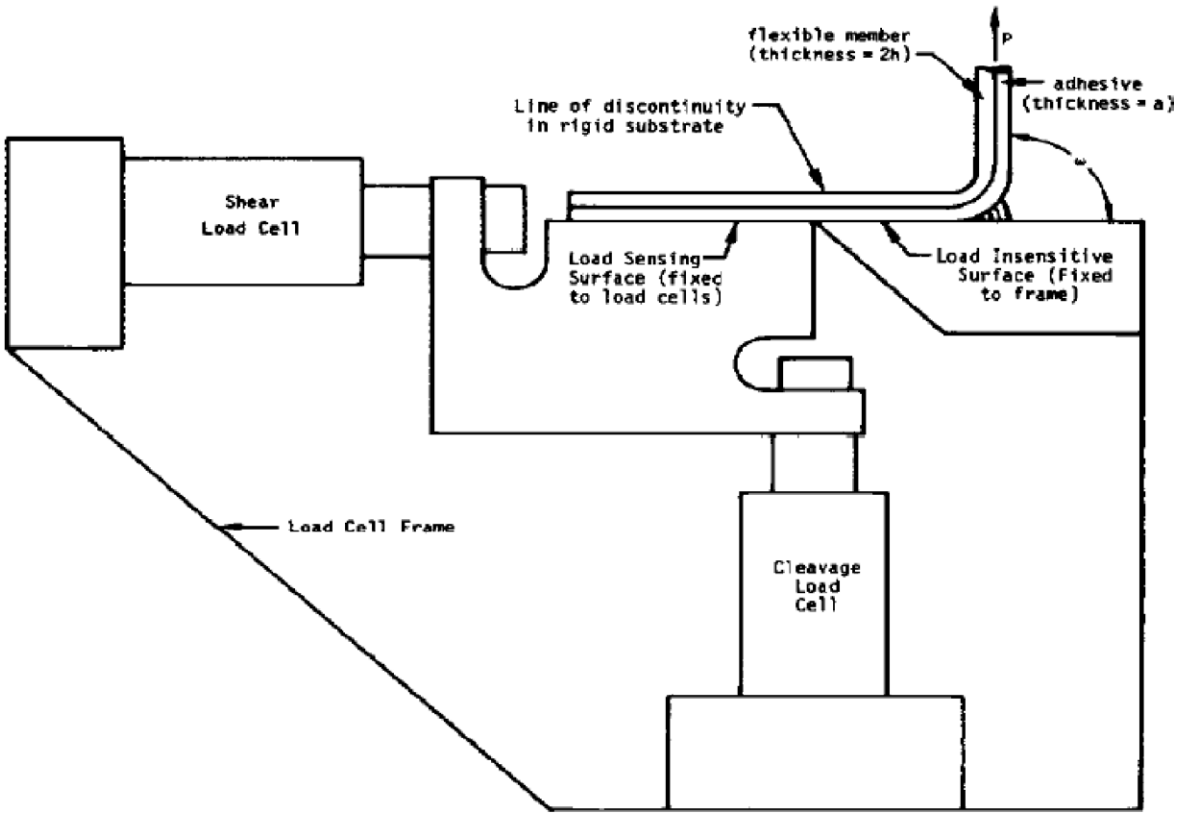

Figure 15. Schematic of the peeling device reproduced with permission from Kaelble and Ho (1974: copyright 1974 AIP Publishing) where the left half of the substrate beam is connected with two shear and traction load cells.

of the adhesive under large stretch. The experiment consists in a T peel test (see figure 4) carried out at different peel rates and temperatures. The peeling force data $F(v)$ were then reduced into master curves, which are in good agreement with the WLF time-temperature equivalence. The link between peel mechanics and rheology of the adhesive is made by using a simplified model based on similar assumptions as Kaelble's model. However, the bond stress distribution was completely neglected and only the deformation of individual fibrils up to debonding was considered. The adherence energy $\Gamma_{\text{app}}\ (v)$ was thus estimated as the work of debonding at a constant strain rate related to the peeling velocity by: $\dot{\varepsilon} = v/a$ in an analog way to equation (26) from Kaelble:

$$\Gamma_{\text{app}}(v) = \frac{F(v)}{b} = h\int_0^{\sigma_c} \sigma(\epsilon)\mathrm{d}\epsilon \qquad (27)$$

where σ_c is again the maximum stress attained in each strand and b is the strip width. However, σ_c was assumed to be limited by two possible failure criteria: cohesive rupture of the adhesive when the tensile strength of the polymer is attained first, or detachment from the substrate when the maximum tensile stress that the interface can withstand is reached first.

The $F(v)$ curves are similar to those of figure 13, but they present two major peaks. The peak at lower velocity was attributed to the transition from cohesive to adhesive debonding, since the transition strain rate was in agreement with the terminal relaxation time (reptation time) of the polymer, which marks the onset of viscous flow. Additionally this peak was shown to disappear upon crosslinking the adhesives and suppressing therefore the possibility of viscous flow and cohesive debonding. The second peak at higher velocity was associated to a combined effect of the glass transition and of the specific T-peel test geometry, on the mechanisms of adhesive debonding. Unlike Kaelble, Gent ant Petrich assumed a constant value of the maximum tensile stress σ_c (which is the only adjustable parameter of the theory), but they took into account the influence of large strain non-linear rheology of the adhesive in uniaxial extension (Gent and Petrich 1969). They pointed out that two adhesives with very similar linear viscoelastic properties, can result in different peeling curves $\Gamma_{\text{app}}(v)$ when they differ significantly in their large strain behavior. This prediction was recently demonstrated by (Villey *et al* 2015). Moreover, the increase of the strength of the interfacial interactions results in a comparatively stronger effect of the differences in non linear properties on the peel force as shown in figure 17.

Another important contribution to the modeling of the peel curve $F(v)$ was proposed by Derail *et al* in a series of papers focusing on peeling of uncrosslinked polybutadiene model polymers (Derail *et al* 1997, 1998) and of several kinds of hot melts PSA adhesives (Gibert *et al* 1999, 2003, Derail *et al* 2004, Marin and Derail 2006). Similarly to the previously cited models, the prediction of the peel force was obtained by combining the analysis of the bending of the

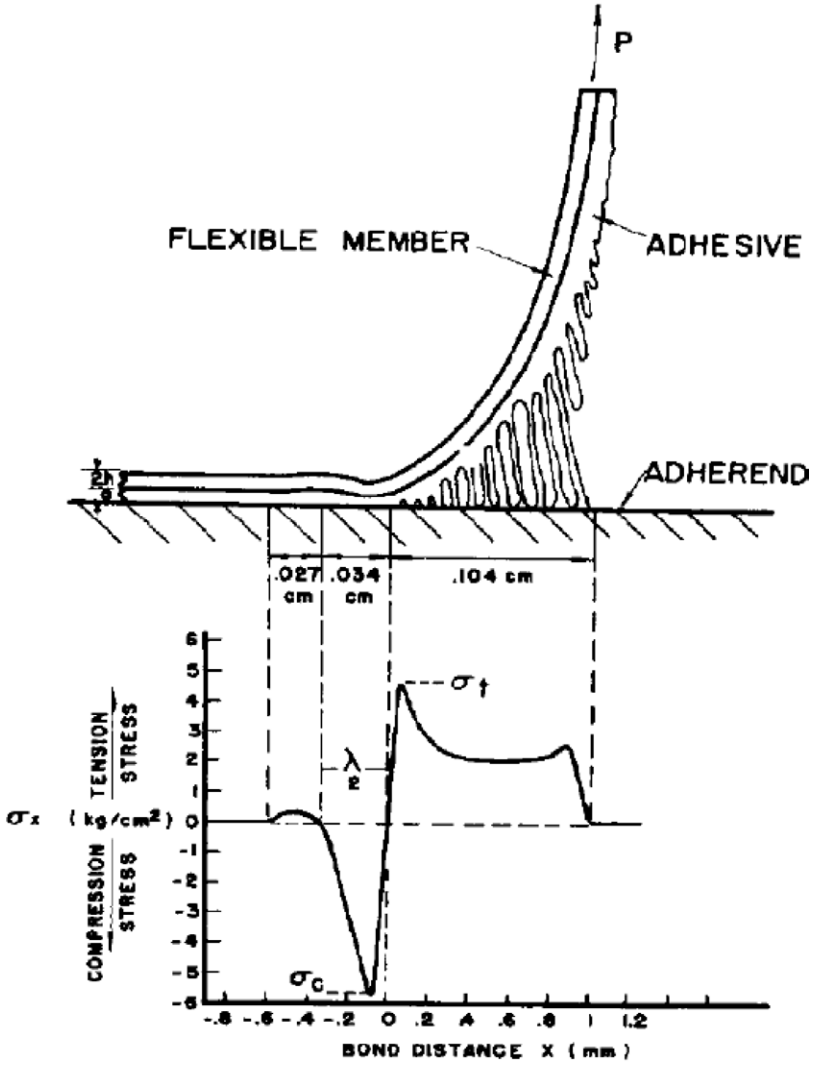

Figure 16. Schematic of the debonding mechanism of a soft adhesive from a rigid surface in a probe tack test along with the measured traction stress profile (reproduced with permission from Kaelble (1965; copyright 2015 AIP Publishing)).

elastic backing (with some complications from plasticity here) with the modeling of the cohesive force applied from the soft viscoelastic adhesive. For the sake of simplicity the flexural profile of the backing was considered as a circular region connected to two straight regions (bonded and unbonded). The cohesive stress of the adhesive was treated again as the uniaxial extension of independent strands. While the confinement effects were neglected, the large strain extension was modeled with a viscoelastic fluid model using parameters extracted from linear rheology and adhesive composition. The peeling curves were reduced to a general master curve using a time-temperature equivalence for a given adhesive and a Deborah number defined as the experimental time divided by the terminal relaxation time of the polymer measured in linear rheology. The same scaling was applied to all peeling regimes (cohesive, slow interfacial, stick-slip, fast interfacial).

The critical point of the analysis is the choice of the criterion for propagation. In the cohesive regime (Derail *et al* 1997) a critical stretch $\lambda_c = 4.5$ was reasonably chosen as a fracture criterion, in agreement with experimental measurements of the fracture strain of the same adhesives under variable uniaxial strain rates. In the adhesive regime, a much more questionable fracture criterion was chosen. Derail *et al* proposed that the fibrils detach when the total work done on the fibril attains a critical value $\sigma_c(\lambda_c - 1)\, h_0 = \text{cst}$, where λ_c is the stretch in the fibril at the debonding point. This fracture criterion is however poorly justified theoretically and the important parameters are not accessible experimentally. Nevertheless, this set of articles provides very interesting measurements on the relation between the structure of the adhesive and their peeling properties. The data set can also be completed by the work of Gower and Shanks on several families of acrylic based PSA adhesives (Gower 2004a, 2004b, 2005, 2006) and by that of Benyahia *et al* on soft block copolymer adhesives for medical applications (Benyahia *et al* 1997, Verdier *et al* 1998). We remark that while the link with rheology in Kaelble's model is related to the loading rate of the zone of stress concentration in the bonded adhesive, this zone is absent in the model of Derail, where the only dynamic length is the radius of curvature of the bent part of the backing and the dissipation seems more related to the finite extension of the adhesive in a

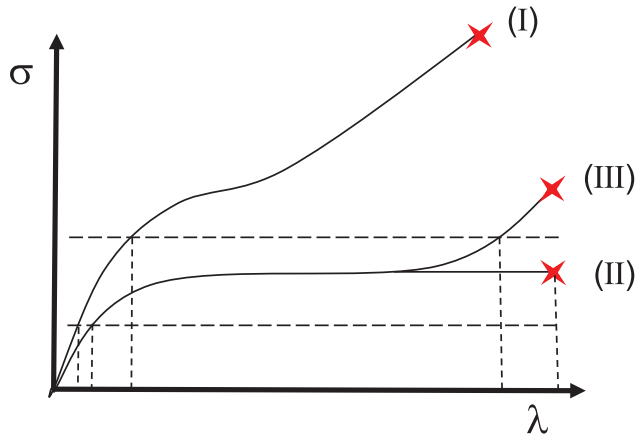

Figure 17. Schematic stress–strain relations for rubbery (I), liquid-like (II) and strain hardening (III) materials. The horizontal dashed lines denote possible levels of the maximum interfacial bond stress σ_c. The vertical dotted lines denote the limiting extensions attainable in each case. Inspired by the original scheme in Gent and Petrich (1969).

cohesive zone (associated to a fibrillated zone) where stretch can be significant.

In the late 1990s, the peeling investigation at 3M was taken over by another scientist, Dave Yarusso, who published an interesting investigation in 1999 concerning the modeling of the 180° peeling of natural rubber based PSA (Yarusso 1999). The deformation of the adhesive was still modeled as the uniaxial extension of individual independent strands. The constitutive law of the adhesive was taken as a linear viscoelastic fluid (the generalized Maxwell model), the parameters of which were fitted on linear rheological measurements. The measured peeling master curves were shown to be consistent with a different fracture criterion based on a critical value of the stored elastic energy (it is indeed a criterion for the failure of each individual strand), but it should be reminded that Yarusso's investigation was limited to uncrosslinked adhesives that can flow and that estimating the stored elastic energy at large strains in soft viscoelastic solids is more complex.

We remark, to conclude, that all the presented descriptions of the peeling of thin soft adhesive layers share the representation of the adhesive deformation as that of a parallel array of independent strands. This description is of course reminiscent of the fibrillar structure often observed in the cohesive zone close to the crack front (Urahama 1989, Verdier *et al* 1998, Chiche *et al* 2005b, Ito *et al* 2014, Villey *et al* 2015). However, the complexity of the local inhomogeneous deformation in the peel test has always hampered the quantitative investigation of these microscale mechanisms, which could only be approached by the probe test investigations described in the following section.

5.3. Microscopic analysis of the debonding mechanisms by the probe tack test

5.3.1. Transition from interfacial debonding to bulk deformation. As discussed in section 5.1, the contact against an imperfect surface (as most surfaces are) leaves small pockets

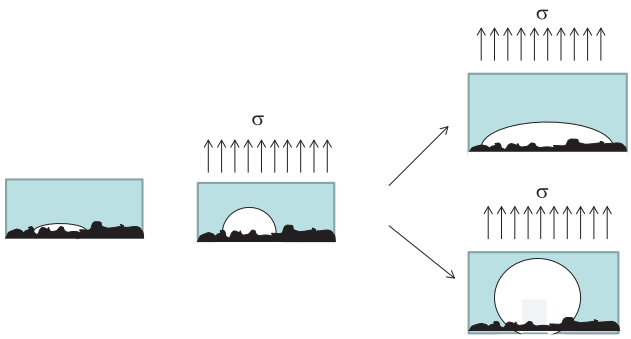

Figure 18. Schematic of early stage of debonding. Cavities grow from defects to hemispheres locally and the macroscopic stress field becomes much flatter promoting the nucleation of cavities randomly distributed along the surface.

of air in valleys that are not in contact. These pockets can be the seed of a localized deformation when a tensile stress is applied to the adhesive layer, leading to either the propagation of interfacial cracks or to the growth of cavities in the bulk that eventually lead to a complex fibrillar structure. This key result was demonstrated experimentally (Lakrout 1998, Zosel 1998, Lakrout *et al* 1999) and described theoretically (Gay and Leibler 1999, Chikina and Gay 2000, Gay 2002) in the late 1990s.

Probe tests, and in particular those carried out with flat-ended probes and visualization tools, provide information on the transient stages of debonding under a more homogeneous and controlled loading, while providing the full stress versus strain curve characteristic of the debonding mechanism and will be addressed here in detail (Shull and Creton 2004). As the probe is lifted from the surface, the average nominal stress σ_N increases. If the material is incompressible, the tensile stress on a highly confined layer ($a \gg h_0$, where a is the radius of the contact area and h_0 is the layer thickness) has a parabolic profile and the maximum tensile stress occurs under the center of the probe (Gent 1994, Ganghoffer and Gent 1995, Creton and Lakrout 2000). Above a certain critical value of local stress, the air pockets trapped at the interface between the surface and the adhesive expand in volume and become optically visible. This expansion process in a soft elastic material has been studied theoretically both at the level of the individual cavity (Williams and Schapery 1965, Gent and Wang 1991, Dollhofer *et al* 2004, Lin and Hui 2004) and at the more collective level of the whole probe (Chikina and Gay 2000, Yamaguchi and Doi 2006, Yamaguchi *et al* 2006).

The two key mechanisms shown in figure 18 have been identified experimentally as (1) a more interfacial mechanism where cavities grow as cracks, mainly along the interface, and (2) a bulk mechanism where cavities grow mainly grow in the direction parallel to the tensile direction, and form cigars (Creton *et al* 2001, Deplace *et al* 2009b).

We use here the beautiful experiments of Yamaguchi *et al* (2007) to illustrate this difference. Yamaguchi *et al* used an instrumented probe tester with an optical prism, to image the shape of the cavities, not in projection as it is usually done, but from a 45° angle which provides a 3D viewing.

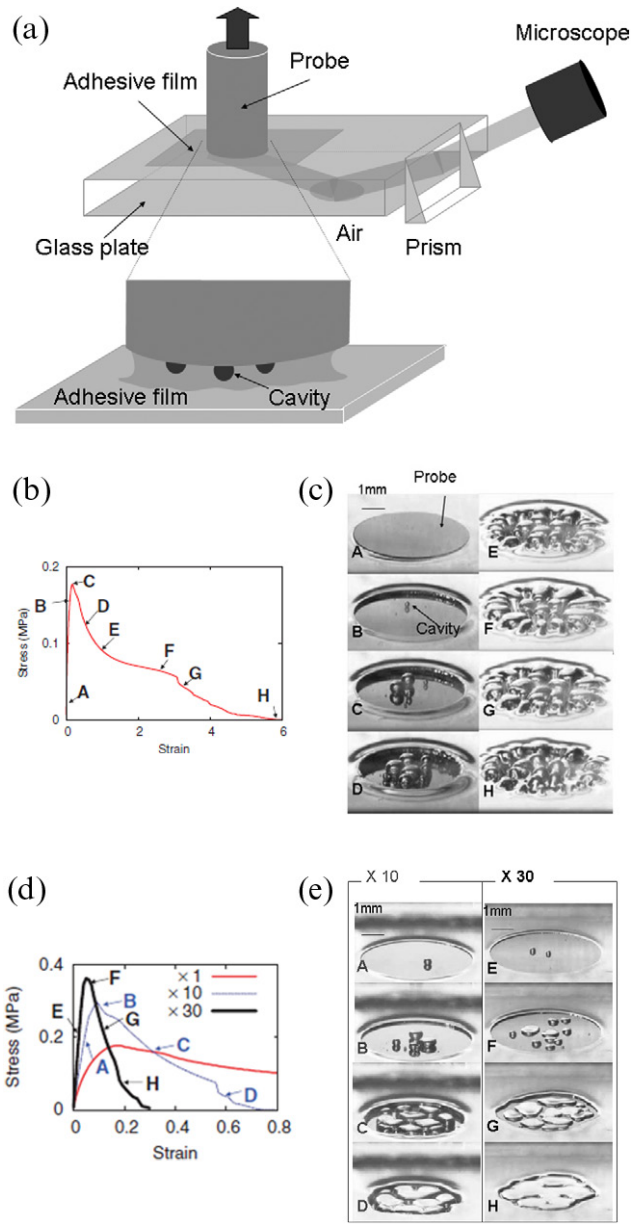

Figure 19. (a) Setup used by Yamaguchi *et al* to observe cavities at a 45° angle. (b) Stress–strain curve of the less crosslinked adhesive and (c) sequential images (A–H) corresponding to the position on this stress–strain curve. (d) Stress–strain curves of all three adhesives. X10 and X30 correspond to ten and thirty times more crosslinker. (e) snapshots of the cavities corresponding to positions on the blue (x10, images A–D)) and red (x30,images E–H) curves. Reprinted with permission from Yamaguchi *et al* (2007; copyright IOP Publishing).

They compared the debonding mechanisms of three differently crosslinked acrylic PSA. As shown in figure 19, the less crosslinked adhesive forms nearly spherical cavities and the initial triple line where the cavity nucleated is actually pinned to the interface. On the other hand, the more crosslinked adhesive forms disk-like cracks that do not grow significantly in the bulk and eventually coalesce at a relatively low level of deformation. Such difference in mechanism can also be obtained by changing the surface chemistry of the interface while keeping the same identical bulk adhesive (Creton *et al* 2001, Schach *et al* 2007).

The transition between bulk growth and interfacial growth of defects is important since this early bifurcation in mechanism leads to vastly different levels of dissipated energy during debonding. If the cavities grow in the bulk, the walls between cavities stretch in the tensile direction, eventually forming bridging fibrils when the walls break and, as shown in figure 19, do not coalesce. On the other hand, the interfacial propagation mechanism leads to the coalescence of the individual cracks nucleated on different defects at the interface, with little deformation of the bulk adhesive.

The transition between interfacial and bulk mechanism can actually be predicted quite well from linear arguments and a detailed derivation was first proposed by Crosby *et al* (2000) for elastic materials and extended by Deplace *et al* (2009b) and Nase *et al* (2008) for viscoelastic adhesives.

Following Hui, Shull and coworkers (Lin and Hui 2004, Shull and Creton 2004) it is useful to analyze the growth of a single defect as shown on figure 20. If we consider the response of an initial penny-shaped interfacial crack ($h_c/R_d \ll 1$) to an increasing hydrostatic tension p representative of the stress state near the center of a very confined layer. For $p/E \ll 1$, we recover the crack driving force from standard linear elasticity theory (Lawn 1993):

$$\mathcal{G} = \frac{3R_dE}{2\pi}\left(\frac{p}{E}\right)^2 \tag{28}$$

As p/E increases, several things happen. The crack begins to inflate in the vertical direction, and the value of h_c in figure 20 increases. The energy release rate also increases in agreement with equation (28), which remains valid for values of p/E less than about 0.4(Lin and Hui 2004).

However, linear elasticity is not valid to describe the deformation of an adhesive at large strains and yet understanding the effect of such complexity on the mechanism is essential. The easiest approximation to our problem of expansion of a crack at the interface is the related (but much simpler) problem of the expansion of a cavity in the bulk of a rubber. If we assume an initial spherical cavity of radius R_0 expanding in a neo-Hookean material of Young's modulus E and use finite strain mechanics, the relation between the applied pressure and the radial stretch is given by (Green and Zerna 1954, Gent and Lindley 1959):

$$p = \frac{1}{6}E\left(5 - \frac{4}{\lambda} - \frac{1}{\lambda^4}\right) \tag{29}$$

It is immediately apparent that this equation does not have a solution for $p > 5/6\ E$. When the hydrostatic traction p approaches the elastic modulus of the material, the cavity should expand indefinitely. This surprising result is analogous to the well-known rubber balloon inflation instability and it is due to the combination of the non linear behavior of the material and the spherical geometry. In real experiments of cavitation in the bulk, the hydrostatic traction applied around the cavity relaxes as the cavity expands (Chikina and Gay 2000, Dollhofer *et al* 2004, Chiche *et al* 2005a). Moreover, the material is typically not neo-hookean and may have a limiting value of the stretch λ where it stiffens and eventually fractures (Gent and Wang 1991, Lin and Hui 2004), so that its bulk fracture

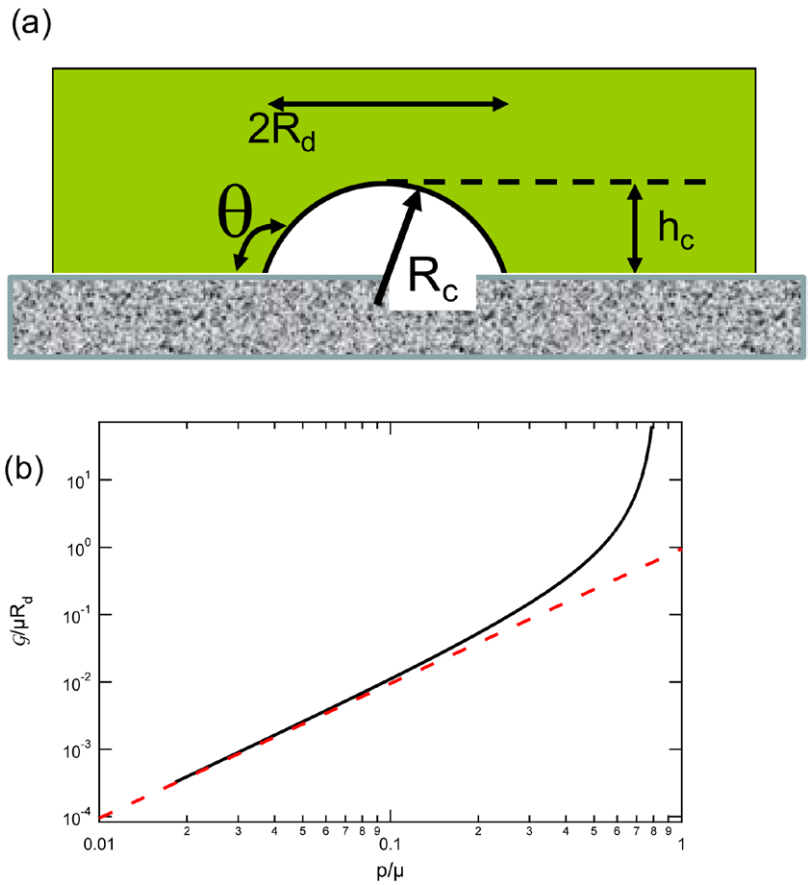

Figure 20. (a) Schematic of a single penny-shaped crack at the interface between a hard surface and the soft material as described in the main text. (b) Normalized energy release rate for a penny-shaped crack growing in the bulk as a function of normalized hydrostatic tensile pressure p. The full line is the prediction for a neo-Hookean material while the dashed line is the linear elastic prediction given by equation (28). Data from Shull and Creton (2004).

energy Γ also matters (Cristiano *et al* 2010) as discussed in more detail section 6.4. For small cavities and/or soft rubbers, such as adhesives, the surface tension of the expanding cavity may also play a role (Dollhofer *et al* 2004, Muralidharan *et al* 2005). Nevertheless, equation (29) predicts a significant expansion of a cavity if the hydrostatic tension exceeds the Young modulus. Experimentally, cavities appear in soft confined materials, at stresses of the order of 3 times the Young's modulus (Lakrout *et al* 1999, Lindner *et al* 2006, Chiche *et al* 2005a), which is not out of line with this simple prediction.

How is this connected to our problem of small crack (R_d, $h_c \ll h$) expansion at the interface? Several scenarios can occur and in the following we have assumed that Γ is a rate independent purely interfacial property (a proper interfacial fracture energy) and that the elastic modulus E is an elastic (rate independent) constant. We also have ignored the details of the large strain properties of the adhesive, limiting the finite strain response to a neo-Hookean behavior.

As discussed above, for $\Gamma/E < R_d$, the initial defects at the interface will propagate following equation (28) as p/E increases, and will eventually coalesce causing the complete detachment of the adhesive from the surface. This regime is commonly encountered when well crosslinked rubbers are debonded from solid surfaces (Nase *et al* 2008, Nase *et al* 2010) or when soft adhesives are debonded from silicone release liners (Josse *et al* 2004). For $R_d < \Gamma/E < h$ the crack will grow first in the bulk but will not propagate along the interface until $p/E \sim 1$. This a direct consequence of the non-linear instability, since, as p approaches 5/6 E, the energy release rate of the interfacial crack $\mathcal{G}$ increases nonlinearly to a much higher value that is determined by the large-strain response of the soft material. The specific value of p/E corresponding to this nonlinear increase depends on the details of the strain energy function that is used to describe the material and can be simulated (Lin and Hui 2004). The example in figure 20 is for a neo-Hookean material. This large increase in $\mathcal{G}$ corresponds to an increase from a value that is below Γ to a value that is above Γ, and the small cracks will grow in an unstable and rapid fashion at the interface and in the bulk until the stress relaxes. This non linear increase in $\mathcal{G}$ leads to a criterion for interfacial cavitation that is coupled to the elastic modulus of the material, and that is insensitive to Γ (Creton *et al* 2001). This situation is typically observed for general purpose PSA (Chiche *et al* 2000, Lindner *et al* 2004). Finally for $\Gamma/E > h$ any cavity at the interface prefers to grow in the bulk and interfacial propagation is excluded. This regime is observed for some high strength PSA (Brown *et al* 2002, Creton *et al* 2009), but it is typically the situation encountered for soft adhesives developing strong chemical bonds (as opposed to Van der Waals bonds) with the surface.

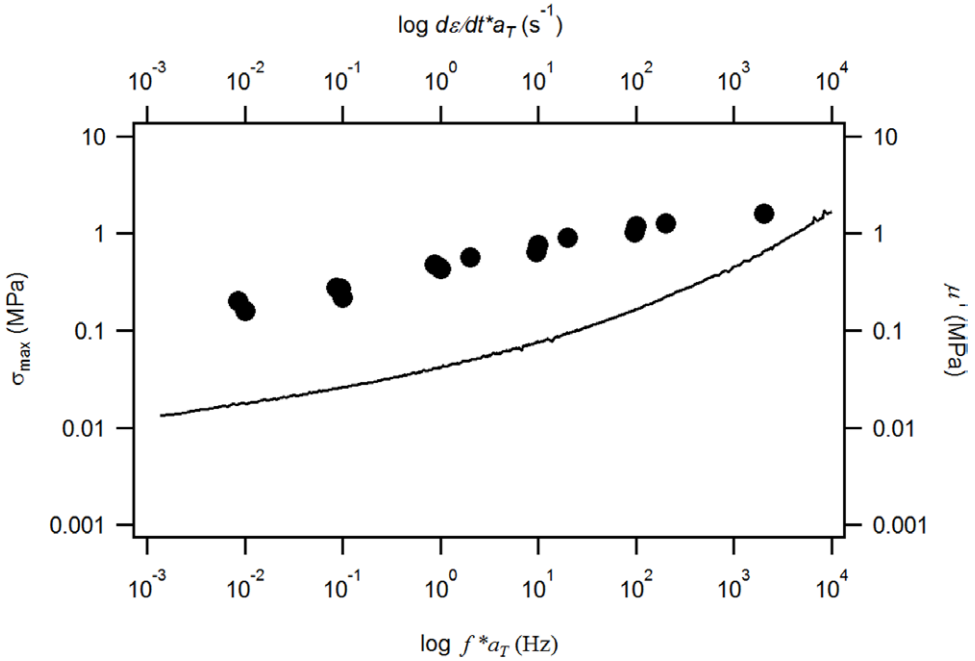

Figure 21. Comparison between the shear storage modulus, μ' as a function of the reduced frequency (fa_T) and maximum stress measured in a probe tack experiment, σ_{max} as a function of $\left(\frac{d\varepsilon}{dt}\right)$ for an acrylic adhesive. The correspondence between fa_T and $d\varepsilon/dt$ was set based on $V_{deb}/h_0 = \omega/2\pi$. The filled symbols represent the actual value of σ_{max}. Data from Lakrout *et al* (1999).

In summary the transition between interfacial and bulk deformation can be approximately predicted by:

$$\frac{\Gamma}{Eh} = 1 \tag{30}$$

i.e. for $\Gamma > Eh$ the initial defects will mainly expand in the bulk of the adhesive layer.

Viscoelasticity will modify in many important ways the behavior of our model soft elastic adhesive. First of all, the fact that the small strain modulus of the material is frequency and temperature dependent, means that the temperature of the test and the probe velocity during debonding will clearly influence the results. In particular, the peak stress measured in a probe test (see figure 5), related to the expansion of cavities, can be plotted as a master curve (using the T-t equivalence) and is markedly dependent on the reduced strain rate (Lakrout *et al* 1999) with a dependency that will typically parallel that of the modulus as shown in figure 21.

Note that this rate dependence of the peak stress in the probe test justifies the rate dependence of the debonding stress used by Kaelble in his model described in section 5.2.

Then the dependence of the interfacial fracture energy Γ on crack velocity (we are speaking now of the microscopic cavity as a penny-shaped crack) and on the linear viscoelastic properties of the soft material $\mu'(\omega)$ and $\mu''(\omega)$, has been extensively studied for nearly elastic rubbers (de Gennes 1996, Baney *et al* 2001, Saulnier *et al* 2004, Barthel and Fretigny 2009). The key idea of these models is that the presence of a crack, even propagating at a constant speed, introduces a singularity at the crack tip where strain amplitudes and strain rates are very inhomogeneous. This spatial heterogeneity in strain rates means that the rate at which energy is dissipated depends on the viscoelastic properties of the adhesive and will vary spatially. For a classical rubbery adhesive, the value of $\mu''(\omega)$ and tan $\delta(\omega)$ increase with decreasing temperature or increasing applied angular frequency ω, leading to a predicted increase of Γ with crack velocity. We stress the fact that all of these models treat the viscoelastic dissipation as a perturbation of the LEFM crack tip stress singularity and thus lead to an intrinsic separability between an interfacial fracture energy $\Gamma(v)$ and the bulk response of the adhesive that can be considered as elastic or viscoelastic in an independent manner. Although quantitative comparisons with experiments suggest that large strain effects cannot be ignored (Gent 1996a, Barthel and Fretigny 2009), we will leave this discussion to the fracture section and assume, as many authors, that the interfacial fracture energy $\Gamma(v)$ can be empirically given by (Maugis and Barquins 1978b):

$$\Gamma(v) = \Gamma_0(1 + \phi(a_T v)) \tag{31}$$

where $\phi(a_T v)$ is a velocity dependent dissipative factor and Γ_0 is the threshold adhesion energy for vanishing crack velocities. If only van der Waals forces are present at the interface, Γ_0 reduces to the thermodynamic Dupré work of adhesion w.

If we now replace E by $3\mu'(\omega)$ and Γ by equation (31) in equation (30), and we assume that we are in the viscoelastic regime, i.e. $\phi(a_T v) >> 1$, we can rewrite the transition condition as:

$$\frac{\Gamma_0 \phi(a_T v)}{3\mu'(\omega) h} = 1 \tag{32}$$

Experimentally, equation (32) can be tested in two different ways. If Γ_0 is fixed, the transition between bulk deformation and interfacial crack propagation is controlled by the

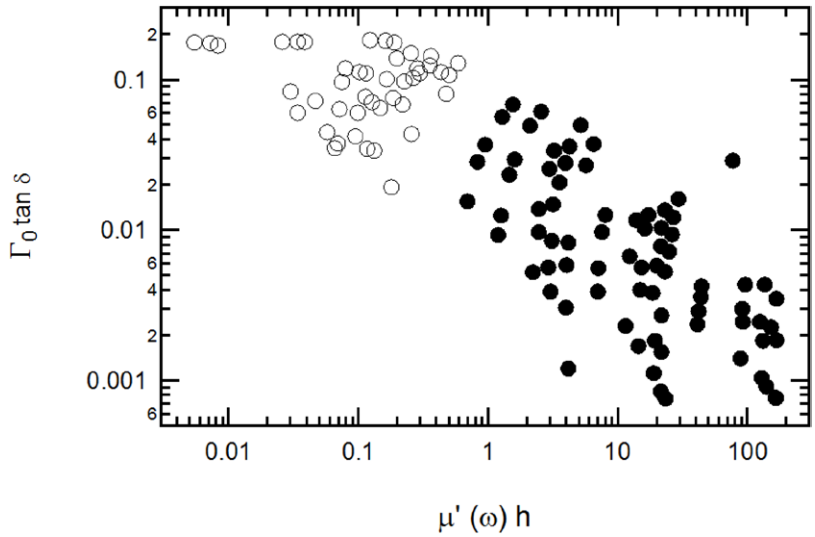

Figure 22. Open symbols represent bulk deformation and black solid symbols interfacial crack propagation. Experiments right at the transition can show both mechanisms due to fluctuations in the sample preparation. Data from Nase *et al* (2008).

viscoelastic properties of the soft adhesive, and if the adhesive is fixed, changing the substrate leads to a change in Γ_0 which in turn affects the transition in mechanism.

It is generally found experimentally (Maugis and Barquins 1978b) that the term $\phi(a_T v)$ has the same frequency dependence as $\tan\delta(\omega)$ so that based on equation (32) if one plots $\Gamma_0 \tan\delta(\omega)$ as a function of $\mu'(\omega)h$ for different materials and substrates, the materials where interfacial debonding mechanisms are observed will appear in different regions of the plot that those who deform in the bulk. This has been tested experimentally for a series of silicone adhesives with different values of $\mu'(\omega)$, h_0 and $\tan\delta(\omega)$. The results are shown in figure 22. It is clear that bulk deformation occurs for low values of $\mu' h_0$ (soft layers) and high values of $\Gamma_0 \tan\delta$ (dissipative layers). The separation between the two regimes is quite abrupt for this system.

5.3.2. Case I: Interfacial crack propagation. Up until this point we have focused the discussion on the energy dissipated by the deformation of the adhesive and not on the nature and strength of the interfacial interactions between the adhesive and the surface that have been bundled into a threshold adhesion energy of Γ_0. For the reversible separation between the two surfaces $\Gamma_0 = w$. Of course for deformable and viscoelastic adhesives this situation is completely hypothetical and separation from the surface always entails significant energy dissipation, both locally near the crack tip and globally in the whole sample. The question is then whether there is a direct relation between w and $\Gamma(v)$. Early papers on adhesion of PSA (Gent and Schultz 1972, Andrews and Kinloch 1973a, 1973b, 1974) argued that the measured $\Gamma(v)$ was directly proportional to an interfacial term without proving that this interfacial term was w. Then systematic experiments studying the adhesion of nearly elastic crosslinked rubbers on glass, supported the validity of equation (31) with $\Gamma_0 = w$ (Maugis and Barquins 1978b). For general polymer interfaces the identification of Γ_0 with w is not correct and Γ_0 can be significantly larger than w due to extraction of interdiffused chains (Raphaël and de Gennes 1992, Brown 1993, Creton *et al* 1994, Léger *et al* 1999, Schach *et al* 2007) or chain extension before fracture due to stronger bonds like covalent (Ahagon and Gent 1975a, 1975b), hydrogen bonding or dipolar interactions (Ahn and Shull 1998a, 1998b).

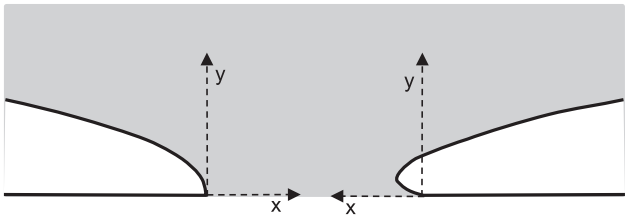

Figure 23. Sketch of the crack front configuration during the interfacial debonding of a soft viscoelastic adhesive and a rigid substrate in the case of low resistance to sliding (left) and high resistance to sliding (right).

Another very important insight came from the elegant experiments of Zhang Newby *et al* (1995) who clearly demonstrated that the influence of the interface on the dissipation $\Gamma(v)$ is not only due to the value of Γ_0 but can be critically affected by the ability of surfaces to slide relative to each other before failure. They prepared three substrates functionalized with fluorinated silanes, hydrogenated silanes and PDMS and peeled the same adhesive from those model surfaces. What they found was that the peel force at an identical peel rate did not scale at all with w (which is a well-defined property here). The mechanism proposed was that in the absence of slippage the deformation field at the crack front is significantly modified as shown in figure 23. This change in crack front shape increases significantly the peel force due to additional shearing in the adhesive layer as demonstrated experimentally (Zhang Newby and Chaudhury 1997, Amouroux *et al* 2001) and theoretically (Krishnan and Hui 2009).

Therefore, a low resistance to friction of the surface is one of the strategies to have a so-called release surface. Such a low resistance to friction can be obtained of course with liquid surfaces, which act as lubricant layers (Lafuma and Quéré

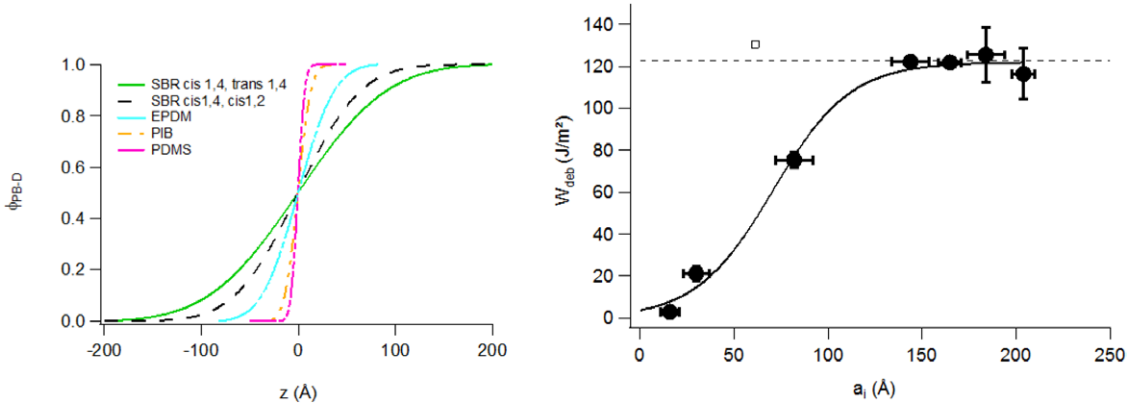

Figure 24. (a) Concentration profile at the interface between deuterated polybutadiene and different polymers. (b) Work of debonding W_{deb} measured by probe tack as a function of interfacial width a_i. Data from Schach *et al* (2007).

2011, Yao *et al* 2013). However, such liquid layers would need reservoirs to maintain the non-sticky character over repeated contacts. A more stable solution from the engineering point of view is to use crosslinked polymers with a very low glass transition temperature and the most commonly used material is silicone rubber (Kinning and Schneider 2002), i.e. PDMS based polymers. However, any other polymer material with a low T_g will also provide a low resistance to friction provided that the adhesive and the surface are strongly immiscible with each other.

While interfacial slippage reduces adhesion, polymer chain interdiffusion across the interface increases the level of interfacial interactions (more van der Waals bonds) or creates topological interactions called entanglements which in both cases increase Γ_0. This correlation between the formation of interfacial entanglements and adhesion has been clearly demonstrated for uncrosslinked high molecular weight polymer melts by Schach *et al* with a series of probe tack experiments coupled with neutron reflectivity measurements of the width of the interface a_i (Schach *et al* 2007). A weak immiscibility (measured by the interaction parameter χ) causes a higher level of chain interpenetration at the interface (Jones and Richards 1999) and increases significantly the value of the work of debonding W_{deb} as shown in figure 24.

Since in this series of experiments, a thick (200 μm) identical layer of polybutadiene, is debonded from thin (100 nm) layers of different polymers, one can infer from these results that the changes in degree of interpenetration at the interface (figure 24(a)) result mainly in changes in Γ_0 which then affect the energy dissipated by the polybutadiene layer during the complex debonding process. Note that the horizontal line in figure 24(b) represents the energy of fracture of the polybutadiene thick layer. As the interfacial width a_i increases from 1 to 15 nm, the failure mechanism changes from interfacial propagation of cracks (figure 23 left) to crack blunting and bulk deformation (figure 23 right) which we will now discuss.

5.3.3. Case II: From bulk deformation to fibril debonding. In some cases bulk deformation becomes dominant over crack front propagation. As shown in figure 12, if the adhesion is significant, the debonding of the soft layer involves the nucleation and growth in the bulk of the adhesive of a large population of initially spherical cavities nucleating and then growing into structures elongated in the tensile direction. An example of this population of cavities for a typical probe tack experiment is shown in figure 25. The cavities appear relatively evenly spaced and of a typical size that is of the order of the thickness of the film (Chikina and Gay 2000, Chiche *et al* 2005a) but depends on the viscoelastic properties of the adhesive (Lakrout *et al* 1999, Peykova *et al* 2012) and on the roughness of the probe (Chiche *et al* 2005a).

The growth of the cavities and in particular the progressive change in shape of the cavities from a sphere to a cylinder with increasing displacement of the probe is a rather complex 3D process where energy is dissipated throughout the adhesive mass. Scaling approaches or simplified approaches have been developed by physicists to describe at least the features of the debonding process in a probe test, where the local loading conditions are better controlled. Gay and coworkers were first to propose a scaling and physically based model of the role of cavitation at the interface (Gay and Leibler 1999, Chikina and Gay 2000) on tackiness. The transition from individual growth of cavities to the collective growth of the foam structure is the most difficult part of the process to model. The rheological properties of the material are complex, the boundary conditions with the adhering surface are not easy to define so that to our knowledge no fully fledged simulations have yet been published reproducing the full complexity of the debonding mechanism of a PSA layer. However, some studies using computational fluid mechanics have simulated the growth of cavities in the bulk of the viscoelastic layer (no interface) and provide some insight on the important role played by elasticity in the deformed adhesive (Yamaguchi and Doi 2006, Papaioannou *et al* 2014).

From an experimental point of view, a recent study (Tanguy *et al* 2014) focused on the measurement of the true tensile stress experienced by the material in the walls between cavities by monitoring, in real time, the projected area of the cavities and of the walls as a function of average layer stretch $\lambda = h/h_0$, and showed that three typical situations can arise as shown in figure 26. If the material is very elastic (Bg1110), the average stress on ligaments between cavities keeps increasing with minor bulk deformation (figure 26(c)). This builds up stress concentration at the edge of the cavities,

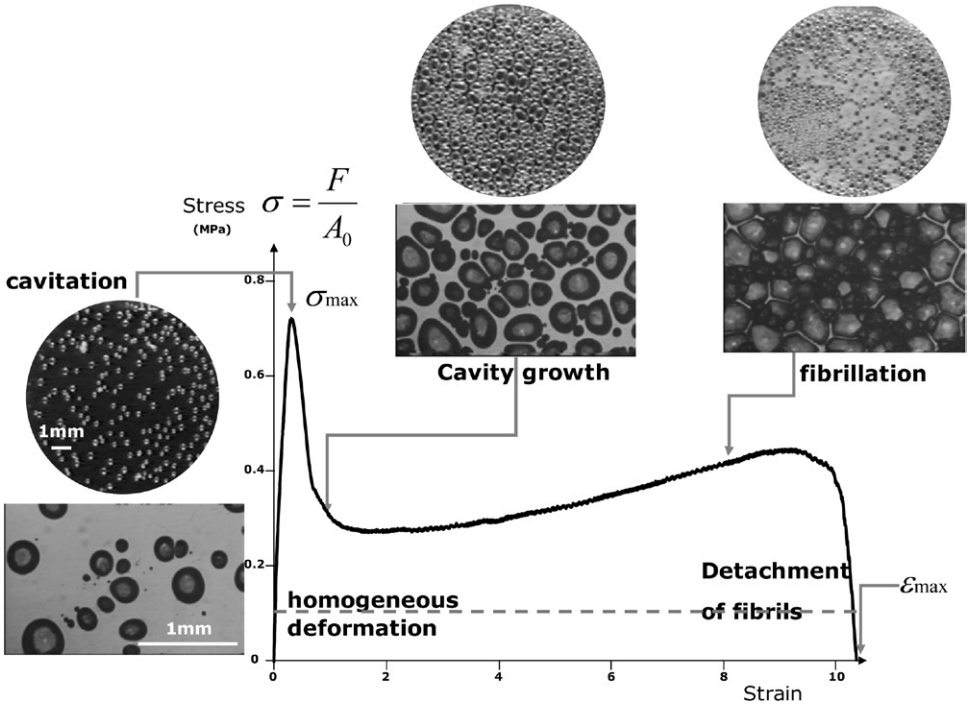

Figure 25. Images of the debonding process in a probe test. The arrows correspond to the point where each picture was taken.

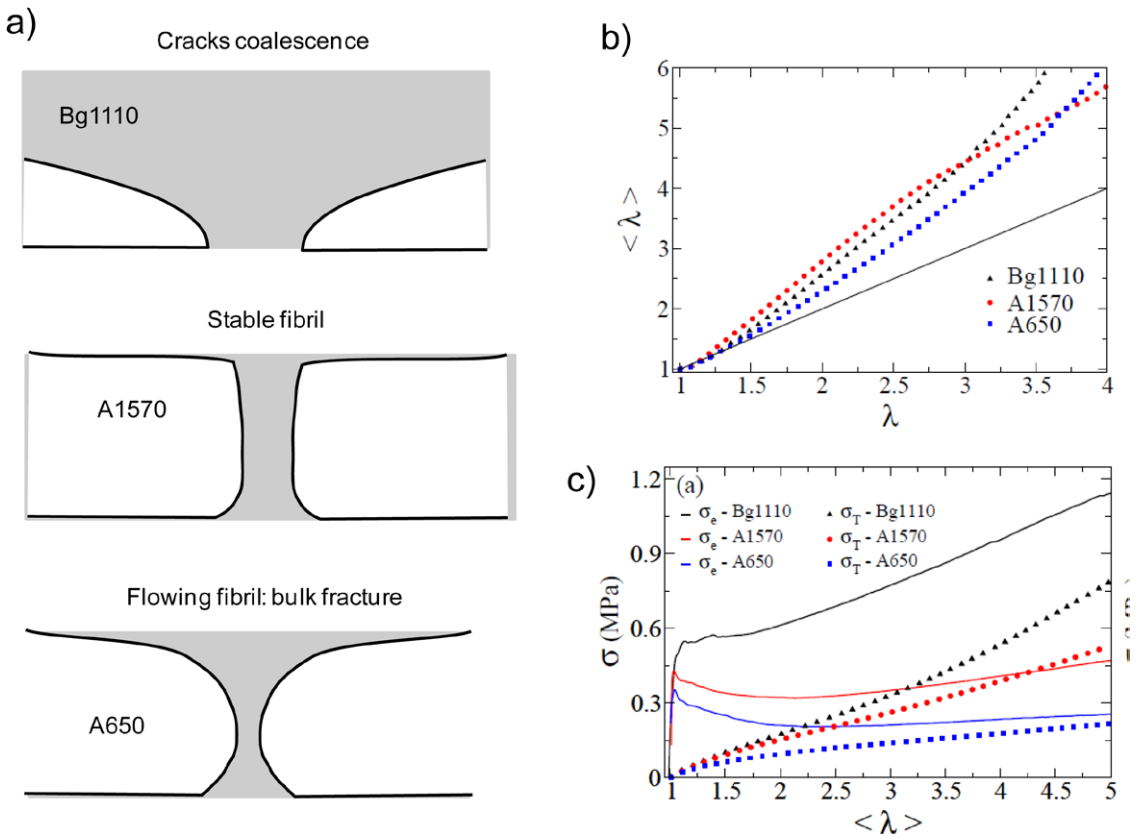

Figure 26. (a) Schematic of the three limiting cases of bulk deformation during debonding. (b) Average stretch in the region between cavities as a function of nominal stretch of the adhesive layer in the tensile direction. (c) Lines represent the average stress in the region between cavities and markers show the tensile stress–strain curve of the adhesive material at comparable strain rates. Bg 1 1 1 0 is the more elastic material, A1570 the optimized one and A650 the more fluid one. Reproduced with permission from Tanguy *et al* (2014; copyright 2014 Elsevier).

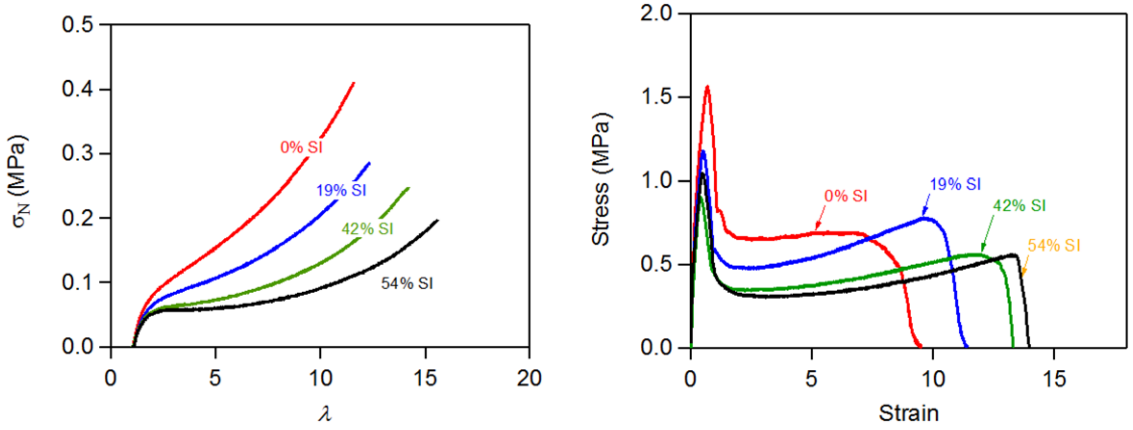

Figure 27. (a) Tensile tests of four different adhesives with nearly identical linear viscoelastic properties, but very different large strain properties. (b) Probe tack tests carried out at similar strain rates with 100 μm thick films of the same adhesive series. Data from Creton *et al* (2005). 0, 19, 42 and 54 % SI correspond to the composition of the block copolymer blend used in the adhesive (see Roos and Creton (2005)).

which propagate as cracks along the interface until complete debonding as discussed in previous sections. If the material is insufficiently elastic (A650), the average true stress remains stable with strain, but the average stretch of the filament diverges (upward curvature in figure 26(b)) and will lead to the unstable shrinking of the ligament up to failure. Finally for an optimized viscoelasticity (A1570), the fibril cross section stabilizes due to strain hardening, the true stress only slightly increases with stretch and the fibril stretch increases at the same rate as the nominal stretch (downward curvature in figure 26(b)) and a stable fibril extends until strain hardening will detach it from the surface.

Although the linear viscoelastic properties predict reasonably well the transition between interfacial crack propagation and bulk deformation, they are clearly not able to predict whether the final failure will occur by a fracture of the extended fibrils, or by a detachment of these fibrils from the surface. This is an essential difference for application properties since a flow or fracture of the fibrils in large strain leads to residues on the probe while a detachment leads to a clean surface. In both cases, to predict or understand these differences it is essential to characterize and understand the non-linear elastic behavior all the way to the failure process. An example of the relevance of extensional properties for the interpretation of tack curves is shown in figure 27. The comparison of the uniaxial tensile curves of figure 27(a) and the probe tack curves of figure 27(b) on the same adhesives show that the nominal stress level in the region where fibrils (or walls between cavities) extend, is controlled by the extensional properties of the adhesive itself.

This characterization of the material properties in uniaxial extension and its connection with the material structure was discussed in section 4 for generic elastic entangled and crosslinked networks. It is useful to extend this analysis to the specific case of PSA's.

The experimental output of a uniaxial tensile test of a PSA is typically a stress versus stretch curve that resembles that of figure 11(a), with a pronounced softening and a stiffening at high strain. Although this nominal stress versus stretch curve is informative by itself, the reduced Mooney stress f^* plotted as a function of $1/\lambda$ such as in figure 11(b) provides more information on the structure of the adhesive. First of all the position of the minimum in reduced stress is clearly representative of the onset point of the stiffening due to finite chain extensibility. Two material parameters can be defined from $f^*(\lambda)$: a reduced modulus at the minimum of f^*, which we will call C_{hard} and a value of stretch at the onset of strain stiffening defined as λ_{hard}. As discussed in section 4, the initial shear modulus of the material μ is due to permanent crosslinks and entanglements. As discussed in section 4, the contribution of entanglements to the stress can either decrease with time due to flow, as in a polymer melt (Doi and Edwards 1986), or decrease with stretch because of chain orientation, in an entangled and crosslinked rubber (Rubinstein and Panyukov 2002). Both mechanisms are active, but the first relaxation mechanism is irreversible and leads to viscoelastic dissipation, while the second mechanism is reversible and leads to non-linear elasticity. Some soft adhesives such as the acrylic networks rely mainly on the first mechanism to obtain the necessary strain softening (Deplace *et al* 2009c), while some others like those based on block copolymers rely mainly on the second mechanism (Roos and Creton 2005).

If the tensile test is performed very slowly so that all relaxation mechanisms have occurred over the time scale of the experiments, we expect μ_x to be related to the C_{hard} of figure 11(b) by:

$$\mu_x \approx C_{\text{hard}} \tag{33}$$

And for a homogeneously crosslinked adhesive, we expect λ_{hard} to be related to the finite extensibility of the crosslinked chains by:

$$\lambda_{\text{hard}} \approx \left(\frac{\rho RT}{C_{\text{hard}}}\right)^{1/2} \tag{34}$$

Where ρ is the density of the polymer. However, experiments are rarely carried out infinitely slowly and the measured $C_{\text{hard}}(\dot{\lambda})$ and λ_{hard} $(\dot{\lambda})$ are usually characteristic of a given stretch rate (Bellamine *et al* 2011, Degrandi-Contraires *et al* 2013). The third parameter that can be extracted from the

Mooney representation of the reduced stress is $C_{soft}(\dot{\lambda})$, characteristic of the softening process due to viscoelastic relaxation and/or presence of entanglements. Although in past studies several definitions have been used for $C_{soft}(\dot{\lambda})$, we feel at this stage that the best way to define it is simply by subtracting $C_{hard}(\dot{\lambda})$, from the initial elastic modulus:

$$C_{soft} \approx \mu - C_{hard} \tag{35}$$

These values of $C_{hard}(\dot{\lambda})$, $C_{soft}(\dot{\lambda})$ and $\lambda_{hard}(\dot{\lambda})$ are the signature of the large strain behavior of the PSA and have a profound effect on the debonding mechanisms as illustrated in figure 29 which can be summarized as follows: If $C_{hard}(\dot{\lambda}) \sim 0$ or cannot be defined, the polymer is a fluid and fibrils, if they form, will shrink and break before detaching from the surface. On the other hand, for a typical lightly crosslinked PSA $C_{hard}(\dot{\lambda}) \sim 10$–30 kPa over the usual stretch rates relevant for adhesive tests and this is sufficient to cause detachment of the fibrils. Given that the initial moduli of the PSAs are generally in the range 30–100 kPa, it is easy to see that the proportion of the modulus due to permanent crosslinks is low, usually less than 30%. The effect of the crosslinking on the tack measurements is illustrated by the example of figure 28. Two PSAs made from an identical blend of acrylic monomers have been first polymerized, then either left uncrosslinked, or lightly crosslinked. Figures 28(a) and (b) show the linear viscoelastic properties of the polymers in the range of frequencies relevant for tack tests and only small differences can be seen. On the other hand, figures 28(d) and (e) show the large strain properties of the same adhesives in uniaxial extension. Although the initial small strain modulus appears indeed identical the curves then significantly diverge. Finally, figure 28(c) shows the results of a tack test carried out on the same adhesives. While the lightly crosslinked adhesive shows a marked plateau at constant nominal stress, typical of PSAs, and an adhesive detachment from the steel substrate, the uncrosslinked material forms filaments that can flow and eventually break before being able to detach. Clearly the strain hardening, which is not necessarily predicted by the linear properties, plays a crucial role in the mechanisms of fibril detachment.

It should be noted that this important effect of a light level of crosslinking can be used to design optimized PSAs with a heterogeneous structure. While linear properties are sensitive to the number of elastic chains per unit volume, the strain hardening process is sensitive to the details of how the chains are connected together and percolate to form a continuous network. This issue is particularly important when adhesive films are prepared from the drying of individual latex particles creating a spatially inhomogeneous structure (Deplace *et al* 2009a, 2009c, Bellamine *et al* 2011, Degrandi-Contraires *et al* 2011, 2013, Foster *et al* 2009).

The parameters extracted from the uniaxial tension test that we have defined can also be used to build a more refined 'application window' of PSAs based on their balance of properties. An example of map as a function of C_{hard} and C_{soft} is given in figure 29. The region on the left side corresponds to more elastic materials than what is necessary for PSA. Typically such materials relax the stress moderately and are too elastic to blunt the cracks as in figure 23(b) and fail by interfacial crack propagation. At the bottom of the graph lie fluids which can be highly sticky, but are not able to detach from the surface without residues. The Dahlquist criterion, which specifies that PSA should not have a shear modulus at 1 Hz above 0.1 MPa, is plotted as a diagonal line and limits the overall modulus $C_{hard} + C_{soft}$. Within the PSA regime one can distinguish different applications of PSA requiring a different balance of properties. Removable PSA are typically soft and weakly adherent, requiring a more elastic character. Labels need to stick on many surfaces and often should not be detachable without damage, while double-sided structural tapes need to use the highest modulus permitted by the Dahlquist criterion.

5.4. *Materials used for pressure-sensitive-adhesives*

This last section on adhesives will address more specifically the materials effect. While a detailed review of the chemistry of PSAs is outside the scope of this review, some general features of the materials can be discussed. In particular, we will address how to obtain the nonlinear viscoelastic properties needed for spontaneous adhesion from polymer design and give some examples.

From the point of view of an adhesive technologist, adhesives can be classified into three categories: (1) reactive soft adhesives, which are applied in the liquid state and become a tough rubber once chemically cured, (2) so-called 'hot-melt' adhesives, which are applied at higher temperatures in the liquid state and then solidify during cooling, generally involving crystallization and (3) pressure-sensitive adhesives (PSA), which adhere by simple mechanical contact without any need of chemical or physical change of state. The properties of the first two categories depend heavily on the details of the chemistry used and on the formulation (for the hot melts in particular) and are reviewed in many specialized technology oriented textbooks (Chaudhury and Pocius 2002, Pocius 2002). On the other hand, pressure-sensitive-adhesives contain relatively few additives and their adhesive behavior is dominated by the rheological properties of the polymer, which is the main component of the adhesive. As a result, it is possible to understand the properties of PSA from polymer physics considerations and this is the focus of this section.

We have seen that polymers used in PSA must have four important properties, according to Dahlquist's criterion, which roughly speaking control their spontaneous bonding behavior and the energy dissipated during debonding. The first is a glass transition temperature well below the usage temperature: PSA rely on rubber elasticity for their properties and this can only occur when polymer chains are mobile. The second is a low shear modulus (10–100 kPa) when tested at a characteristic frequency of 1 Hz. This condition implies that the strain energy necessary to conform to even rough surfaces at deformation rates of the order of 1 s^{-1} should be of the order of the gain in surface energy when forming an interface and has been discussed in section 5.1. The third one is an elastic character at low frequency or long times, which prevents

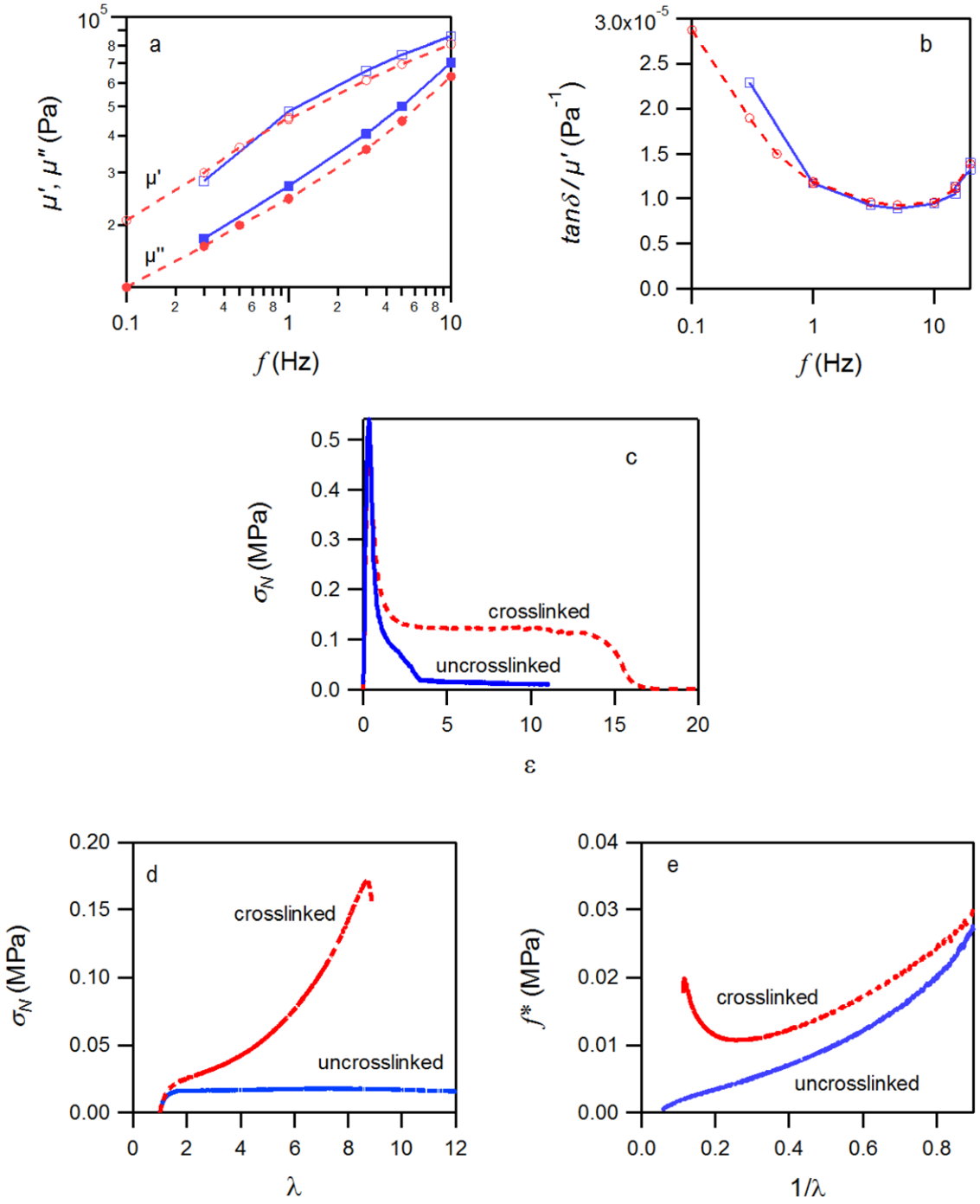

Figure 28. Effect of crosslinking of an acrylic PSA. Solid red line: uncrosslinked material, dashed blue line: crosslinked material. (a) Linear rheology: evolution of the elastic μ' (empty symbols) and dissipative μ''(filled symbols) moduli as a function of the frequency. (b) Evolution of the ratio tan δ/μ'; (c) stress–strain tack curves. Tack experiments were performed at 10 μm s^{-1} on stainless steel; (d) tensile test: nominal stress σ_N versus strain tensile curves. (e) Tensile tests: f^* versus $1/\lambda$ of the same tensile results. Data from Deplace *et al* (2009b).

or slows down creep. These three necessary conditions guarantee spontaneous adhesion and clean removal from most surfaces. Yet to achieve large energy dissipation upon debonding and become a useful adhesive in the practical sense, a fourth condition must be met, the material must have a significant degree of viscoelasticity in small and large strain. This fine adjustment of the viscoelastic properties while satisfying the first three conditions is at the core of the know-how of PSA manufacturers.

Such a combination of requirements on the macroscopic properties can in principle be obtained from any polymer with a low glass transition temperature, by adjusting its molecular weight, and crosslinking density, but in practice only a few families of polymers are used to manufacture PSA. Table 1 lists some families of PSA with some selected experimental references focusing on those families of adhesives.

It is worthwhile now to translate the physical and rheological properties that are required to display adhesion into

Table 1. Families of PSA with typical monomers used in the polymer and selected references.

Family	Type of polymer	Tg adjustement	Non-linear rheology adjustment	Applications	References
Acrylic	Poly n-butyl acrylate, Poly (2-ethylhexyl acrylate)	Comonomers	Chemical crosslinking	UV and oxidation resistant, all purpose	Tobing *et al* 2001, Gower and Shanks 2004b, Lakrout *et al* 2001, Lindner *et al* 2006
Natural rubber	Natural rubber	Tackifying resin	Strain induced crystallization, chemical crosslinking	Cheap, high Strength	Sherriff *et al* 1973, Aubrey and Sherriff 1980
A-B-A Block copolymers	Styrene-isoprene-styrene	Tackifying resin	Physical crosslinking by polystyrene domains	High strength, does not work above 70 °C	Nakajima 1992, Gibert *et al* 1999, Daoulas *et al* 2004, Creton *et al* 2005
Silicones	Polydimethylsiloxane, polyvinylsiloxane	MQ resin	Chemical crosslinking	High and low T resistance, biocompatible, low adhesion	Lin *et al* 2007
Polyisobutylene	Polyisobutylene + butyl rubber	Tackifying resin	Chemical crosslinking	Biocompatibility, good UV, oxidation resistance	Krenceski and Johnson 1989

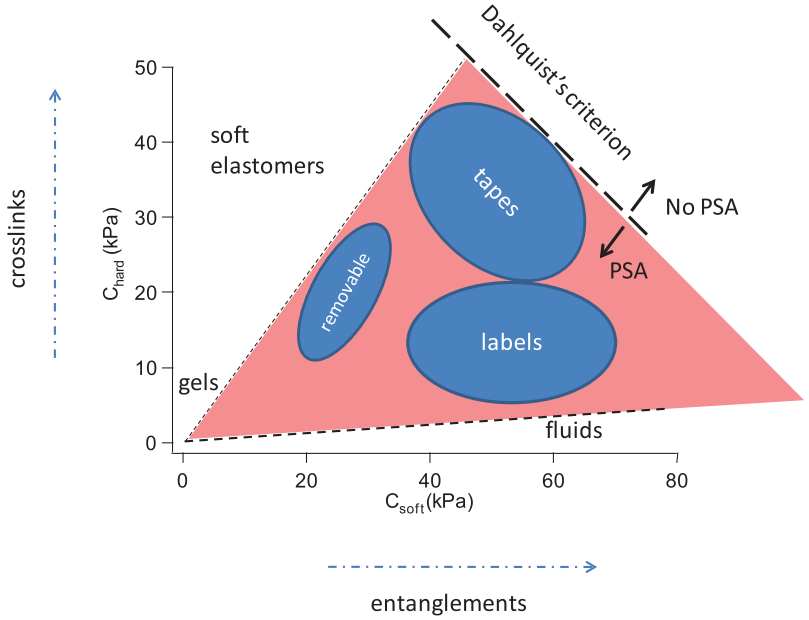

Figure 29. Application map of PSA as a function of the two large strain parameters C_{hard} and C_{soft} representing the crosslink and entanglement densities respectively at the relevant strain rate.

polymer chain architecture. Since the modulus must be below 0.1 MPa at 1 Hz, it is clear that glassy and semi-crystalline polymers cannot be the main component to make a PSA. However, classically crosslinked rubbers cannot be used either, since they typically reach elastic shear moduli μ of several hundreds of kPA and up to several MPa with a level of viscoelasticity insufficient to relax the stress singularity at the edge of a growing cavity and blunt the crack (see equation (32) and figure 29). As a result, while rubbers have some level of adhesion on solid surfaces (like a tire on the road), they always debond by interfacial crack propagation without forming fibrils. The optimum level of crosslinking is a crucial parameter to optimize for all families of PSA (Zosel 1991, Gower and Shanks 2004a, Deplace *et al* 2009a) and depends markedly on the application but is typically just above the point of percolation of the network (the gel point) so that the polymer is highly stretchable but cannot flow (Jensen *et al* 2009).

Zosel, pointed out also in a seminal paper that a low entanglement density was a necessary condition to reach good adhesive properties (Zosel 1985). This is understandable since entanglements are temporary crosslinks and a shear modulus μ at room temperature of 0.1 MPa corresponds to an average molecular weight between entanglements of roughly 25 000 g mole^{-1} (Rubinstein and Colby 2003). The earliest PSA were made with a blend of natural rubber and a low molecular weight resin with a T_g above room temperature (Sherriff *et al* 1973, Aubrey and Sherriff 1980, Butler 1989). In this case the cohesion comes from the high molecular weight of the natural rubber and its physical crosslink structure. The role of the resin is to lower the plateau modulus by diluting the entanglement network and to increase the T_g of the blend an hence the viscoelastic dissipation at the strain rates relevant for debonding. The second very common family of PSA is that of acrylic polymers (Dale *et al* 1989, Satas 1989, Gower and Shanks 2004a, Lindner *et al* 2006). They are usually copolymers containing a combination of monomers used to adjust both T_g and entanglement density ν_e (although not independently). Because of their bulky side chains, acrylate monomers have sufficiently low entanglement densities to function as PSA without any additives. However, the adjustment of the rheological properties has to occur by synthesizing copolymers with different monomer compositions rather than by simply mixing ingredients, which makes them less attractive as model systems for physicists. In PSA based on acrylate monomers, a polar group, typically acrylic acid, is usually added to provide better interactions with the surface, and to introduce physical crosslinks (in addition to entanglements) increasing the elongational viscosity and stabilizing the fibrillar structure once it is formed. A third widespread family that has been highly studied by polymer physicists is the styrene-isoprene-styrene (SIS) block copolymer family (Daoulas *et al* 2004, Marin and Derail 2006, Creton *et al* 2009). PSA based on SIS copolymers are physically crosslinked by spherical polystyrene domains. A typical formulation would have about 40 wt% of a combination of triblock and diblock copolymers and 60 wt% of low molecular weight additives miscible with the polyisoprene (PI) domain only, which reduce the plateau modulus and adjust the glass transition temperature as described above (Nakajima 1992, Gibert *et al* 1999).

Finally, two more specialty families deserve to be mentioned. Silicone PSA (Sobieski and Tangney 1989, Lin *et al* 2007, 2009) do exist and are based on similar criteria as acrylics, i.e. a combination of monomers to adjust T_g and entanglement network. However, silicone PSA also use the so-called MQ resin, denser silica-like nanoparticles that are incorporated to increase dissipative processes during deformation. The other specialty family is that of hydrophilic PSA (Roos *et al* 2002, Feldstein *et al* 2006) and hydrocolloid PSA (Ferrari *et al* 1995). Both are used for medical applications

and should stick on wet or at least humid surfaces (skin or mucosa). They are usually composed of a significant proportion of very hydrophilic monomers, but controlling the change in properties occurring with variable water content is still a significant challenge so that applications only typically work for a limited time period. This is clearly the area in greatest need of a better understanding.

6. Fracture of soft polymer networks

In the previous sections we focused on adhesion problems, i.e. situations where typically a thin layer of soft adhesive is sandwiched between two stiffer layers and is being detached from one of these layers. While this detachment process is clearly a fracture process, there are some specific aspects that are worthwhile pointing out now to distinguish it from the more general problem of fracture:

(1) the locus of failure is at or near the interface. This situation is inherently asymmetric around the crack plane and interfacial interactions and bulk interactions are generally not the same;
(2) the soft deformable adhesive film is almost always confined so that hydrostatic stresses play a key role in the fracture mechanisms;
(3) soft adhesives are often very viscoelastic and highly deformable. Not only the SSY condition is never fulfilled, but dissipative zones are always extending over the complete layer thickness. In other words, a value of the adherence energy can only be viewed as an apparent fracture energy Γ_{app}, i.e. as the property of a structure and not of a material or an interface.

The fracture problems that we will now address will be different from the above. Bonds broken during crack propagation will generally be the same that insure bulk cohesion, hydrostatic stresses will only play a role near the crack tip and Γ will be understood as a material property if the sample is large enough to satisfy the SSY condition (see introduction). Furthermore, and because we are now investigating bulk properties, the type of materials where fracture occurs by crack propagation are predominantly elastic, i.e. $\mu'(\omega) \gg \mu''(\omega)$ and are well crosslinked, i.e. $\mu_x \geqslant \mu_e$.

Nevertheless, there is a clear analogy between the mechanisms of adherence and the mechanisms of fracture in the bulk and it is our goal to point out to the reader the similarities between the two cases.

From a historical point of view, fracture of soft elastic materials cannot be dissociated from fracture of rubbers. Several researchers in the late 1950s and early 1960s, used Griffith's energy balance approach of fracture mechanics to treat and understand quite a wide range of failure phenomena in elastomers (Rivlin and Thomas 1953, Thomas 1955, Greensmith 1960, Andrews 1961, Gent *et al* 1965, Lake and Thomas 1967). Circumventing the difficulty of finite strains and of the nonlinearity of the material properties in calculating stress fields, they showed experimentally that the energy necessary to propagate a crack in the bulk Γ, either called 'critical strain energy release rate' $\mathcal{G}_c$ or 'tearing energy' T in the original papers, was a characteristic of the rubber itself and was independent of the geometry of the test piece.

Two important insights that dominate the modern vision of polymer networks fracture today were established during that period. First, Greensmith *et al* (1960) determined that the tear energies were highly dependent on crack propagation rate and temperature, varying from around 0.1 kJ m^{-2} at very low rates (or elevated temperatures), to 100 kJ m^{-2} for rapid growth (or lower temperatures). These variations paralleled qualitatively the variation of linear viscoelastic properties observed with rate and temperature. This led to the conclusion that the rate dependence of the fracture energy can be attributed to viscoelastic energy dissipation in the bulk. Then Lake and coworkers (Lake and Lindley 1965) determined that even in the absence of viscoelastic dissipation (high temperature, low crack velocity) the threshold value of Γ was still three orders of magnitude larger than the Dupré work of adhesion w.

We will now first address the physics underlying these two seminal results before discussing more recent developments concerning the role of large strains in the fracture propagation mechanisms, with a special focus on the physics of the crack tip blunting effect and the growth of internal defects towards cavities and fibrils. Analogies will thus be established between fracture of soft materials and the mechanisms of debonding of soft adhesives, focusing on scale separation of the different dissipation mechanisms.

6.1. Threshold fracture energy

As mentioned above Lake and coworkers (Lake and Lindley 1964, 1965, Lake and Thomas 1967) showed that in the absence of viscoelastic dissipation (at high temperature far from the T_g of the rubber or with oil-swollen rubbers), a minimum amount of mechanical energy Γ_0 of about 50–100 J m^{-2} was required for a crack to propagate, for a broad range of elastomers differing widely in other strength properties. Lake and Thomas (Lake and Thomas 1967) predicted from simple molecular arguments a threshold value of Γ_0 of the order of 20 J m^{-2}, scaling with $\nu_x^{-1/2}$ value where ν_x is the density of crosslinks. They proposed that this rate independent dissipation process was due to the fact that when any of the main chain bonds breaks, the total bond energy of each bond of the stretched chain is irreversibly lost. Therefore the minimum energy necessary to break the chain is proportional to the length of that chain, i.e. to the number of C-C bonds comprising that chain N_x. Assuming that only the chains crossing the plane of the crack will break, Γ_0 is then given by:

$$\Gamma_0 = N_x U_b \Sigma \tag{36}$$

where Σ is the areal density of chains crossing the interface and U_b is the bond energy of a C-C bond (350 kJ mol^{-1}). For a homogeneously crosslinked network, Σ and ν_x are not independent and one can write:

$$\Sigma \approx \nu_x a N_x^{1/2} \tag{37}$$

where a is the size of the monomer. Substituting equation (37) into equation (36), Γ_0 can then be rewritten as:

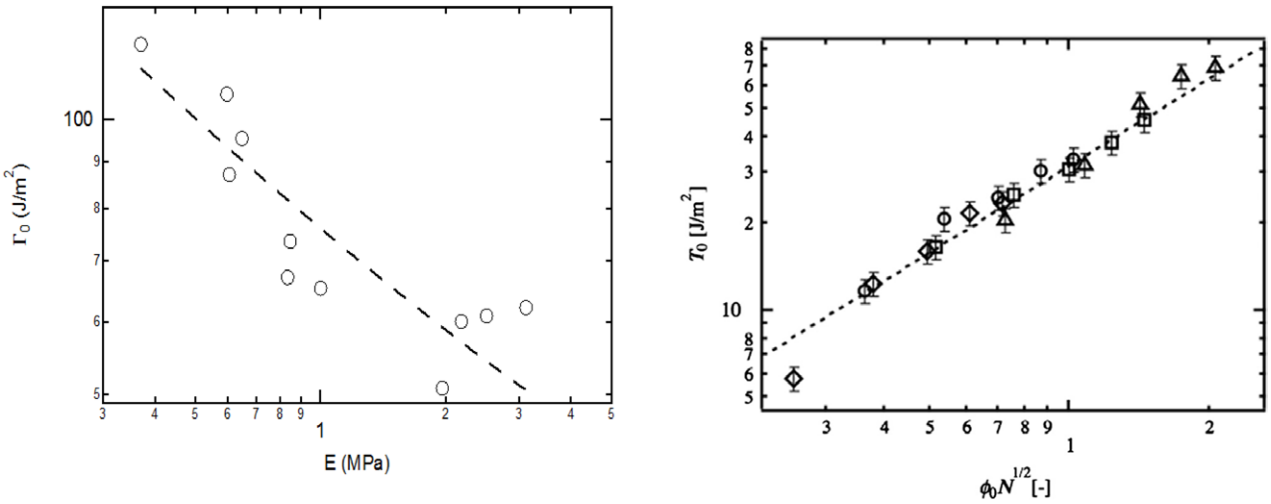

Figure 30. (a) Threshold fracture energy Γ_0, versus Young's modulus E for elastomers (data from Bhowmick *et al* (1983)) and (b) threshold fracture energy (original symbol T_0) of a series of model hydrogels based on the tetra-PEG segments. ϕ_0 is the monomer concentration in the gel and N is the number of monomers in each chain. Reproduced with permission from Sakai (2013; copyright 2013 Elsevier).

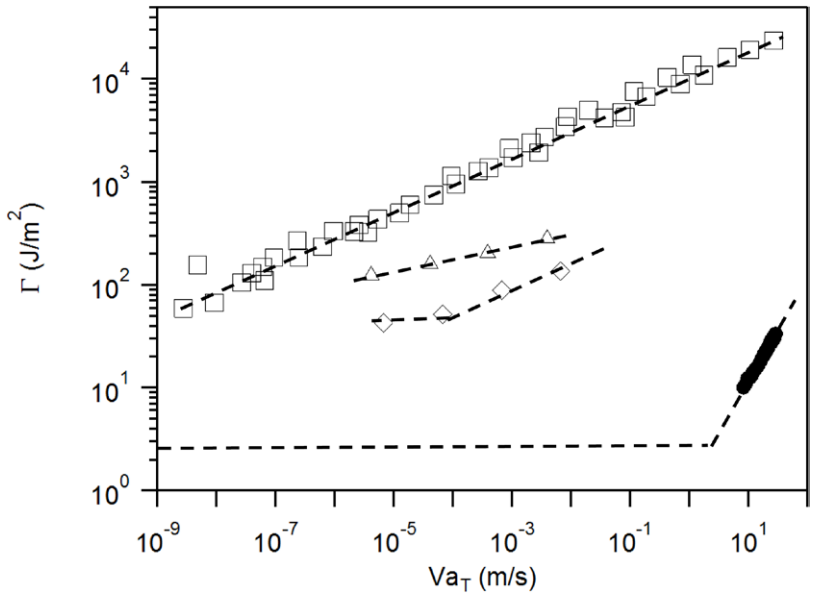

Figure 31. (a) Fracture energy Γ as a function of propagation velocity or reduced propagation velocity for different materials. (□) Master curve at 25 °C for a styrene-butadiene rubber ($T_g = -25$ °C) tested with the trouser tear geometry. Data from Gent *et al* (1994). (◇) Polyurethane rubber ($T_g = -55$ °C) at 25 °C tested with the single edge notch geometry. Data from Cristiano *et al* (2011). (△) Double network hydrogel at 25 °C. Data from Tanaka *et al* (2005). (●) Gelatin gel (5 wt% polymer) at room temperature in the pure shear geometry. Data from Baumberger *et al* (2006a). Horizontal lines are values of Γ_0 when reported.

$$\Gamma_0 \approx N_x U_b \nu_x a N_x^{1/2} \approx U_b \nu_x a N_x^{3/2} \approx \frac{U_b a \rho}{M_0} N_x^{1/2} \tag{38}$$

where ρ is the monomer density and M_0 is the molar mass of the monomer.

This equation is valid for both elastomers and swollen gels since the difference between the two cases is mainly contained in ρ, which for elastomers is a bulk unswollen density ρ_0 of the order of 10^3 kg m^{-3} and for gels it is simply $\rho = \rho_0\ \phi_p$ where ϕ_p is the polymer volume fraction.

If the chains in the network are Gaussian, the elastic modulus is $E = 3\,\nu_x k_B T$, so that equation (38) can be rewritten as:

$$\Gamma_0 \approx U_b a \left(\frac{\rho}{M_0}\right)^{3/2} (3k_B T)^{1/2} E^{-1/2} \tag{39}$$

In other words, the threshold fracture energy Γ_0 is predicted to scale with the inverse square root of the elastic modulus, a classic yet not very intuitive result. It should be noted however that this simple model ignores any imperfections or heterogeneities in the network as well as the presence of entanglements.

This prediction can then be tested with model systems. Experimental evidence of the Lake and Thomas prediction are shown in figure 30 and show that for both rubbers and

hydrogels the key idea behind the Lake and Thomas model seems to be correct (see equations (39) and (38)).

A key point beyond scaling is however the quantitative agreement. A more general version of equation (36) can be written as (Akagi *et al* 2013):

$$\Gamma_0 \approx N_x U_b \nu_x L \tag{40}$$

While N_x and v_x are physically well defined quantities that can be obtained (within a factor of 2) from bulk elasticity experiments and U_b cannot be too different from the bond energy of a C-C bond, the distance L over which energy is irreversibly dissipated upon fracture, can only be estimated from fracture experiments. In unfilled rubbers threshold fracture energies are of the order of 50–100 J m^{-2} (Ahagon and Gent 1975b, Gent and Tobias 1982, Bhowmick *et al* 1983, Bhowmick 1988). For $\mu_x \sim 0.5$ MPa and $M_0 = 100$ Dalton, we have a prediction of $\Gamma_0 \sim 25$ J m^{-2}, in very good agreement with the experimental values, suggesting that the original insight of Lake and Thomas was basically correct and L is of the order of the mesh size of the molecular network.

6.2. *Fracture of rubber at finite crack propagation velocity*

In the previous section we have seen that at propagation threshold conditions, i.e. slow fracture very far from the glass transition temperature, the fracture of at least simple network rubbers can be well understood with simple molecular arguments. However, this ceases to be the case as the temperature decreases and becomes closer to the glass transition temperature of the rubber, or the rate at which the networks are broken increases. In this case Γ depends both on the rate and temperature at which the experiments are carried out and on the architecture of the crosslinked network in a fully analogous way to the adhesive case, so that the empirical equation (31) relating Γ and crack velocity remains valid. Several examples of measurements of $\Gamma(v)$ for typical networks as a function of rate and temperature are given in figure 31 and show that the fracture energy increases very significantly with the crack propagation velocity. The functional form of $\Gamma(v)$ is generally similar to that found for adhesion, i.e. a threshold value Γ_0 and a power-law dependence at higher crack velocities, i.e. $\phi(a_T v) \sim v^n$. The value of the exponent n has been reported to vary between 0.1 and 1 depending on the material and examples reported in figure 31 include two rubbers and two crosslinked gels (Gent *et al* 1994, Tanaka *et al* 2005, Baumberger *et al* 2006a, Cristiano *et al* 2011).

Since the force to break a highly energetic covalent bond does not increase that significantly with deformation rate, it is obvious that the measured increase in fracture energy with rate is due to a change in how the energy is transferred from the loading point to the fracture point. This is the realm of solid mechanics and it is important to focus now on larger length scales than the molecular scale. An interesting result shown in figure 31 is the possibility to construct a master curve from fracture data measured at different temperatures by using velocity shifts of the horizontal axis. This result was interpreted early on as proof of the viscoelastic nature of the dissipative processes involved at the crack tip (Ahagon and Gent 1975b, Plazek *et al* 1988, 1983, Bhowmick 1986, Gent *et al* 1994) in an analogous way to what has been discussed for adhesives in section 5. Based on this insight many researchers in physics and mechanics have sought to account quantitatively for the dissipation of energy during fracture by using linear viscoelastic properties of the material. Although a detailed review of these models is beyond the scope of this paper, it is worthwhile to mention the pioneering efforts of Knauss (Mueller and Knauss 1971), Schapery (Schapery 1975a, 1975b, 1975c) and Christensen (Christensen and Wu 1981), who calculated the stress fields ahead of a propagating crack assuming infinitesimal strains and linear viscoelasticity and introducing a cohesive zone to remove the singularity. And more recently, the scaling approach of de Gennes (de Gennes 1988, 1997, de Gennes and Troian 1990), which estimates the energy dissipation of a crack propagating in a viscoelastic medium as a function of propagation velocity, and the contribution of Persson who extended the model to a more general linear viscoelastic rheology (Persson *et al* 2005, Persson and Brener 2005). Despite making sound scaling predictions these models and their variations (Saulnier *et al* 2004, Barthel and Fretigny 2009) always significantly underpredict the actual dissipation measured at the crack tip during fracture at a set velocity. The reason is evident when one looks at the frequencies involved. Typically a well crosslinked rubber is used about 40–50 °C above its glass transition temperature mainly to avoid viscoelastic losses and heating during normal use. At that temperature the ratio of the dissipative versus storage component of the 1 Hz modulus is well below 0.1. As pointed out by Gent in his landmark paper (Gent 1996a), when comparing the master curves of the fracture energy and that of the elastic modulus (taking the glass transition temperature as a common reference), the strong increase in the fracture energy occurs between $V = 10^{-20}$ and 10^{-8} m s^{-1}, while the increase in dissipation due to linear viscoelasticity occurs between $\omega = 10^{-4}$ and 10^{2} rad s^{-1}. Following a simple dimensional argument, if a crack moves at a velocity V and we assume that the dissipation occurs over a characteristic length scale L_0, the characteristic dissipation frequency should be $\omega = V/L_0$. However the dissipation ranges observed by Gent imply that the size of the dissipative zone at the crack tip would be of the order of $L_0 \sim 10^{-12}$ m, which is below atomic dimensions. Hence, the simple linear viscoelastic calculation, which assumes that dissipation depends on frequency alone and not on strain amplitude, must be incorrect.

What is missing in this picture is the role played by large strain elasticity and localized damage in controlling the size of the dissipative zone and the nature of dissipation.

6.3. *Crack tip analysis: crack blunting, large strain effects*

For many years large strain elasticity was completely absent from the physical picture of the crack tip and the few papers being published on the subject (Knowles and Sternberg 1973, 1974, Stephenson 1982, Geubelle and Knauss 1994) did not permeate beyond the mechanics community. The development of other types of soft materials, such as gels, which are very relevant for life sciences, have since then fostered a renewed

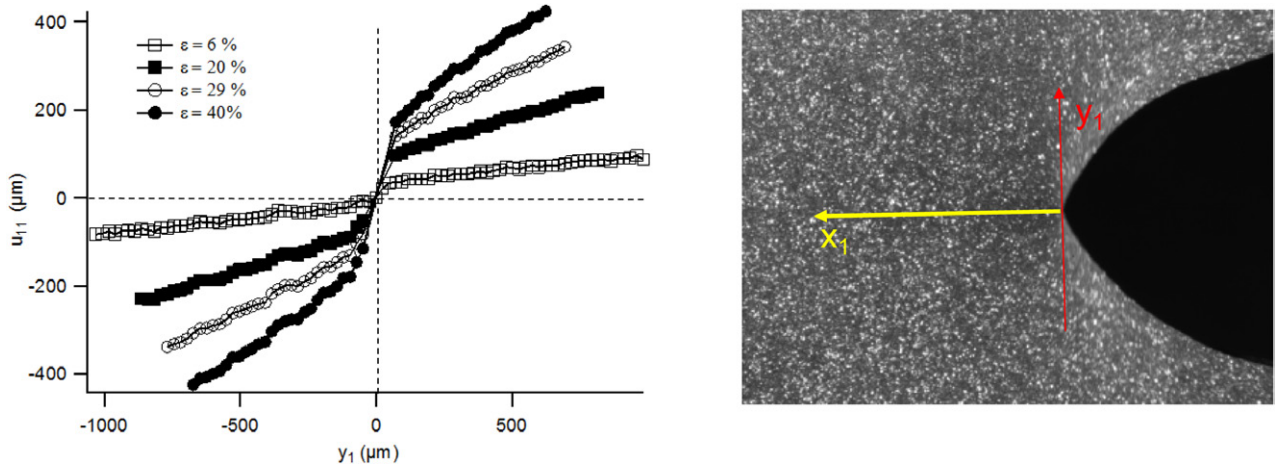

Figure 32. Displacement at the crack tip as measured by DIC in filled elastomers. u_{11} is the displacement of a point along the red line as a function of its position. The crack tip is at the origin. There is clearly a localized highly stretched region while outside of this zone u_{11} is linear with position and corresponds to the macroscopic strain applied to the pure shear sample. Data from Mzabi *et al* (2011).

interest in the solid mechanics and the physics community in a better understanding of the fracture mechanics of soft materials.

As discussed in the introduction, the important quantity to assess is the elasto-adhesive length $\ell_{EA} = \Gamma/E$. Based on the experimental results of figures 30 and 31, the elasto-adhesive length for tough rubbers (E ~1 MPa) ranges between 50 μm and 1 cm, and for gels (E ~ 5–50 kPa) it ranges between 200 μm and 1 cm, but can reach values larger than 10 cm for the tough gets described in section 7. Below this length scale the crack tip strains are larger than 100% and the material response and properties are well into its non linear regime.

This argument has been first proposed by Hui *et al* in their seminal paper (Hui *et al* 2003), based on the following approximate treatment, which considers the change of crack tip radius with increasing loading on a slit-like crack in a soft material. In each step of the loading the crack is treated as a plane stress elliptical crack of half length c and half height b in a uniformly stressed infinite plane. The radius of curvature at the crack tip ρ is:

$$\rho = \frac{b^2}{c} \tag{41}$$

And the tensile stress at the crack tip is:

$$\sigma_{max} = \frac{2\sigma c}{b} = 2\sigma\sqrt{\frac{c}{\rho}} \tag{42}$$

The question is now to determine, for such a crack, the increase in σ_{max} as a function of the applied remote stress σ. For small strain elasticity, the relation between local stress and remote stress is fixed by LEFM and an increase in remote stress σ will always lead to an increase in local stress σ_{max} until the crack propagates as discussed in the introduction. However, if finite strains are allowed and ρ can change with increasing loading, σ_{max} progressively ceases to increases with σ and tends toward $2E$ as the remote stress σ approaches the modulus E. This situation is called elastic blunting by Hui *et al*.

The assumptions in (Hui *et al* 2003) are very stringent and do not consider other failure mechanisms than crack propagation nor the effect of strain stiffening on the crack tip stresses, but the general message should be that for materials where the cohesive strength exceeds the elastic modulus, a large highly stretched region of size of the order of Γ/E exists near the crack tip during crack propagation.

Yet most real soft materials cannot deform to infinite strains with the same modulus and experience strain stiffening at large strains or damage micromechanisms at the molecular level, which modify the stress field. Hence, the tip of a blunted crack usually contains a highly stretched region very elongated in the tensile direction and rather narrow in the crack propagation direction. Such a highly stretched region at the tip of the crack has been simulated (Long *et al* 2011) and can be directly visualized nowadays by digital image correlation (Kwon *et al* 2011, Mzabi *et al* 2011). As shown in figure 32 for the tip of a crack in a filled styrene-butadiene rubber, the measured strain field directly ahead of the crack tip is not singular in both directions, but has been measured to decrease roughly as $x^{-0.4}$ in front of the crack tip and is nearly constant in the transverse direction over a height approaching 50–100 μm very close to the tip.

The presence of this highly stretched region in a blunt crack was simulated by Hui and coworkers (Krishnan *et al* 2008, Long *et al* 2011) who also suggested that such a crack should propagate by the nucleation of smaller cracks in the highly strained zone. Mzabi *et al* (2011) proposed the following model, inspired by Brown's models for crack growth in a craze in glassy polymers (Brown 1991) and for the fracture of double network gels (Brown 2007), which bridge macroscopic loading and local growth of a small micro crack of length c_l in the center of this highly strained zone. According to the deformation field observed at the crack tip by Mzabi *et al* the strained zone can be approximately described as a homogeneously strained initially square zone of undeformed height H_0. We can then define an approximate local energy release rate g_{local} using the analogy of this local loading with the pure shear test (Mzabi *et al* 2011):

$$g_{local} = WH_0 \tag{43}$$

where W is the local strain energy density, that can be approximated by:

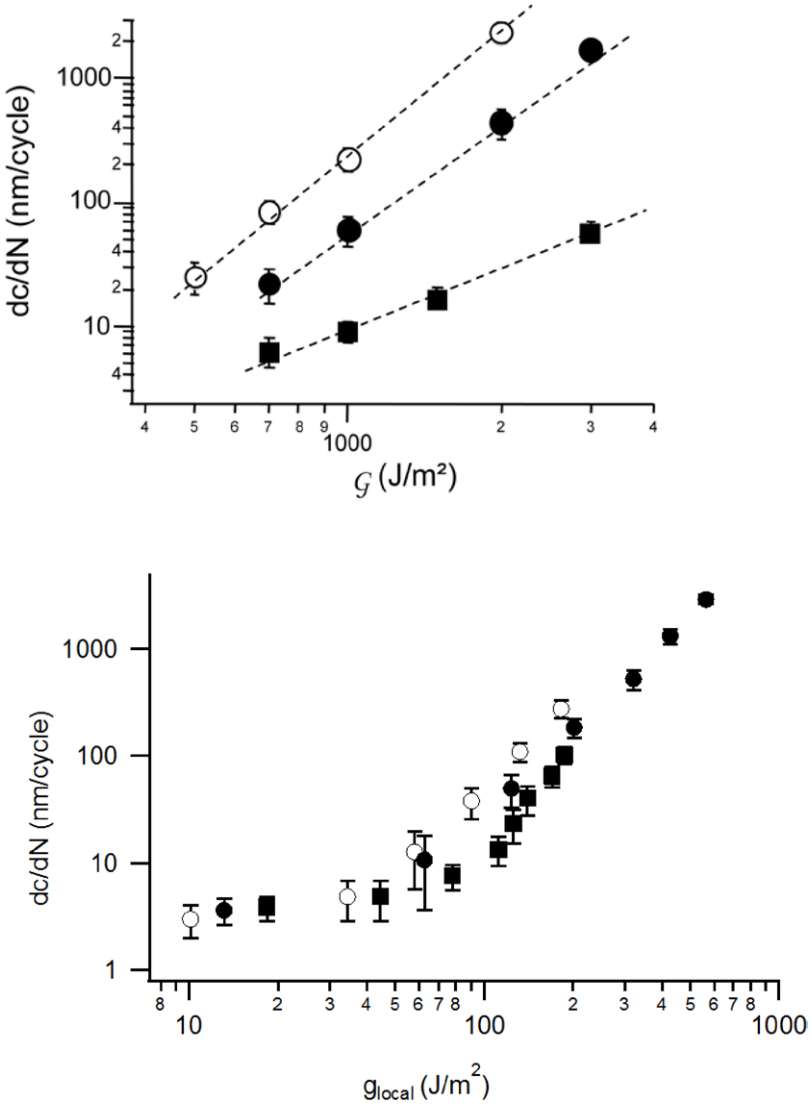

Figure 33. (a) Plot of dc/dn as a function of applied macroscopic energy release rate $\mathcal{G}_{\max}$ for a series of filled and unfilled rubbers and (b) plot of the same dc/dn as a function of g_{local}. ○ unfilled SBR rubber, ■ 20 vol% carbon black, low crosslinking density; ● 20 vol% carbon black, low crosslinking density. Data from Mzabi *et al* (2011).

$$W = \int_0^{\varepsilon_{\max}} \sigma \mathrm{d}\varepsilon \tag{44}$$

where $\varepsilon_{\max}$ is defined as the strain at the closest point to the crack tip that can be measured ~ 15 μm, and the integral is carried out over the unloading curve in uniaxial tension. We now illustrate how this concept of g_{local} can be used with an example of analysis of crack propagation in a series of elastomers in cyclic fatigue. A classic test for engineering rubbers is the resistance to crack propagation in cyclic fatigue (Mars and Fatemi 2004). A sinusoidal tensile load is applied to a prenotched sample in the pure shear geometry (figure 7). Since in the pure shear geometry the applied energy release rate is independent of crack length, this geometry applies a macroscopic energy release rate varying from 0 to $\mathcal{G}_{\max}$.

Typically the results are presented in terms of dc/dn, i.e. the differential increase in length of the crack dc per cycle as a function of applied $\mathcal{G}_{\max}$. Changes in formulation parameters like adding nanofillers or changing the crosslink density by a factor of two, can change the crack velocity by up to two orders of magnitude (Mzabi *et al* 2011). Yet if the strain field ahead of accommodated cracks (after 50 000 cycles) is characterized by DIC, it is possible to extract from the measurement an approximate value of $\varepsilon_{\max}$ and H_0 and then to estimate from equation (43) a value of g_{local} for each crack tip measurement. Figure 33 shows the value of dc/dn as a function of $\mathcal{G} = \mathcal{G}_{max}$ and as a function of g_{local} for three different materials. While the data plotted as a function of the applied macroscopic $\mathcal{G}_{\max}$ are very scattered, they collapse on a single master curve when plotted as a function of g_{local}.

Although this result has been obtained for a single system, it implies that the actual failure of covalent bonds at the crack tip may be controlled by the energy released locally (in a small region close to the crack tip) and that tough soft materials are actually able to shield crack tip bonds by dissipating energy over a larger volume further away from the tip.

The measured g_{local} of equation (43) quantifies approximately the elastic energy seen by the micro crack in the highly

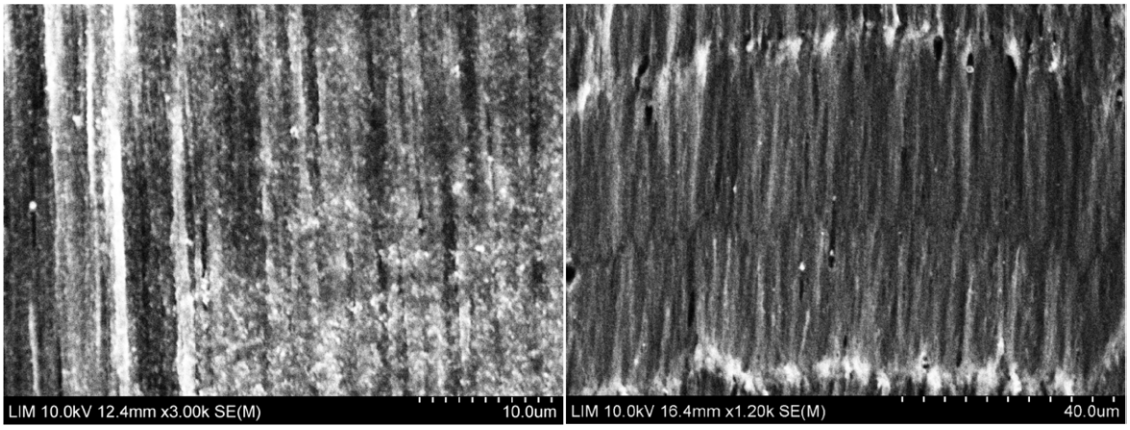

Figure 34. SEM image of the crack front showing the fibrillar structure. Images from (Mzabi 2010).

oriented zone of size ~ 15 μm right in front of the tip of the crack. Moreover, observations made by SEM and optical microscopy of the crack front show the local development of a fibrillar structure (see figure 34) (Beurrot *et al* 2010, Mzabi 2010). The connection between g_{local} and the local stress σ_{f} at the point where molecular fracture occurs (ranging between the inter-crosslink distance ~5 nm and the fibril size ~1 μm) can be done in three steps as proposed by Hui *et al* for glassy polymers presenting an analogous crazing structure (Hui *et al* 1992a). First a local stress intensity factor k_{local} associated to g_{local} by:

$$k_{\text{local}} = \sqrt{E_{\text{eff}} g_{\text{local}}} \tag{45}$$

can be defined, where E_{eff} is now an effective unloading modulus of the material. The local stress field in this oriented zone can then be related to k_{local} by:

$$\sigma(x) = \frac{k_{\text{local}}}{\sqrt{2\pi x}} \tag{46}$$

And finally the fracture propagation criterion can be set at the molecular scale by equating the characteristic stress estimated with equation (46) at a distance l_{fib} over which continuum mechanics breaks down with the critical stress to break the covalent bonds of the rubber σ_f giving:

$$\sigma_f = \frac{\sqrt{E_{\text{eff}} g_{\text{local}}}}{\sqrt{2\pi l_{\text{fib}}}} \tag{47}$$

relating effectively g_{local} with the molecular fracture stress (controlling crack propagation) through a fibril diameter length scale l_{fib}, which in principle could be measured experimentally.

This concept of local mechanics, and in particular damage and dissipation near the crack tip is a focus of current research interest both in fracture of gels (Baumberger *et al* 2006b, Seitz *et al* 2009, Baumberger and Ronsin 2010) and in fracture of rubbers (Trabelsi *et al* 2002, Mzabi *et al* 2011, Brüning *et al* 2013, Rublon *et al* 2013, Zhang *et al* 2015). Finding adapted and quantitative micromechanical models for the crack tip, accounting for both the non-linear elasticity, anisotropy (as induced by crystallization or polymer orientation for example) and damage, is clearly an important future challenge.

6.4. *Fracture by cavitation*

Until now we have considered fracture in uniaxial tension. However, when incompressible soft materials are loaded under a nearly hydrostatic tensile stress, failure generally occurs by the formation of cavities. This phenomenon often called cavitation in the literature is of great practical interest since soft materials are often loaded in confined geometries for example in coatings or adhesives (see section 5.3). Furthermore, a dilatant stress of considerable magnitude is set up near hard fillers (Cho *et al* 1987, Cho and Gent 1988) and at the tip of a sharp crack (Gent 1990) so that cavities of various sizes often appear in front of cracks (Hui *et al* 2003).

Yet, the details of the cavity nucleation and growth are still incompletely understood and a reliable cavitation criterion based on materials properties is still lacking. A variety of models have been proposed to describe the expansion of a pre-existing cavity as a function of the elastic properties of the material, its surface tension or its fracture energy (Ball 1982, Hou and Abeyaratne 1992, Polignone and Horgan 1993, Ganghoffer and Schultz 1995, Horgan and Polignone 1995, Chang and Pan 2001, Fond 2001, Dollhofer *et al* 2004, Biwa 2006, Volokh 2007, Lopez-Pamies 2009). However, experimental studies in well controlled conditions have been much less available to the theoretical community. The earliest documented evidence of the cavitation process is rather old (Busse 1938, Yerzley 1939) and experiments were carried out with commercial rubbers (neoprene and natural rubber) using a relatively confined geometry called ‘poker-chip’. The rubber disks were glued to a cylindrical sample holder and stretched in the thickness direction. Both studies observed that the stress-strain curve obtained in that geometry showed a marked and irreversible softening above a well-defined value of stress and noted that the fracture surfaces after failure contained the evidence of what they called ‘internal cracks’ or macroscopic cavities.

Some years later Gent and Lindley (Gent and Lindley 1959) used the same ‘poker-chip’ geometry on natural rubber formulations to carry out their widely known systematic investigation. They prepared vulcanized rubber disks of identical diameter and different thicknesses varying therefore the aspect ratio (i.e. the level of confinement). They

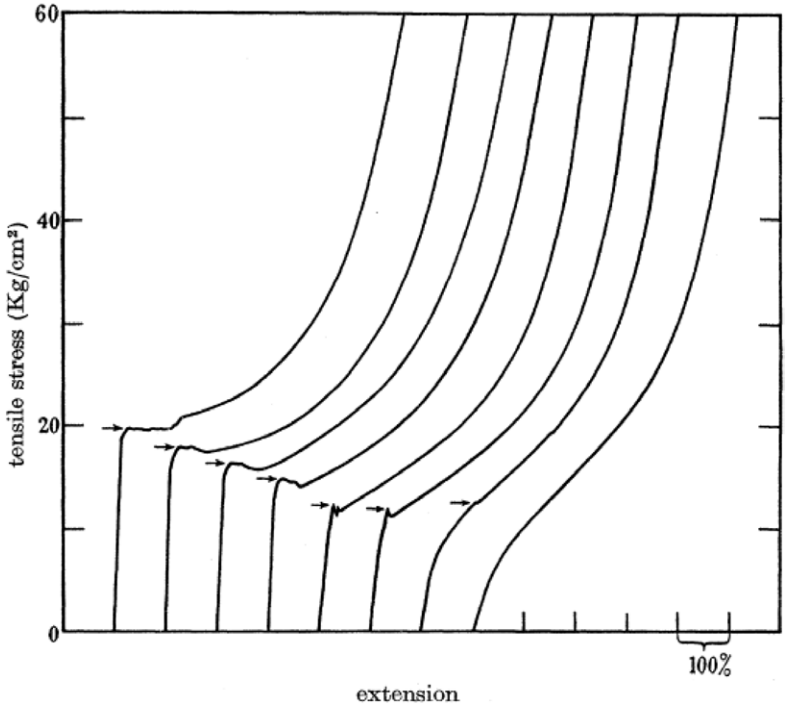

Figure 35. Experimentally determined load-extension relations for bonded rubber cylinders of vulcanizate D. Test-piece dimensions: diameter, 2 cm; thickness (from left to right), 0.056, 0.086, 0.145, 0.183, 0.32, 0.365, 0.565, 0.98 cm. Data shifted horizontally. Reproduced with permission from Gent and Lindley (1959; copyright 1959 The Royal Society of London).

found that the critical stress (defined as the apparent yield point in the stress-strain curve) decreased as the test-piece thickness was increased from very small values, becoming substantially constant for moderately thick samples as shown in figure 35.

Post mortem observations showed that a series of small internal cracks were formed in the thin disks (uniformly distributed across the section), and only one or two large cracks were formed in the centre in moderately thick disks. This result has been since completed by real-time x-ray tomography observations showing that the cavities actually appear progressively and toward the center of the sample first (Bayraktar *et al* 2008a). The switch from multiple growth of small cavities to single growth of a large cavity as the ratio between diameter and thickness of the sample decreases has also been recently predicted by finite element simulations (Lefèvre *et al* 2015). Interestingly the fact that the yield stress increases with degree of confinement is counterintuitive and contrary to cavity expansion simulation results (Lefèvre *et al* 2015) and suggests that there is more than the expansion of a cavity in the observed damage mechanism.

Maybe the most important observation of Gent and Lindley's seminal work is however that (for a fixed geometry) the apparent yield point in the stress-strain curves of the poker-chip samples is a reproducible material constant proportional to the elastic modulus. This certainly brought Gent and Lindley to name this internal cracking process a cavitation process and to model it as a simple deformation process (i.e. independent of initial cavity size) rather than as a fracture process. They used the elastic theory of cavity inflation developed by Green and Zerna (Green and Zerna 1954) for neo-Hookean behaviour to justify that the apparent yield point in the stress-strain curve appeared when the local hydrostatic pressure reached a critical value of $5E/6$ (where E is the small strain Young's modulus of the rubber). This criterion of critical pressure proportional to the modulus was also confirmed by the studies of Cho and Gent (Cho and Gent 1988) using layers of transparent silicone rubber bonded to two steel balls or to two parallel steel cylinders. Optical observations showed the presence of large cavities in the rubber layers concomitantly with the occurrence of the apparent yield stress. Note that this connection between the modulus of the material and the apparent yield stress due to cavity formation was also made for much softer thin confined layers of adhesives (see figures 21 and 25) where fracture of the material and large deformation coexist (Lakrout *et al* 1999, Brown and Creton 2002, Chiche *et al* 2005a).

Coming back to elastomers, for thinner layers (layer thickness less than 5% of sphere diameter) two interesting effects were observed. (1) In a continuous tensile test the critical stress increased markedly above the elastic modulus. (2) If on the other hand the load was kept constant just below the critical value, cavities progressively appeared over time. These two results seem to indicate that the material is in a metastable state when the applied stress exceeds the small strain elastic modulus. These early results showed a strong correlation between the critical stress (described as the apparent yield point) and the elastic modulus of the rubber, while post-mortem observations and common sense point to a fracture process, which should introduce the idea of defect size and should not be necessarily proportional to the modulus.

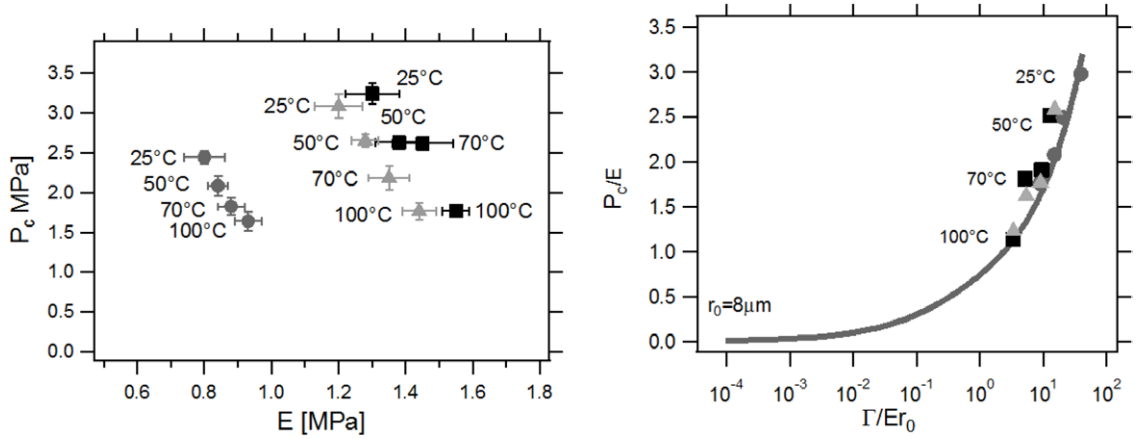

Figure 36. (a) Cavitation strength P_c as a function of Young's modulus E for three different materials and different temperatures. (b) Same data replotted to show the dependence of the cavitation strength P_c on both the elastic modulus E and the fracture energy Γ in dimensionless form. The dashed line is the prediction of the model with $r_0 = 8$ μm. Data from Cristiano *et al* (2010).

This apparent discrepancy has been pointed out theoretically (Gent and Wang 1991, Lin and Hui 2004) and recently re-examined experimentally. Using a series of unfilled and fully transparent model polyurethanes synthesized directly in a disc-like confined sample holder, Cristiano *et al* (2010) studied the effect of network architecture and temperature on the onset of cavitation. Combining experiments and simulation, they found that while the modulus of their network increased with temperature (as expected for any unfilled rubber), the critical hydrostatic stress P_c to observe cavitation decreased markedly with temperature (figure 36(a)) in clear contradiction with earlier results from Gent and Lindley (Gent and Lindley 1959) and models based on cavity expansion by deformation alone (Hou and Abeyaratne 1992, Lopez-Pamies *et al* 2011, Lefèvre *et al* 2015).

They also presented an improved model taking into account the importance of the fracture energy Γ measured in mode I (double edge notch geometry) on the onset of cavitation. Using a penny-shape precursor crack in an infinite medium as an idealized geometry and a nonlinear constitutive model with exponential hardening as in (Seitz *et al* 2009) they were able to predict the relation between the pressure P and energy release rate $\mathcal{G}$ as a function of initial crack size. This non-linear elastic model was able to properly fit the dependence of the pressure P_c at the onset of cavitation on both the Young's modulus and the fracture energy Γ by using a constant value of the initial crack radius $r_0 = 8$ μm (figure 36(b)). The elasto-adhesive length Γ/E, (which varied between 25 and 320 μm depending on the temperature and material) is here much larger than the initial crack radius implying that nonlinear elasticity must be used to calculate $\mathcal{G}$. This result will be even more relevant for cavitation in adhesives (section 5.3) where the modulus is typically one to two orders of magnitude lower. Interestingly, the model suggests that resistance to fracture by cavitation P_c can be improved by increasing both the mode I fracture toughness Γ of the material and its degree of strain hardening which effectively reduces the applied $\mathcal{G}$ at a fixed stress level. This combination of stiffening at low λ and high value of Γ is precisely what has recently been discovered in double network gels and elastomers (Nakajima *et al* 2013b, Ducrot *et al* 2014) and will be discussed in section 7.2.

6.5. *Conclusions and some remarks on damage mechanisms*

We have seen in this section that the fracture of soft materials is inherently a multi-scale process with at least three important length scales. At the molecular level the bonds break and some energy dissipation occurs by the Lake-Thomas mechanism. If only this molecular mechanism is active (as in figure 30) the fracture process is called threshold fracture. However, in the general case two other important dissipative mechanisms are active and couple to the failure of chemical bonds. Far from the crack tip the viscoelastic nature of the soft material can dissipate energy if the applied strain rate near the crack tip is in the range of strain rates where the material is dissipative. Then locally, very close to the crack tip, but over a region of the order of 50–100 μm, the material is highly deformed and generally experiences some concomitant damage such as cavitation (section 6.3) and stringing or some diffuse bond breakage.

For natural rubber, which is able to strain crystallize, it has been known for quite a while that the crystallization ahead of a propagating crack has a significant toughening effect (Thomas and Whittle 1970, Huneau 2011). While modern x-ray techniques have allowed to map the crystallizing region and to investigate dynamic effects (Trabelsi *et al* 2002, Beurrot-Borgarino *et al* 2013, Candau *et al* 2014), a full micromechanical model is still lacking to connect the extent of strain-induced crystallization and the measured value of the fracture energy Γ.

For filled rubbers the questions becomes more complex due to the inherently heterogeneous structure of the material and the local confinement introduced by the presence of nanofillers. For example it has been shown that nanocavities can appear above a true stress of the order of 25 MPa even in uniaxial extension (Zhang *et al* 2012, 2013). The presence of such nanocavities has also recently been detected directly in front of the crack tip (Zhang *et al* 2015).

7. New trends

In this chapter, we will present and briefly discuss some new trends in adhesion and fracture of soft materials. Rather than listing the very large literature reporting novel soft materials with ever exciting new properties we will focus on three new concepts, which in our opinion deserve attention and couple polymer physics and mechanics. The first one is the use of labile bonds in solid materials, i.e. bonds that can be broken and reformed leading to self-healing properties and viscoelastic properties without permanent damage. The second concept is that of interpenetrated networks, also called double networks, where having cocontinuous networks in the material leads to tremendous increases in toughness. Finally the third concept is that of biomimetism for reversible adhesion. The investigation of the reversible adhesion of insects, lizards and other small animals has led to a wealth of new science inspired by the adhesive features occurring in nature.

7.1. Labile bonds in adhesion and fracture of soft materials

It is common to distinguish solids and liquids by their macroscopic mechanical behavior. Solids resist creep and cannot deform indefinitely without permanent damage (fracture). On the other hand liquids have the ability to flow and change shape without any permanent damage, but cannot maintain static loads for long times. Liquids only contain weak intermolecular bonds that can readily exchange, while classic soft solids, in addition to these weak bonds, contain a network of connected strong bonds that never spontaneously break and give the solid character. In between these two extremes it is possible to make materials containing also stronger bonds than the typical van der Waals bonds of liquids, but still able to be dynamic (break and reform). Materials containing such bonds of intermediate energy can self-assemble and form so-called supramolecular structures (Sijbesma *et al* 1997, Lange *et al* 1999, Cordier *et al* 2008, Aida *et al* 2012, Narita *et al* 2013) or in the case of filled systems can form dynamically the bonds between filler and polymer (Carlsson *et al* 2010, Lin *et al* 2010, Haraguchi *et al* 2011, Rose *et al* 2013).

The role of these non permanent bonds on adhesion and fracture has been the focus of much attention in the materials science community in particular because of their self-healing properties. It is an engineer's dream to design a material that can repair itself after it has been fractured and this would of course be particularly desirable for long–term performance where for example fatigue cracks can propagate slowly over time and eventually cause the catastrophic failure of the material. If mechanisms existed whereby the crack, opened by the mechanical stress, could self-heal and reform the same chemical bonds across the crack faces, the lifespan of the mechanical part would be greatly increased. Of course this self-healing property requires some molecular mobility, which is a natural property of liquids. Therefore any self-healing material must possess simultaneously the properties of solids and liquids. For a homogeneous material the diffusion coefficient D and the viscosity η are closely coupled by the Stokes-Einstein relation:

$$D\eta = \frac{k_B T}{6\pi r_H} \tag{48}$$

Where r_H is the hydrodynamic radius of the diffusing particle. Equation (48) basically states that it is very difficult to have molecular diffusion (required for healing of cracks) without flow (which is generally undesirable in solids).

Any viable strategy for self-healing must therefore break this paradox. Cordier *et al* developed a new elastomer made from oligomers connected by multiple hydrogen bonds (Cordier *et al* 2008). These oligomers are dynamic, but there is always a large number of closed bonds so that the material behaves as a solid and displays rubber elasticity while remaining completely soluble and processable like a thermoplastic. Most interesting are its self-healing properties. When the material is cut, it can be reassembled and can retrieve its original strength, as long as the surfaces are freshly cut (Maes *et al* 2012). Tack experiments have been carried out between plates and the increase in adhesion energy with time is represented in figure 37.

The claimed healing mechanism here is not interdiffusion of chains (although it must occur), but rather the reformation of supramolecular bonds across the interface until the density of bonds reaches its equilibrium bulk value after a few minutes. While such healing behavior is commonly observed with polymer melts (Jud *et al* 1981, Schach and Creton 2008), which flow at long times, the supramolecular elastomers of Cordier *et al* deform like crosslinked rubbers showing significant strain hardening as shown in figure 38.

A second example is the use of labile bonds in combination with permanent bonds (Haraguchi and Song 2007, Miquelard-Garnier *et al* 2009, Carlsson *et al* 2010, Sun *et al* 2012, Narita *et al* 2013, Rose *et al* 2013, Tuncaboylu *et al* 2013, Kean *et al* 2014, Long *et al* 2014). In this case the solid character and resistance to creep is provided by the covalent bonds, which are generally rather dilute, and the viscoelastic dissipation, which is necessary to resist fracture, is provided by the labile bonds. A particularly interesting example of this toughening mechanism is the case of nanocomposite hydrogels (Carlsson *et al* 2010, Lin *et al* 2010, 2011), where polymers can adsorb reversibly on nanoparticles and introduce dissipative mechanisms during deformation by breaking and reforming, while the permanent bonds make sure that the shape is maintained as the load is removed. This non permanent adsorption mechanism has also been recently used to obtain macroscopic adhesion between wet living tissues (Rose *et al* 2014).

The effect of such labile bonds on fracture should be twofold. On the one hand the breakable bonds should favor stress redistribution between covalent bonds and reduce stress concentration, and on the other hand each stretched chain able to break will irreversibly dissipate the elastic energy stored in the chain due to the Lake-Thomas mechanism (Long *et al* 2014) described in section 6.1. Both mechanisms should lead to increased fracture toughness and indeed this type of gel is usually more extensible and breaks at higher values of stress than an equivalent gel with covalent bonds only. Yet an important notion is that of the characteristic exchange time of the labile bonds. If the bonds can exchange much faster than the rate at which polymer chains are being stretched, they should

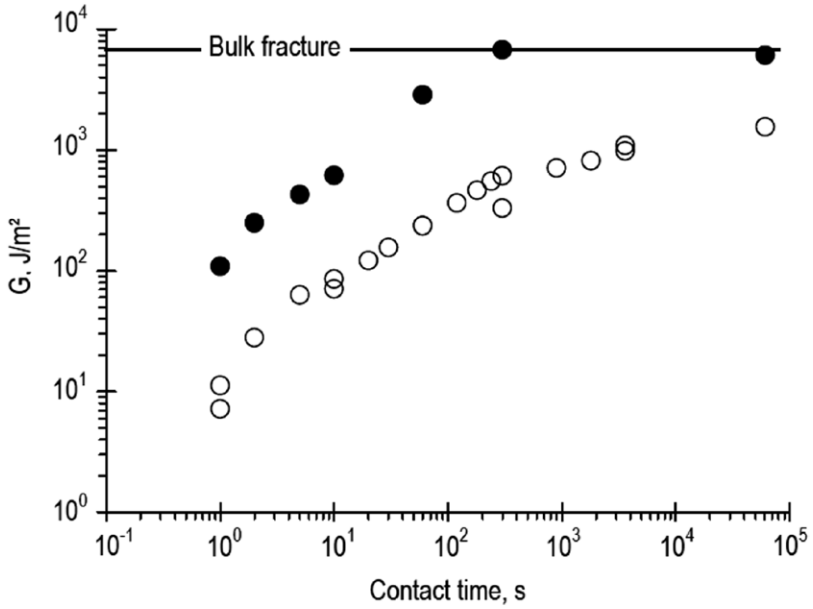

Figure 37. Fracture energy of healed supramolecular rubber as a function of contact time. Open circles represent melt pressed surfaces, while the filled circles represent freshly broken fracture surfaces. Bulk fracture is only achieved for these freshly broken surfaces. Reproduced with permission from Maes *et al* (2012; copyright 2012 Royal Society of Chemistry).

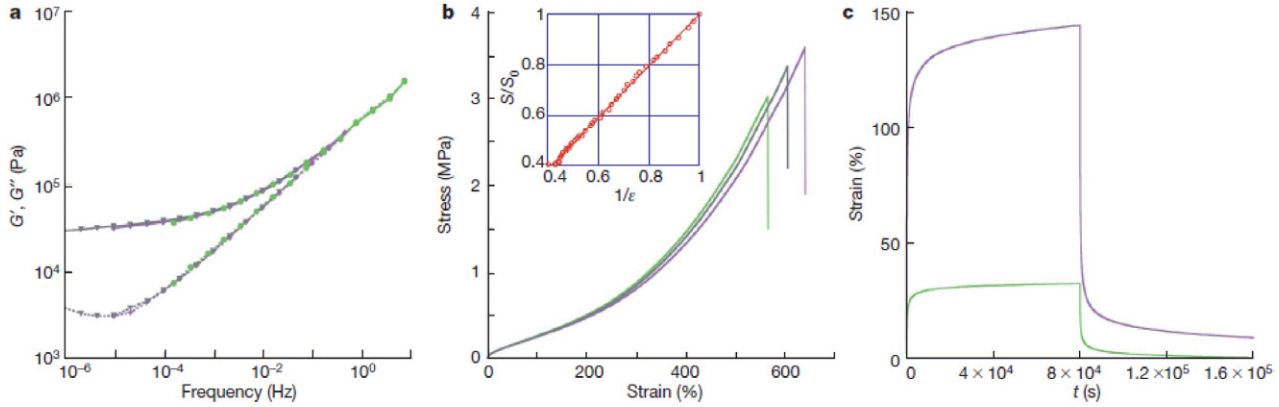

Figure 38. (a) Frequency dependence of the storage (top, μ') and loss (bottom, μ'') moduli of the supramolecular elastomer obtained by classical time–temperature superposition shifts (note that G′ and G″ are used for the storage moduli in the original figure). The reference temperature is 50 °C and measurements were performed at 50 °C (green circles), 70 °C (purple diamonds) and 90 °C (black triangles). (b) Stress–strain curve of supramolecular rubber. Data for three samples are shown. The inset shows that the cross-section area varies, as the inverse of the tensile deformation confirms incompressibility. (c) Creep–recovery experiment of the same elastomer for an applied stress of 5,000 Pa (green) and 20,000 Pa (purple). Figure reproduced with permission from Cordier *et al* (2008; copyright 2008 Nature).

be invisible, while if the strain rate is much faster than the inverse of the characteristic exchange time the labile bonds should act as permanent bonds. Systematic experiments with notched samples have only been reported in a limited number of cases and indeed an increase in the fracture energy Γ has been observed when labile and permanent bonds were present (Lin *et al* 2010). However, experiments were carried out as a function of composition rather than as a function of strain rate. It is therefore still difficult to relate the characteristic exchange time of the labile bonds with the macroscopic fracture energy.

7.2. Interpenetrated networks for fracture toughness

A particularly difficult combination of properties to obtain simultaneously is a perfectly reversible elastic behavior (with no hysteresis) and mechanical toughness. This has been for many years a very important limiting factor for hydrogels for example.

Hydrogels are extremely important in processed food but also in biological tissues and biomedical applications (Peppas *et al* 2000, Calvert 2009). From the materials point of view hydrogels are polymer networks highly swollen with water. At short times (or high strain rates) their mechanical behavior is dominated by rubber elasticity and they essentially behave as very soft rubbers. However, when immersed in water they can also exchange water with the surrounding medium in response to an applied stress (Hui and Muralidharan 2005, Cai and Suo 2012). This phenomenon, called poroelasticity, only occurs at long times for macroscopic gels. The characteristic time scale of the water exchange depends on the characteristic size of the

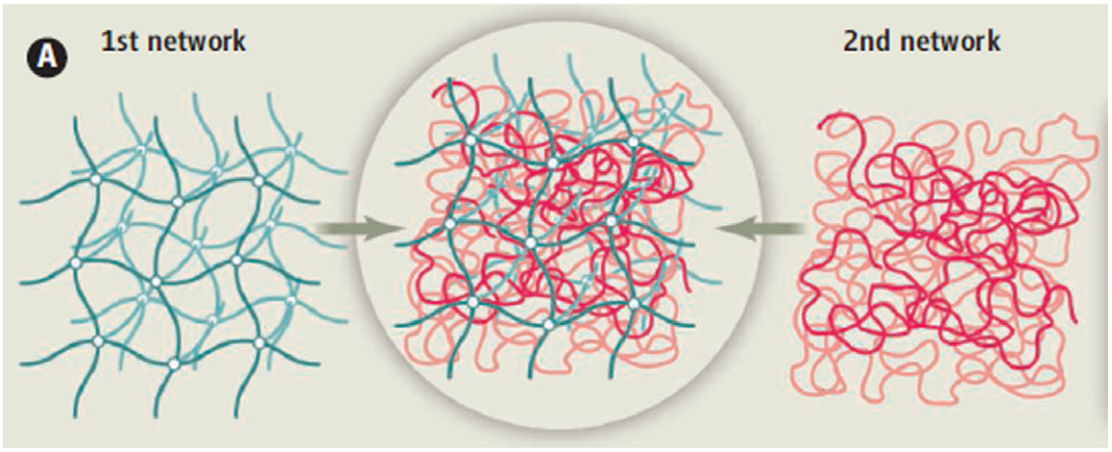

Figure 39. Schematic of the fabrication of a double network gel. The first network is initially synthesized in its Gaussian configuration. Then it is swollen in the second monomer. At this stage the first network is swollen isotropically, but the material is not tough. The second monomer is then polymerized and the interpenetrated networks are formed. Note that the second network chains are Gaussian. Reproduced with permission from Gong (2014: copyright 2014 AAAS).

system and is controlled by the so-called collective diffusion coefficient, which is typically in the range of 10^{-12} cm^2 s^{-1}.

Because they are highly swollen in water (10% polymer is typical), chemically crosslinked hydrogels are usually very elastic (Sakai *et al* 2010, Sakai 2013) and while they can be extensible, they are typically not very tough when they are notched as discussed in section 6.1. One strategy to make these chemical gels tough is to introduce viscoelastic dissipative processes, for example by introducing labile bonds as discussed in the previous section. However, this method always leads to significant strain rate dependence of the mechanical behavior even after many loading cycles and often to irreversible residual deformation upon unloading after the first cycle (Tuncaboylu *et al* 2011, 2013, Sun *et al* 2012, Rose *et al* 2013).

Jian Ping Gong and her group (Gong *et al* 2003, Tanaka *et al* 2005, Gong 2010, Ahmed *et al* 2014) have developed since 2003 a completely different toughening method, which does not rely on viscoelastic dissipation by monomer friction, but rather on irreversible dissipation (Webber *et al* 2007) by the Lake-Thomas mechanism. The synthesis of interpenetrated networks is achieved by sequences of synthesis, swelling and polymerization (Gong 2014). These interpenetrated composites are constituted of two elastic networks with different levels of prestretch and maximum extensibility. The principle is shown in figure 39. In the gels developed by Gong, one of the networks is stiff and highly prestretched, while the other is very extensible and at its reference configuration. This combination of properties leads to a simultaneous high stiffness (due to the high stress necessary to break the first network) and high extensibility controlled by the second network. A micromechanical model for the toughening effects has been proposed by Brown (Brown 2007) while Tanaka obtained similar qualitative predictions with a more macroscopic approach (Tanaka 2007).

We describe here Brown's model. As the sample is deformed, the bonds of the first network break progressively and this occurs until the first network is fully broken into pieces. This internal breaking of bonds eventually leads to the 'yielding' of the soft gel at a yield stress σ_y that is illustrated by the uniaxial step-cycle loading tensile curves carried out as a function of λ shown in figure 40 (Nakajima *et al* 2013b). Brown hypothesizes that the crack only propagates in such a gel when the elastic energy per unit volume W_{2nd} stored in the second network (once the first is broken) times the deformed thickness of the yielded zone exceeds the fracture energy of the second network alone Γ_2. This is equivalent to defining a local energy release rate in the yielded zone, in analogy with the modeling of the craze region in glassy polymers (Brown 1991). This defines a value for the maximum thickness of the deformed yielded zone at the crack tip $\lambda_{max}\, H_0$, which has been observed experimentally for such gels (Yu *et al* 2009). In the original model H_0, i.e. the undeformed thickness of the yielded zone, is given by the following expression:

$$H_0 \sim \frac{2\Gamma_2}{(\lambda_{max} - 1)^2 E_2} \tag{49}$$

where λ_{max} is the limiting extensibility of the second network. Since the fracture of the first network into pieces occurs at nearly constant stress σ_y, the macroscopic fracture energy Γ of the gel is given by:

$$\Gamma \sim \sigma_y H_0(\lambda_{max} - 1) \sim \frac{2\sigma_y \Gamma_2}{(\lambda_{max} - 1)E_2} \tag{50}$$

This model suggests that a large toughness can be obtained by combining a high yield stress (due to the breaking of the 1st network) and a low elastic modulus of the second network. This can generally obtained by a large contrast in crosslinking density between the two networks (Gong 2010, Nakajima *et al* 2013a, 2013b, Ahmed *et al* 2014). However, the detailed effect of the crosslinking density on each parameter of equation (49) is difficult to check independently and more complete data sets would be needed to validate the model.

The relevance of the toughening effect induced by the multiple network structure has been recently demonstrated to be more general by Ducrot *et al* on fully hydrophobic (and unswollen) elastomers (Ducrot *et al* 2014). Using interpenetrating networks of poly-methyl-acrylate and poly-ethyl-acrylate, they were able to increase the fracture energy of the

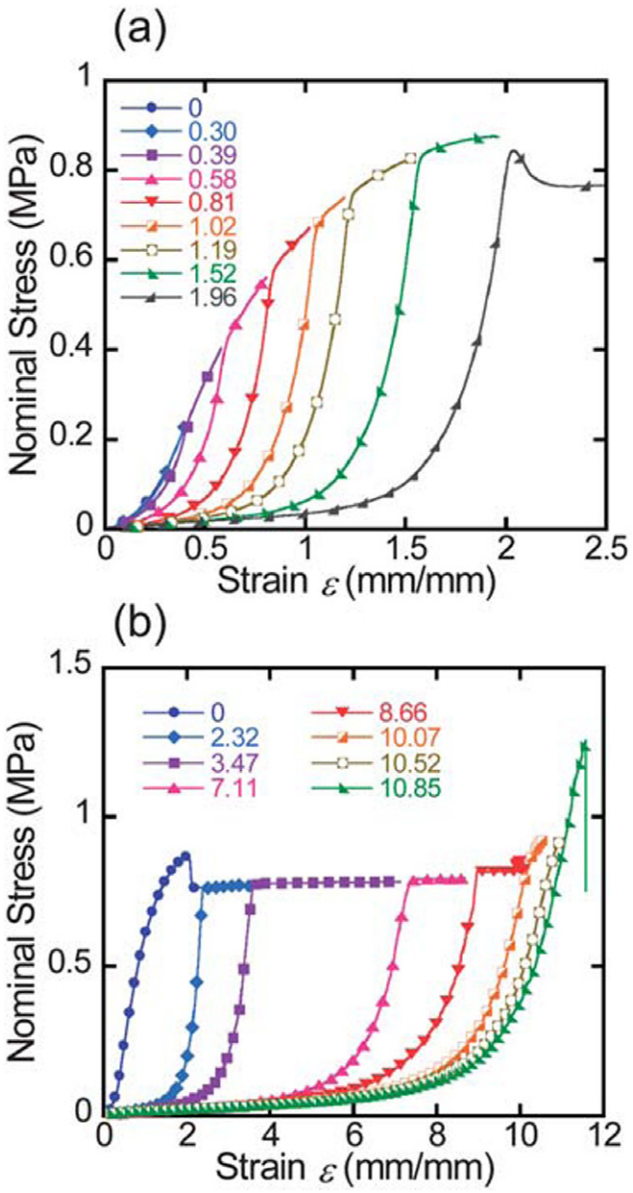

Figure 40. Tensile hysteresis loops of double network (DN) gels in (a) the pre-necking region and (b) the necking/hardening regions measured in a cyclic tensile test. The necking occurs at a well defined value of the stress. The symbol numbers denote the pre-experienced strain, ε_{max}, before measurement of each stress–strain curve. The tensile velocity was fixed at 100 mm min^{-1}. Reproduced with permission from Nakajima *et al* (2013b; copyright 2013 Royal Society of Chemistry).

original network from 50 J m^{-2} to about 2–5 kJ m^{-2} even if a necking was not obtained in uniaxial tension, since the sample rather broke before σ_y could be reached.

The mechanism of bond breakage of the first network was elegantly demonstrated and mapped spatially and temporally during crack propagation by using chemoluminescent molecules, as shown in figure 41.

Interestingly the experiments of Ducrot *et al* show that the breakdown of the first network chains occurs close to the crack tip well before the material yields macroscopically and causes a significant toughening. Moreover the size of the damage zone at the crack tip and the fracture toughness can be tuned by the respective volume fractions of the two or more networks.

7.3. *Biomimetic adhesion of soft materials*

The third recent development in the field of soft adhesives is the so-called biomimetic approach to adhesion of soft materials through a controlled topography of the surface. This topic has been extensively reviewed by others (del Campo and Arzt 2008, Meyers *et al* 2008) so we will simply highlight some fundamental working principles. In 2000, Autumn *et al* published a landmark paper on the adhesion mechanisms of gecko feet (Autumn *et al* 2000). This paper demonstrated that the gecko can bond well and quickly release the contact on a variety of surfaces with the help of millions of 50–100 nm contact spatulae as shown in figure 42. Each one of these spatulae can withstand strong forces in shear, but can be easily released if peeled off (Tian *et al* 2006). For a more recent discussion of the adhesion of gecko's sophisticated feet see (Autumn *et al* 2014) while for a discussion of adhesion and locomotion of insects see (Gorb 2008, Zhou *et al* 2014, Labonte and Federle 2015).

Although a direct copy of the structure of the gecko's feet appears impossible, several working principles have been used to design synthetic biomimetic reversible adhesives. The first important principle is the notion of contact splitting, i.e. replacing a large area of contact, which is sensitive to stress concentrations at the edges, with many small areas of contact, which are less sensitive to it (Arzt *et al* 2003, Glassmaker *et al* 2004, Hui *et al* 2004, Spolenak *et al* 2005a). This can be easily understood by using contact mechanics. The detachment force of a hemispherical contact is proportional to its radius R, while the density of hemispherical contacts per unit area scales with $1/R^2$. Hence, replacing a large contact with a great number of smaller ones leads to an enhancement of the detachment stress, which scales as the inverse of the radius R of the contacts. The efficiency of this strategy is illustrated in figure 43 for the feet of different animal species.

Since the seminal paper of Arzt *et al* (2003), highlighting design criteria, many new fibrillar surfaces have been developed to achieve reversible and relatively weak adhesion, in particular to create adhesive pads for the locomotion of robots on vertical walls or even on a ceiling (Geim *et al* 2003, Yurdumakan *et al* 2005). While the first generation of surfaces was composed of straight pillars, it was soon realized that such structures buckle and are not adapted to rough surfaces. Current improved versions use tilted soft pillars (Yang *et al* 2012), which provide some compliance and adaptability to rough surfaces, or pillars with more complex shapes such as mushroom shapes (Spolenak *et al* 2005b, Hossfeld *et al* 2013), which suppresses the stress concentrations at the edges.

A very different strategy for removable attachment pads was proposed by Crosby and coworkers (King *et al* 2014). The working principle of these pads does not rely on multicontacts, but rather on the combination of a very stiff yet flexible fabric core (which cannot easily store elastic energy under stretch but can bend), and the presence of a soft skin layer of elastomeric material (polyurethane in the original version) to provide some adhesion. This combination, which the authors call a 'draping' adhesive, provides very high detachment forces when sheared while being easily removed by peeling and can be reattached many times without surface

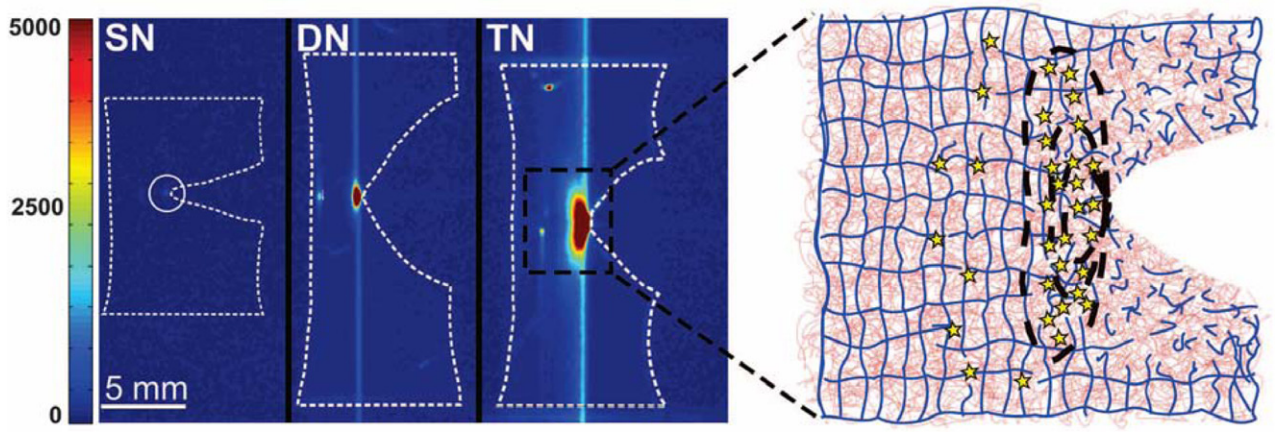

Figure 41. Intensity-colorized images of propagating cracks on notched samples containing a chemoluminescent cross-linker in the first network, showing the light emission due to the breakage of bonds in a single network (SN), double network (DN), and triple network (TN). The size and geometry of the sample are shown with a white dashed line. (Right) Schematic of the sacrificial bond-breaking mechanism in front of the crack tip for the multiple network; the first network is represented in blue, and the second and third networks are in red. Reproduced with permission from Ducrot *et al* (2014; copyright 2014 AAAS).

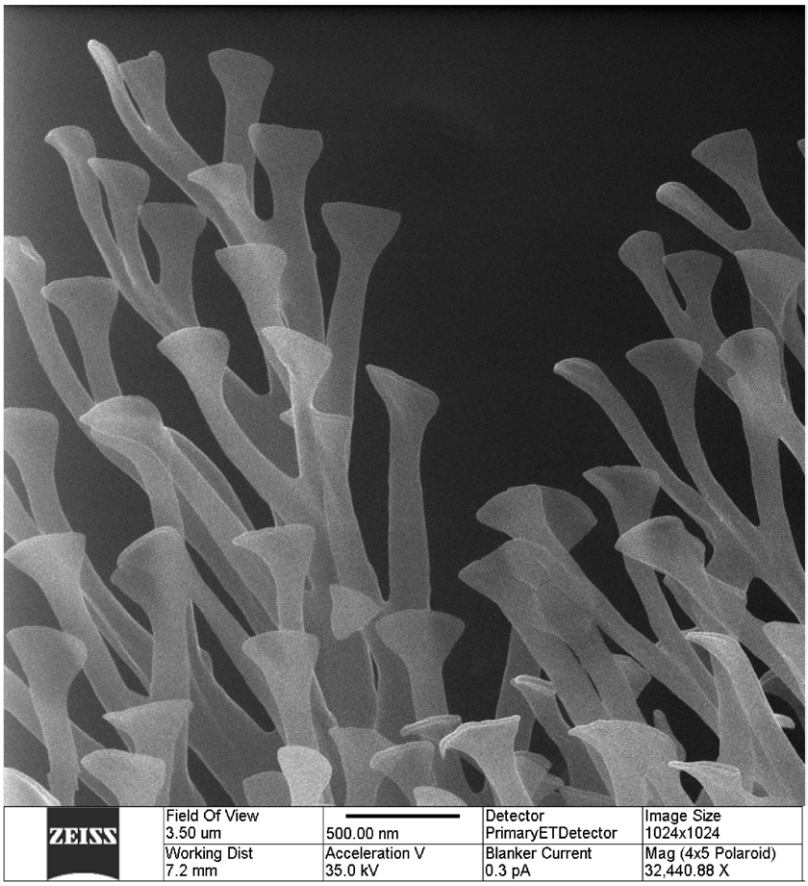

Figure 42. High resolution helium-ion image of the adhesive spatula at the tip of the gecko's feet (Autumn *et al* 2014). Courtesy of Autumn (Lewis and Clark) and Yang (Zeiss).

contamination. The high resistance to shear can be understood in analogy with the strong increase of the peeling force of PSA at vanishing angle discussed in section 5.2.

8. Unifying picture

We have tried to cover in this review a broad picture of the current state of the art in adhesion and fracture of soft materials. Although the similarities between these two processes have often been pointed out, in particular by Gent in a landmark paper (Gent 1996a), the connection was often only made between the molecular scale of the material properties and the macroscopic fracture toughness. We made a specific effort to introduce, define and discuss the importance of intermediate length scales (100 nm–100 μm) in these problems and to integrate the current understanding of the viscoelasticity and

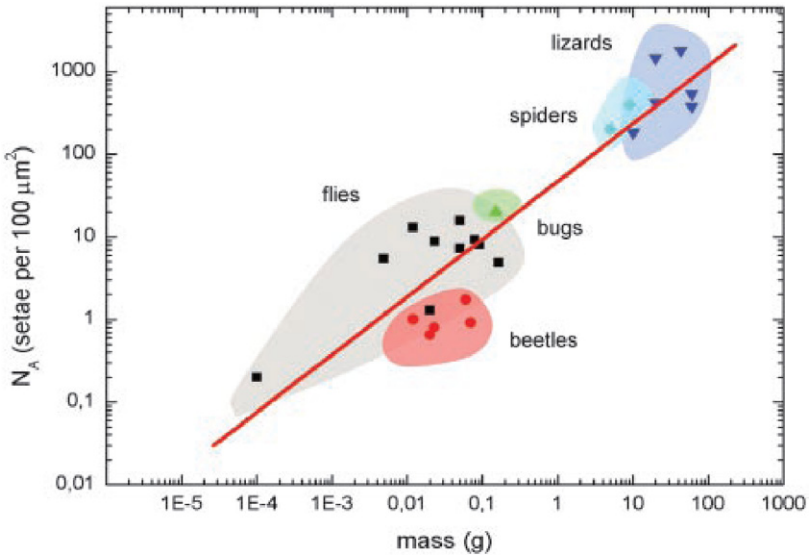

Figure 43. Dependence of the terminal element density (NA) of the attachment pads on the body mass (m) in hairy-pad systems of diverse animal groups. Figure reproduced from Arzt *et al* (2003; copyright 2003 PNAS).

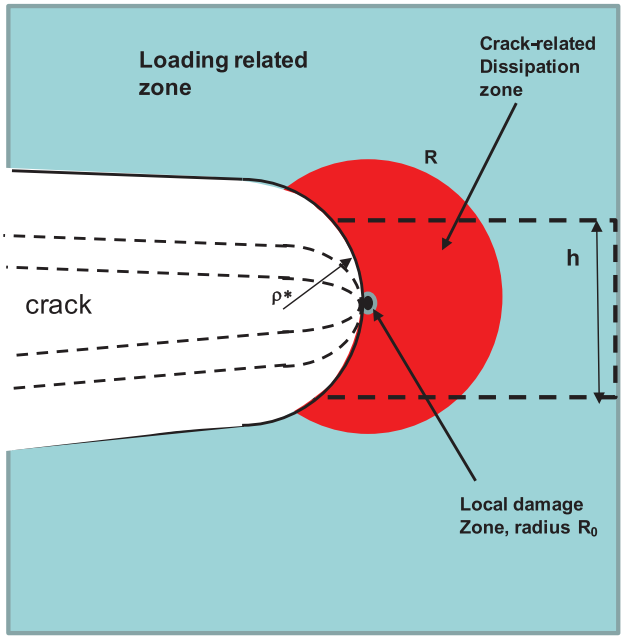

Figure 44. Schematic of a propagating crack in a soft material showing the radius of the dissipative zone R, the radius of the local damage zone R_0, the thickness of the sample h as well as several crack tip radii that also represent the size of the large strain zone.

damage mechanisms in the material at the molecular level with the mechanics of soft materials at the micron scale such as cavitation, stringiness, fibril detachment, into a global view of fracture and adhesion that can be sketched in figure 44, and applies to different length scales (macroscopic crack or debonding front, edge of a microscopic growing defect or cavity in the bulk or at the interface).

A key point of this unified picture is the spatial separation between three different scales of dissipation. Far from the crack tip, there is a zone (in light blue) where the dissipation of the material is dominated by the far-field loading conditions. If the material is elastic, no dissipation occurs in that region. The zone of size R delimited in red is the zone where the dissipation of the material is dominated by the propagation of the crack. The dissipated energy in this region is generally called Γ. Finally, the black zone of size R_0 close to the tip is where local damage and molecular fracture generally occurs, inducing an energy dissipation named Γ_{local}. For the crack to propagate, the Griffith condition must be considered independently at the two scales R and R_0, resulting in the definition of two different energy release rates, named respectively $\mathcal{G}$ and g_{local}.

Based on this general picture, we can now discuss different situations to explain the separate role played by large strains and dissipative processes. The sizes R and R_0 of the two crack related dissipative regions need to be compared with two important geometric parameters, which are the crack length c and the smallest sample size h, as well as with the size of the region affected by large strain caused by the presence of the crack tip. This is represented by the radius of the opened propagating crack ρ^*, which corresponds to the elastoadhesive length $\ell_{\text{EA}} = \frac{\Gamma}{E}$, if R remains small related to the sample thickness h.

Let's first discuss the case of a long crack in a large medium. In the case of small-scale yielding discussed in the introduction (with both large strain and dissipation limited to a small region), the energy transfer is clearly established by LEFM concepts like $\mathcal{G}$ and K and fracture propagation is determined by the condition $\mathcal{G} = \Gamma(v)$. If the dissipative region remains small (the red zone collapses into the black one), but the region where large strain is developed becomes large, i.e. if $R \ll \rho^*$, $\mathcal{G}$ can still be defined and evaluated through the method or Rivlin and Thomas or the J integral and $\mathcal{G} = \Gamma_{\text{local}}$ is a proper propagation criterion. This is the case for both the threshold fracture of elastomers (section 6.1) and reversible adhesion of elastomers to solid surfaces (section 5.3.2).

When both large strain and energy dissipation occur over a large region, i.e. $R \sim \rho^*$, alternative strategies must be found. One way to approach the problem is to define a local energy

release rate g_{local} applied to the black zone and then set the propagation criterion as $g_{local} = \Gamma_{local}$ (see section 6.3). Then the problem becomes to relate g_{local} to the energy release rate $\mathcal{G}$ applied to the red zone, which requires modeling the material response in the large strain region. The difference between the two representing the energy dissipated inside the red zone.

We remark that if the dissipation associated to the far-field loading is not negligible, the classical energy release rate $\mathcal{G}$ cannot be unambiguously defined. When the material response in this region can be considered linear viscoelastic, one convenient strategy to obtain an approximate value of $\mathcal{G}$ is to include the macroscopic relaxation of the material in the estimate of the elastic energy effectively releasable. In practice, this means using the elastic calculation for the sample and substituting the elastic modulus by $\mu'(t)$ or $\mu'(\omega)$ as discussed in section 5.3.2 and also used by Bhuyan *et al* (2013). In the cases where large deformations are relevant over the whole sample, like in fracture of pure shear samples, another strategy to better estimate $\mathcal{G}$ or g_{local} is to consider the soft elastic solution, and then estimate the strain energy density $W(\lambda)$ at the point of crack propagation by using the *unloading* stress-strain curve rather than the loading curve (section 6.3).

The review shows that elasto-adhesive length, $\ell_{EA} = \Gamma/E$ plays a unifying role between fracture and adhesion. In the bulk fracture case, we can unambiguously define a macroscopic fracture energy $\Gamma(v)$ that is a material property and is independent of sample geometry for sufficiently large samples ($\Gamma(v)/E <$ sample size). In the adhesion case, large strain and dissipation generally affect the whole thickness of the sample and the debonding does not occur any longer by the propagation of a stress singularity. Therefore, the macroscopic dissipation can only be interpreted as an apparent fracture energy $\Gamma_{app}(v)$, which critically depends on sample geometry (in particular layer thickness h). We remark that although $\Gamma_{app}(v)$ is not a material property, the condition $\Gamma_{app}(v)/E > h$ is a sufficient condition to identify this regime, since $\Gamma_{app}(v)$ is generally smaller than $\Gamma(v)$.

So far we have discussed the extension of LEFM to the propagation of macroscopic fracture in a soft dissipative material. However, a propagating macroscopic peel front or a propagating crack are often preceded by the growth of micro cracks, cavities and highly oriented fibrils. This is particularly true during debonding of very soft adhesives, but also for fracture of tough soft materials. In this review we have shown that the global picture presented above of how elastic energy flows to the crack tip and is dissipated can also be applied at smaller scale, to the propagation of microfracture defects in the bulk or at the interface, which becomes part of the damage zone at the macroscale.

At the microscopic scale, Γ_{local} can be used to construct a local elasto-adhesive length Γ_{local}/E that should be compared with the size of defects R_d in order to determine if these defects will either grow as cracks ($\Gamma_{local}/E < R_d$) or expand as bulk cavities (section 5.3.1). However at the local scale, the material properties may be quite different in particular because of the orientation of polymer fibrils in the direction of the tensile opening stresses so that E should rather be substituted by an E_{local} in the estimation of the local elasto-adhesive length.

The same reasoning can be applied to the growth of cavities in the bulk of a soft material, which should be interpreted as the propagation of a blunted crack of length $R_d < \Gamma_{local}/E_{local}$ (section 6.4).

In both these cases the detailed study of the micromechanisms of fracture (section 5.3), which vary significantly depending on the large strain properties of the materials, provides crucial information, which can then be used as input for the macroscopic propagation of a peel front (section 5.2) or a crack.

This last point brings us now to summarize the main insights on materials properties and their characterization. Clearly both the strong adhesives and tough soft materials discussed in this review require the existence of important molecular dissipative mechanisms (see section 5 and 7), coexisting with a molecular percolating network preventing macroscopic flow. In order to predict the fracture toughness of soft materials or their adhesive properties it is essential to characterize the strain-rate dependence as well as the strain dependence of these dissipative mechanisms. Uniaxial tensile experiments carried out at different strain rates are highly complementary with classical frequency dependent linear viscoelastic measurements. For polymer based soft adhesives, we propose to represent the reduced stress f^* as a function of I/λ (section 5.3.3) to separate the small-strain shear modulus μ into a permanent (C_{hard}) and non-permanent (C_{soft}) component and we propose to use these large strain parameters to draw a properties map (figure 29). Furthermore systematic cycles of loading and unloading at large strains are also essential to separate damage mechanisms from viscoelasticity for all the complex and dissipative soft materials treated in this review.

9. Open questions and conclusion

To conclude the review we propose now a discussion of some open challenges that need to be addressed to understand better these rather complex processes.

Maybe the most important experimental challenge is that of collecting better experimental data at the scale of the process zone close to the crack tip, using newly available techniques. In experimental mechanics, techniques such as (1) digital image correlation to measure displacement fields (Hild *et al* 2015), or (2) birefringence mapping to measure stresses or levels of local anisotropy, (3) or infrared observations to map temperatures changes and characterize dissipative processes, have significantly increased their spatial resolution and are better adapted to large strains, and thus hold great potential while having still been only sparsely used to characterize fracture of soft materials.

Wide angle x-ray scattering has been used in the past to characterize static strain induced crystallization (Trabelsi *et al* 2002), but recently the wide availability of synchrotrons has made it possible to carry out time-resolved experiments with unprecedented spatial resolution (Brüning *et al* 2013, Rublon *et al* 2013, Zhang *et al* 2015), which can map damaged regions around the crack tip. Local crystallization, but also nanocavitation (with small and ultra small angle x-ray

scattering) can be characterized in this way. If the heterogeneities are larger (100 nm–100 μm), x-ray computed microtomography (micro-CT) is becoming increasingly available and the reconstruction algorithms provide excellent spatial resolution when sufficient contrast in density is present (Bayraktar *et al* 2008b, Jago 2012).

At the more molecular scale mechanochemistry has proved to be a powerful technique to investigate molecular damage mechanisms in cracks. Mechanoluminescent molecules have been used to map individual bond breakage more quantitatively (Chen and Sijbesma 2014, Ducrot *et al* 2014, Kean *et al* 2014), and mechanophores are only starting to be used to map dissipative mechanisms in fracture problems (Zhang *et al* 2014).

On the modeling side many important challenges remain both on the materials modeling side and on the mechanics modeling side.

When the dissipative zone at the crack tip is affected by multiple mesoscale damage mechanisms such as cavitation, fibrillation and local fractures, the mechanical properties of the damaged materials cannot be simply predicted from the constitutive law of the undamaged material. These mechanisms should either be treated in detail as an evolving structure or by a suitable homogeneization procedure that includes the details of the damage into an effective constitutive law. This is currently still rarely done for soft materials, but a combination of detailed characterization of large strain properties and creative modeling strategies should be the way to progress in this area.

A more philosophical question underlying all the discussed approaches is the level of separability between the energy dissipated in the bulk deformation (the blue zone of figure 44) and an energy dissipation mechanism Γ (the red zone of figure 44) that can be unambiguously related to the propagation of a crack, this concept is so far only empirically validated on a limited number of systems and a general framework is missing.

Somewhat related to the above is the correct criterion for the detachment from the surface or breakage in the bulk of a microscopic and highly strained fibril. At the molecular scale, fracture of a covalent bond should be stress related as demonstrated for example by AFM single molecule experiments (Merkel *et al* 1999), fracture of single molecules in flow (Nguyen *et al* 1997) or fracture of block copolymers at the interface between glassy polymers (Creton *et al* 2002). However, when it comes to a micron scale soft viscoelastic fibril, should we consider a stress or an energy based criterion? In this case the difficulty lies in the combination of poorly defined geometry of the fibril and complex material properties, which makes even estimating the local stress or a g_{local} very difficult.

As discussed above in addition to the mesoscopic damage mechanisms such as cavitation and microcracks, the material itself dissipates energy in a non-trivial way when deformed in large strain. The molecular origin of this dissipation is generally either molecular viscosity (nonlinear viscoelasticity) or damage through irreversible breakage of polymer chains (Lake-Thomas mechanism). More recently the use of reversible labile bonds (also referred to as sacrificial bonds), which are able to break under stress and reform and hence dissipate energy as discussed in section 7 also called sacrificial bonds have been introduced in soft materials (Sun *et al* 2012, Grande *et al* 2015). Although some level of permanent bonds is probably necessary to avoid creep, the optimum ratio of reversible to permanent bonds to maximize Γ is a subject of current study, as is the effect of the characteristic rate at which these sacrificial bonds can break and reform.

Although we limited our review to soft solids, which do not flow at long times, the distinction between soft viscoelastic solids and viscoelastic fluids can be subtle at short or intermediate times. Soft adhesives actually combine large strain non-linear elasticity with significant viscoelasticity and lie exactly at the interface between liquids (with which they share the deformability and strong strain rate dependent behavior) and soft elastic solids (with which they share the capability to store elastic energy and the finite deformability). Two modeling options are then possible: (1) keeping a clear reference configuration and introducing a time-dependent viscoelastic behavior into a non-linear elastic model or (2) modeling a fluid and introducing elasticity as a time-dependent additional stress tensor. Some recent efforts to combine both approaches (Glassmaker *et al* 2008, Deplace *et al* 2009a, Padding *et al* 2011, 2012) are promising but the field is still in its infancy.

Overall we feel that after many years of relative stagnation, a strong interest in the mechanics of soft living and artificial tissues in biology and medicine combined with a push toward developing stronger and lighter structures in industry, has fueled an increasing number of materials science studies creating new materials with improved mechanical properties. Yet the understanding of how soft materials can combine strength and toughness with a low elastic modulus and a large reversible deformability remains incomplete and will be the key to develop new applications such as soft robots, artificial muscles or transparent ionically conducting materials. New experimental, analysis and modeling techniques powered by the progress in electronics and software can now give unprecedented time and space resolved information on the structure, dynamics and damage mechanisms in soft materials and we feel that there are outstanding opportunities for curious physicists to enter the field and make a significant contribution.

Acknowledgments

We thank Herbert Hui for a helpful suggestion on presenting Hugh Brown' model and Ken Shull for his careful reading of the manuscript and very helpful suggestions.

References

Ahagon A and Gent A N 1975a Effect of interfacial bonding on the strength of adhesion *J. Polym. Sci. Polym. Phys. Ed.* **13** 1285–300

Ahagon A and Gent A N 1975b Threshold fracture energies for elastomers *J. Polym. Sci. Polym. Phys. Ed.* **13** 1903–11

Ahmed S, Nakajima T, Kurokawa T, Anamul Haque M and Gong J P 2014 Brittle–ductile transition of double network hydrogels: Mechanical balance of two networks as the key factor *Polymer* **55** 914–23

Ahn D and Shull K R 1998a Effects of methylation and neutralization of carboxylated poly(n-butyl acrylate)on the interfacial and bulk contributions to adhesion *Langmuir* **14** 3637–45

Ahn D and Shull K R 1998b Effects of substrate modification on the interfacial adhesion of acrylic elastomers *Langmuir* **14** 3646–54

Aida T, Meijer E W and Stupp S I 2012 Functional supramolecular polymers *Science* **335** 813–7

Akagi Y, Sakurai H, Gong J P, Chung U-I and Sakai T 2013 Fracture energy of polymer gels with controlled network structures *J. Chem. Phys.* **139** 144905

Amouroux N, Petit J and Léger L 2001 Role of interfacial resistance to shear stress and adhesive peel strength *Langmuir* **17** 6510–7

Andrews E H 1961 Stresses at a crack in an elastomer *Proc. Phys. Soc. London* **77** 483–98

Andrews E H and Kinloch A J 1973a Mechanics of adhesive failure I. *Proc. R. Soc.* A **332** 385–99

Andrews E H and Kinloch A J 1973b Mechanics of adhesive failure II *Proc. R. Soc.* A **332** 401–14

Andrews E H and Kinloch A J 1974 Mechanics of elastomeric adhesion *J. Polym. Sci. Polym. Symp.* **46** 1–14

Arzt E, Gorb S and Spolenak R 2003 From micro to nano contacts in biological attachment devices *Proc. Natl Acad. Sci.* **100** 10603–6

Aubrey D W and Sherriff M 1980 Peel adhesion and viscoelasticity of rubber-resin blends *J. Polym. Sci. Poly. Chem. Ed.* **18** 2597–608

Autumn K, Liang Y A, Hsieh S T, Zesch W, Chan W P, Kenny T W, Fearing R and Full R J 2000 Adhesive force of a single gecko foot-hair *Nature* **405** 681–5

Autumn K, Niewiarowski P H and Puthoff J B 2014 Gecko adhesion as a model system for integrative biology, interdisciplinary science, and bioinspired engineering *Annu. Rev. Ecol. Evol. Syst.* **45** 445–70

Ball J M 1982 Discontinuous equilibrium solutions and cavitation in non-linear elasticity *Phil. Trans. R. Soc.* A **306** 557–611

Baney J M, Hui C-H and Cohen C 2001 Experimental investigations of a stress intensity factor based description of the adhesion of viscoelastic materials *Langmuir* **17** 681–7

Barquins M and Maugis D 1988 Stick-slip and peeling of adhesive tapes *Adhesion* ed K W Allen vol 12 (London: Elsevier)

Barthel E and Fretigny C 2009 Adhesive contact of elastomers: effective adhesion energy and creep function. *J. Phys. D: Appl. Phys.* **42** 195302

Barthel E and Haiat G 2002 Approximate model for the adhesive contact of viscoelastic spheres *Langmuir* **18** 9362–70

Baumberger T, Caroli C and Martina D 2006a Fracture of a biopolymer gel as a viscoplastic disentanglement process *Eur. Phys. J.* E **21** 81–9

Baumberger T, Caroli C and Martina D 2006b Solvent control of crack dynamics in a reversible hydrogel *Nat. Mater.* **5** 552–5

Baumberger T and Ronsin O 2010 A convective instability mechanism for quasistatic crack branching in a hydrogel *Eur. Phys. J.* E **31** 51–58

Bayraktar E, Bessri K and Bathias C 2008a Deformation behaviour of elastomeric matrix composites under static loading conditions *Eng. Fract. Mech.* **75** 2695–706

Bayraktar E, Isac N, Bessri K and Bathias C 2008b Damage mechanisms in natural (Nr) and synthetic rubber (Sbr): nucleation, growth and instability of the cavitation*. *Fatigue Fract. Eng. Mater. Struct.* **31** 184–96

Bellamine A, Degrandi E, Gerst M, Stark R, Beyers C and Creton C 2011 Design of nanostructured waterborne adhesives with improved shear resistance *Macromol. Mater. Eng.* **296** 31–41

Benyahia L, Verdier C and Piau J M 1997 The mechanisms of peeling of uncross-linked pressure sensitive adhesives *J. Adhes.* **62** 45–73

Beurrot-Borgarino S, Huneau B, Verron E and Rublon P 2013 Strain-induced crystallization of carbon black-filled natural rubber during fatigue measured by *in situ* synchrotron x-ray diffraction *Int. J. Fatigue* **47** 1–7

Beurrot S, Huneau B and Verron E 2010 *In situ* sem study of fatigue crack growth mechanism in carbon black-filled natural rubber *J. Appl. Polym. Sci.* **117** 1260–9

Bhowmick A. K 1986 Tear strength of elastomers over a range of rates, temperatures and cross-linking—tearing energy-spectra *J. Mater. Sci.* **21** 3927–32

Bhowmick A K 1988 Threshold fracture of elastomers *J. Macromol. Sci. Rev. Macromol. Chem. Phys.* **C28** 339–70

Bhowmick A K, Gent A N and Pulford C T R 1983 Tear strength of elastomers under threshold conditions *Rubber Chem. Technol.* **56** 226–32

Bhuyan S, Tanguy F, Martina D, Lindner A, Ciccotti M and Creton C 2013 Crack propagation at the interface between soft adhesives and model surfaces studied with a sticky wedge test *Soft Matter* **9** 6515–24

Bird R B, Armstrong R C and Hassager O 1987 *Dynamics of Polymeric Liquids: Vol 1 Fluid Mechanics* (New York: Wiley)

Biwa S 2006 Cavitation in finite elasticity with surface energy effects *Int. J. Non-Linear Mech.* **41** 1084–94

Bouchaud E and Paun F 1999 Fracture and damage at a microstructural scale *Comput. Sci. Eng.* **1** 32–8

Briggs L J 1950 Limiting negative pressure of water *J. Appl. Phys.* **21** 721–2

Briggs L J 1951 The limiting negative pressure of acetic acid, benzene, aniline, carbon tetrachloride, and chloroform *J. Chem. Phys.* **19** 970–2

Brown H R 1991 A molecular interpretation of the toughness of glassy polymers *Macromolecules* **24** 2752–6

Brown H R 1993 Effects of chain pull-out on adhesion of elastomers *Macromolecules* **26** 1666–70

Brown H R 2007 A model of the fracture of double network gels *Macromolecules* **40** 3815–18

Brown K R and Creton C 2002 Nucleation and growth of cavities in soft viscoelastic layers under tensile stress *Eur. Phys. J.* E **9** 35–40

Brown K, Hooker J C and Creton C 2002 Micromechanisms of tack of soft adhesives based on styrenic block copolymers *Macromol. Mater. Eng.* **287** 163–79

Brüning K, Schneider K, Roth S V and Heinrich G 2013 Strain-induced crystallization around a crack tip in natural rubber under dynamic load *Polymer* **54** 6200–5

Busse W F 1938 Physics of rubber as related to the automobile *J. Appl. Phys.* **9** 438–51

Butler G L 1989 Natural rubber adhesives *Handbook of Pressure Senstitive Adhesive Technology* ed D Satas (Princeton, NJ: Van Nostrand-Reinhold)

Cai S and Suo Z 2012 Equations of state for ideal elastomeric gels *Europhys. Lett.* **97** 34009

Calvert P 2009 Hydrogels for soft machines *Adv. Mater.* **21** 743–56

Candau N, Laghmach R, Chazeau L, Chenal J M, Gauthier C, Biben T and Munch E 2014 Strain-induced crystallization of natural rubber and cross-link densities heterogeneities *Macromolecules* **47** 5815–24

Carlsson L, Rose S, Hourdet D and Marcellan A 2010 Nano-hybrid self-crosslinked pdma/silica hydrogels *Soft Matter* **6** 3619–31

Chang W J and Pan J 2001 Cavitation instability in rubber with consideration of failure *J. Mater. Sci.* **36** 1901–9

Chaudhury M K and Pocius A V eds 2002 *Surfaces, Chemistry and Applications* (Amsterdam: Elsevier)

Chen Y and Sijbesma R P 2014 Dioxetanes as mechanoluminescent probes in thermoplastic elastomers *Macromolecules* **47** 3797–805

Chiche A, Dollhofer J and Creton C 2005a Cavity growth in soft adhesives *Eur. Phys. J.* E **17** 389–401

Chiche A, Pareige P and Creton C 2000 Role of surface roughness in controlling the adhesion of a soft adhesive on a hard surface *C. R. Acad. Sci. Paris IV* **1** 1197–204

Chiche A, Zhang W H, Stafford C M and Karim A 2005b A new design for high-throughput peel tests: statistical analysis and example *Meas. Sci. Technol.* **16** 183–90

Chikina I and Gay C 2000 Cavitation in adhesives *Phys. Rev. Lett.* **85** 4546–9

Cho K and Gent A N 1988 Cavitation in model elastomeric composites *J. Mater. Sci.* **23** 141–4

Cho K, Gent A N and Lam P S 1987 Internal fracture in an elastomer containing a rigid inclusion *J. Mater. Sci.* **22** 2899–905

Christensen R M and Wu E M 1981 A theory of crack growth in viscoelastic materials *Eng. Fract. Mech.* **14** 215–25

Ciccotti M, Giorgini B, Vallet D and Barquins M 2004 Complex dynamics in the peeling of an adhesive tape *Int. J. Adhes. Adhes.* **24** 143–51

Cordier P, Tournilhac F, Soulie-Ziakovic C and Leibler L 2008 Self-healing and thermoreversible rubber from supramolecular assembly *Nature* **451** 977–80

Creton C 2003 Pressure-sensitive-adhesives: an introductory course *MRS Bull.* **28** 434–9

Creton C, Brown H R and Shull K R 1994 Molecular weight effects in chain pullout *Macromolecules* **27** 3174–83

Creton C and Fabre P 2002 Tack *The Mechanics of Adhesion* ed D A Dillard and A V Pocius (Amsterdam: Elsevier)

Creton C, Hooker J C and Shull K R 2001 Bulk and interfacial contributions to the debonding mechanisms of soft adhesives: extension to large strains *Langmuir* **17** 4948–54

Creton C, Hu G J, Deplace F, Morgret L and Shull K R 2009 Large-strain mechanical behavior of model block copolymer adhesives *Macromolecules* **42** 7605–15

Creton C, Kramer E J, Brown H R and Hui C Y 2002 Adhesion and fracture of interfaces between immiscible polymers: from the molecular to the continuum scale *Adv. Polym. Sci.* **156** 53–136

Creton C and Lakrout H 2000 Micromechanics of flat probe adhesion tests of soft viscoelastic polymer films *J. Polym. Sci.* B **38** 965–79

Creton C and Leibler L 1996 How does tack depend on time of contact and contact pressure? *J. Polym. Sci.* B **34** 545–54

Creton C, Roos A and Chiche A 2005 Effect of the diblock content on the adhesive and deformation properties of Psas based on styrenic block copolymers *Adhesion: Current Research and Applications* ed W G Possart (Weinheim: Wiley-Vch)

Cristiano A, Marcellan A, Keestra B J, Steeman P and Creton C 2011 Fracture of model polyurethane elastomeric networks *J. Polym. Sci.* B **49** 355–67

Cristiano A, Marcellan A, Long R, Hui C Y, Stolk J and Creton C 2010 An experimental investigation of fracture by cavitation of model elastomeric networks *J. Polym. Sci. B Polym. Phys.* **48** 1409–22

Crosby A J and Shull K R 1999a Adhesive failure analysis of pressure-sensitive adhesives *J. Polym. Sci.* B **37** 3455–72

Crosby A J and Shull K R 1999b Debonding mechanisms of pressure-sensitive-adhesives *22nd Annual Meeting* (Panama City: The Adhesion Society) pp 320–2

Crosby A J, Shull K R, Lakrout H and Creton C 2000 Deformation modes of adhesively bonded elastic layers *J. Appl. Phys.* **88** 2956–66

Dahlquist C A 1969 Pressure-sensitive adhesives *Treatise on Adhesion and Adhesives* ed R L Patrick (New York: Dekker)

Dale W C, Paster M D and Haynes J K 1989 Mechanical properties of acrylic pressure-sensitive adhesives and their relationships to industry standard testing *J. Adhes.* **31** 1–20

Daoulas K, Theodorou D N, Roos A and Creton C 2004 Experimental and self-consistent field theoretical study of styrene block copolymer self-adhesive materials *Macromolecules* **37** 5093–109

De D and Gent A N 1996 Tear strength of carbon-black-filled compounds *Rubber Chem. Technol.* **69** 834–50

De Gennes P G 1979 *Scaling Concepts in Polymer Physics* (Ithaca, NY: Cornell University Press)

De Gennes P G 1988 Fracture d'un adhésif faiblement réticulé *C. R. Acad. Sci. Paris II* **307** 1949–53

De Gennes P G 1989 Weak adhesive junctions *J. Phys.* **50** 2551–62

De Gennes P G 1996 Soft adhesives *Langmuir* **12** 4497–500

De Gennes P G 1997 *Soft Interfaces* (Cambridge: Cambridge University Press)

De Gennes P G and Troian S M 1990 Sur la fracture des adhésifs caoutchoutiques *C. R. Acad. Sci. Paris II* **311** 389–92

Degrandi-Contraires E, Lopez A, Reyes Y, Asua J M and Creton C 2013 High shear strength waterborne polyurethane/acrylic soft adhesives *Macromol. Mater. Eng.* **298** 612–23

Degrandi-Contraires E, Udagama R, Bourgeat-Lami E, Mckenna T, Ouzineb K and Creton C 2011 Mechanical properties of adhesive films obtained from pu-acrylic hybrid particles *Macromolecules* **44** 2643–52

Del Campo A and Arzt E 2008 Fabrication approaches for generating complex micro- and nanopatterns on polymeric surfaces *Chem. Rev.* **108** 911–45

Deplace F, Carelli C, Langenfeld A, Rabjohns M A, Foster A B, Lovell P A and Creton C 2009a Controlled sparse and percolating cross-linking in waterborne soft adhesives *ACS Appl. Mater. Interfaces* **1** 2021–29

Deplace F, Carelli C, Mariot S, Retsos H, Chateauminois A, Ouzineb K and Creton C 2009b Fine tuning the adhesive properties of a soft waterborne adhesive from rheological measurements *J. Adhes.* **85** 18–54

Deplace F, Rabjohns M A, Yamaguchi T, Foster A B, Carelli C, Lei C H, Ouzineb K, Keddie J L, Lovell P A and Creton C 2009c Bottom-up design of a soft-soft nanocomposite from polymer colloid particles *Soft Matter* **5** 1440–7

Derail C, Allal A, Marin G and Tordjeman P 1997 Relationship between viscoelastic and peeling properties of model adhesives. Part 1. Cohesive fracture *J. Adhes.* **61** 123–57

Derail C, Allal A, Marin G and Tordjeman P 1998 Relationship between viscoelastic and peeling properties of model adhesives. Part 2. The interfacial fracture domains *J. Adhes.* **68** 203–28

Derail C, Cazenave M N, Gibert F X, Marin G, Kappes N and Lechat J 2004 Rheological properties of hot-melt pressure-sensitive adhesive (hmpsas) based on styrene-isoprene copolymers. Part 2: innovative molecular design from predictive formulation *J. Adhes.* **80** 1131–51

Deruelle M, Hervet H, Jandeau G and Léger L 1998 Some remarks on Jkr experiments *J. Adhes. Sci. Technol.* **12** 225–47

Doi M and Edwards S F 1986 *The Theory of Polymer Dynamics* (Oxford: Oxford University Press)

Dollhofer J, Chiche A, Muralidharan V, Creton C and Hui C Y 2004 Surface energy effects for cavity growth and nucleation in an incompressible neo-Hookean material—modeling and experiment *Int. J. Solids Struct.* **41** 6111–27

Ducrot E, Chen Y, Bulters M, Sijbesma R P and Creton C 2014 Toughening elastomers with sacrificial bonds and watching them break *Science* **344** 186–9

Dugdale D S 1960 Yielding of steel sheets containing slits *J. Mech. Phys. Solids* **8** 100–4

Edwards S F and Vilgis T A 1988 The tube model-theory of rubber elasticity *Rep. Prog. Phys.* **51** 243–97

Erb R A and Hanson R S 1960 The tensile strength and tacky behavior of polymeric liquids *Trans. Soc. Rheol.* **4** 91–116

Feldstein M M, Kulichikhin V G, Kotomin S V, Borodulina T A, Novikov M B, Roos A and Creton C 2006 Rheology of poly(N-vinyl pyrrolidone)-poly(ethylene glycol) adhesive blends under shear flow *J. Appl. Polym. Sci.* **100** 522–37

Ferrari F, Bertoni M, Bonferoni M C, Rossi S, Caramella C and Waring M J 1995 Comparative-evaluation of hydrocolloid dressings by means of water-uptake and swelling force measurements 2. *Int. J. Pharmaceutics* **117** 49–55

Fond C 2001 Cavitation criterion for rubber materials: a review of void-growth models *J. Polym. Sci.* B **39** 2081–96

Foster A B, Lovell P A and Rabjohns M A 2009 Control of adhesive properties through structured particle design of water-borne pressure-sensitive adhesives *Polym.* **50** 1654–70

Fuller K N G and Tabor D 1975 The effect of surface roughness on the adhesion of elastic solids *Proc. R. Soc.* A **A345** 327–42

Ganghoffer J F and Gent A N 1995 Adhesion of a rigid punch to a thin elastic layer *J. Adhes.* **48** 75–84

Ganghoffer J F and Schultz J 1995 A new theoretical approach to cavitation in rubber *Rubber Chem. Technol.* **68** 757–72

Gardon J L 1963a Peel adhesion. I. Some phenomenological aspects of the test. *J. Appl. Polym. Sci.* **7** 625–41

Gardon J L 1963b Peel adhesion. II. A theoretical analysis *J. Appl. Polym. Sci.* **7** 643–65

Gay C 2002 Stickiness—some fundamentals of adhesion *Integr. Comp. Biol.* **42** 1123–6

Gay C and Leibler L 1999 Theory of tackiness *Phys. Rev. Lett.* **82** 936–9

Geim A K, Dubonos S V, Grigorieva I V, Novoselov K S, Zhukov A A and Shapoval S Y 2003 Microfabricated adhesive mimicking gecko foot-hair *Nat. Mater.* **2** 461–3

Gent A N 1990 Cavitation in rubber: a cautionary tale *Rubber Chem. Technol.* **63** 49–53

Gent A N 1994 Compression of rubber blocks *Rubber Chem. Technol.* **67** 549–58

Gent A N 1996a Adhesion and strength of viscoelastic solids Is there a relationship between adhesion and bulk properties? *Langmuir* **12** 4492–6

Gent A N 1996b A new constitutive relation for rubber *Rubber Chem. Technol.* **69** 59–61

Gent A N and Kaang S Y 1987 Effect of peel angle upon peel force *J. Adhes.* **24** 173–81

Gent A N, Lai S M, Nah C and Wang C 1994 Viscoelastic effects in cutting and tearing rubber *Rubber Chem. Technol.* **67** 610–8

Gent A N and Lindley P B 1959 Internal rupture of bonded rubber cylinders in tension *Proc. R. Soc.* A **249** 195–205

Gent A N, LindleyP B and Thomas A G 1965 Cut growth and fatigue of rubbers. I. The relationship between cut growth and fatigue *Rubber Chem. Technol.* **38** 292–300

Gent A N and Petrich R P 1969 Adhesion of viscoelastic materials to rigid substrates *Proc. R. Soc.* A **310** 433–48

Gent A N and Schultz J 1972 Effect of Wetting Liquids on the strength of adhesion of viscoelastic materials *J. Adhes.* **3** 281–294

Gent A N and Tobias R H 1982 Threshold tear strength of elastomers *J. Polym. Sci. Polym. Phys. Ed.* **20** 2051–8

Gent A N and Tompkins D A 1969 Nucleation and growth of gas bubbles in elastomers *J. Appl. Phys.* **40** 2520–5

Gent A N and Wang C 1991 Fracture mechanics and cavitation in rubber-like solids *J. Mat. Sci* **26** 3392–5

Geubelle P and Knauss W 1994. Finite strains at the tip of a crack in a sheet of hyperelastic material: I. Homogeneous case *J. Elast.* **35** 61–98

Gibert F X, Allal A, Marin G and Derail C 1999 Effect of the rheological properties of industrial hot-melt and pressure-sensitive adhesives on the peel behavior. *J. Adhes. Sci. Technol.* **13** 1029–44

Gibert F X, Marin G, Derail C, Allal A and Lechat J 2003 Rheological properties of hot melt pressure-sensitive adhesives based on styrene-isoprene copolymers. Part 1: a rheological model for Sis-Si formulations *J. Adhes.* **79** 825–52

Giesekus H 1982 A simple constitutive equation for polymer fluids based on the concept of deformation-dependent tensorial mobility *J. Non-Newton. Fluid Mech.* **11** 69–109

Glassmaker N J, Hui C Y, Yamaguchi T and Creton C 2008 Detachment of stretched viscoelastic fibrils *Eur. Phys. J.* E **25** 253–266

Glassmaker N J, Jagota A, Hui C Y and Kim J 2004 Design of biomimetic fibrillar interfaces: 1. Making contact *J. R. Soc. Interface* **1** 23–33

Gong J P 2010 Why are double network hydrogels so tough? *Soft Matter* **6** 2583–90

Gong J P 2014 Materials both tough and soft *Science* **344** 161–2

Gong J P, Katsuyama Y, Kurokawa T and Osada Y 2003 Double-network hydrogels with extremely high mechanical strength *Adv. Mater.* **15** 1155–8

Gorb S N 2008 Biological attachment devices: exploring nature's diversity for biomimetics *Phil. Trans. R. Soc.* A **366** 1557–74

Gower M D and Shanks R A 2004a The effect of chain transfer agent level on adhesive performance and peel master-curves for acrylic pressure sensitive adhesives *Macromol. Chem. Phys.* **205** 2139–50

Gower M D and Shanks R A 2004b The effect of varied monomer composition on adhesive performance and peeling master curves for acrylic pressure-sensitive adhesives *J. Appl. Polym. Sci.* **93** 2909–17

Gower M D and Shanks R A 2005 Comparison of styrene with methyl methacrylate copolymers on the adhesive performance and peeling master curves of acrylate pressure sensitive adhesives *Macromol. Chem. Phys.* **206** 1015–27

Gower M D and Shanks R A 2006 Acrylic acid level and adhesive performance and peel master-curves of acrylic pressure-sensitive adhesives *J. Polym. Sci.* B **44** 1237–52

Grande A M, Garcia S J and Van Der Zwaag S 2015 On the interfacial healing of a supramolecular elastomer *Polymer* **56** 435–42

Green A E and Zerna W 1954 *Theoretical Elasticity* (Oxford: Oxford University Press)

Greensmith H W 1960 Rupture of rubber. VII. Effect of rate of extension in tensile tests *J. Appl. Polym. Sci.* **3** 175–82

Greensmith H W 1963 Rupture of rubber. X. The change in stored energy on making a small cut in a test piece held in simple extension. *J. Appl. Polym. Sci.* **7** 993–1002

Greensmith H W, Mullins L and Thomas A G 1960 Rupture of rubber *Trans. Soc. Rheol.* **4** 179–89

Greenwood J A and Williamson J B P 1966 Contact of nominally flat surfaces *Proc. R. Soc.* A **A295** 300–19

Griffith A A 1920 *Phil. Trans. R. Soc.* A **A221** 163–98

Haiat G, Phan Huy M C and Barthel E 2002 The adhesive contact of viscoelastic spheres *J. Mech. Phys. Solids* **51** 69–99

Han K, Ciccotti M and Roux S 2010 Measuring nanoscale stress intensity factors with an atomic force microscope *Europhys. Lett.* **89** 66003

Haque M A, Kurokawa T and Gong J P 2012 Anisotropic hydrogel based on bilayers: color, strength, toughness, and fatigue resistance *Soft Matter* **8** 8008–16

Haraguchi K and Song L 2007 Microstructures formed in co-cross-linked networks and their relationships to the optical and mechanical properties of pnipa/clay nanocomposite gels *Macromolecules* **40** 5526–36

Haraguchi K, Uyama K and Tanimoto H 2011 Self-healing in nanocomposite hydrogels *Macromol. Rapid Commun.* **32** 1253–8

Hild F, Bouterf A and Roux S 2015 Damage measurements via dic *Int. J. Fract.* **191** 77–105

Horgan C O and Polignone D A 1995 Cavitation in nonlinearly elastic solids: a review *Appl. Mech. Rev.* **48** 471–85

Hossfeld C K, Schneider A S, Arzt E and Frick C P 2013 Detachment behavior of mushroom-shaped fibrillar adhesive surfaces in peel testing *Langmuir* **29** 15394–404

Hou H S and Abeyaratne R 1992 Cavitation in elastic and elastic plastic solids *J. Mech. Phys. Solids* **40** 571–92

Hui C-Y and Muralidharan V 2005 Gel mechanics: a comparison of the theories of Biot and Tanaka, Hocker, and Benedek *J. Chem. Phys.* **123** 154905

Hui C Y, Glassmaker N J, Tang T and Jagota A 2004 Design of biomimetic fibrillar interfaces: 2. Mechanics of enhanced adhesion *J. R. Soc. Interface* **1** 35–48

Hui C Y, Jagota A, Bennison S J and Londono J D 2003 Crack blunting and the strength of soft elastic solids. *Proc. R. Soc.* A **403** 1489–516

Hui C Y, Lin Y Y and Baney J M 2000 The mechanics of tack: viscoelastic contact on a rough surface *J. Polym. Sci.* B **38** 1485–95

Hui C Y, Ruina A, Creton C and Kramer E J 1992a Micromechanics of crack growth into a craze in a polymer glass *Macromolecules* **25** 3948–55

Hui C Y, Xu D B and Kramer E J 1992b A fracture model for a weak interface in a viscoelastic material (small scale yielding analysis) *J. Appl. Phys.* **72** 3294–304

Huneau B 2011 Strain-induced crystallization of natural rubber: a review of x-ray diffraction investigations *Rubber Chem. Technol.* **84** 425–52

Hyun K, Wilhelm M, Klein C O, Cho K S, Nam J G, Ahn K H, Lee S J, Ewoldt R H and Mckinley G H 2011 A review of nonlinear oscillatory shear tests: Analysis and application of large amplitude oscillatory shear (Laos) *Prog. Polym. Sci.* **36** 1697–753

Ito K, Shitajima K, Karyu N, Fujii S, Nakamura Y and Urahama Y 2014 Influence of the degree of crosslinking on the stringiness of crosslinked polyacrylic pressure-sensitive adhesives *J. Appl. Polym. Sci.* **131** 40336

Jago K L G 2012. x-Ray computed microtomography of rubber *Rubber Chem. Technol.* **85** 387–407

Jensen M K, Bach A, Hassager O and Skov A L 2009 Linear rheology of cross-linked polypropylene oxide as a pressure sensitive adhesive *Int. J. Adhes. Adhes.* **29** 687–93

Jones R A L and Richards R W 1999 *Polymers at surfaces and interfaces* (Cambridge: Cambridge University Press)

Josse G, Sergot P, Dorget M and Creton C 2004 Measuring interfacial adhesion between a soft viscoelastic layer and a rigid surface using a probe method *J. Adhes.* **80** 87–118

Jud K, Kausch H H and Williams J G 1981 Fracture mechanics studies of crack healing and welding of polymers *J. Mater. Sci.* **16** 204–10

Kaelble D H 1959 Theory and analysis of peel adhesion: mechanisms and mechanics *Trans. Soc. Rheol.* **3** 161–80

Kaelble D H 1960 Theory and analysis of peel adhesion: bond stresses and distributions *Trans. Soc. Rheol.* **4** 45–73

Kaelble D H 1964 Theory and analysis of peel adhesion: rate-temperature dependence of viscoelastic interlayers *J. Colloid Sci.* **19** 413–24

Kaelble D H 1965 Peel adhesion: micro-fracture mechanics of interfacial unbonding of polymers *Trans. Soc. Rheol.* **9** 135–63

Kaelble D H 1969 Peel Adhesion: influence of surface energies and adhesive rheology *J. Adhes.* **1** 102–123

Kaelble D H 1971 Cavitation in viscoelastic media. *Trans. Soc. Rheol.* **15** 275–96

Kaelble D H 1992 Theory and analysis of peel adhesion: adhesive thickness effects *J. Adhes.* **37** 205–214

Kaelble D H and Ho C L 1974 Biaxial bond stress analysis in peeling *Trans. Soc. Rheol.* **18** 219–35

Kean Z S, Hawk J L, Lin S, Zhao X, Sijbesma R P and Craig S L 2014 Increasing the maximum achievable strain of a covalent polymer gel through the addition of mechanically invisible cross-links *Adv. Mater.* **26** 6013–18

King D R, Bartlett M D, Gilman C A, Irschick D J and Crosby A J 2014 Creating gecko-like adhesives for 'real world' surfaces *Adv. Mater.* **26** 4345–51

Kinning D J and Schneider H M 2002 Release coatings for pressure sensitive adhesives *Surfaces, Chemistry and Applications* 1st edn, ed M Chaudhury and A V Pocius (Amsterdam: Elsevier)

Knowles J K and Sternberg E 1973 An asymptotic finite-deformation analysis of the elastostatic field near the tip of a crack *J. Elast.* **3** 67–107

Knowles J K and Sternberg E 1974 Finite-deformation analysis of the elastostatic field near the tip of a crack: reconsideration and higher-order results *J. Elast.* **4** 201–33

Krenceski M A and Johnson J F 1989 Shear, tack, and peel of polyisobutylene: effect of molecular weight distribution *Polym. Eng. Sci.* **29** 36–43

Krishnan V R and Hui C Y 2009 Finite strain stress fields near the tip of an interface crack between a soft incompressible elastic material and a rigid substrate *Eur. Phys. J.* E **29** 61–72

Krishnan V R, Hui C Y and Long R 2008 Finite strain crack tip fields in soft incompressible elastic solids *Langmuir* **24** 14245–53

Kwon H J, Rogalsky A D and Kim D W 2011 On the measurement of fracture toughness of soft biogel *Polym. Eng. Sci.* **51** 1078–86

Labonte D and Federle W 2015 Scaling and biomechanics of surface attachment in climbing animals *Phil. Trans. R. Soc.* B **370** 20140027

Lafuma A and Quéré D 2011 Slippery pre-suffused surfaces *Europhys. Lett.* **96** 56001

Lake G J and Lindley P B 1964 Cut growth and fatigue of rubbers. II. Experiments on a noncrystallizing rubber *J. Appl. Polym. Sci.* **8** 707–721

Lake G J and Lindley P B 1965 The mechanical fatigue limit for rubber *J. Appl. Polym. Sci.* **9** 1233–51

Lake G J and Thomas A G 1967 The strength of highly elastic materials *Proc. R. Soc.* A **300** 108–19

Lakrout H 1998 Micromécanismes de la pégosité des polymères fondus *PhD Thesis* Université Denis Diderot, Paris

Lakrout H, Creton C, Ahn D and Shull K R 2001 Influence of molecular features on the tackiness of acrylic polymer melts *Macromolecules* **34** 7448–58

Lakrout H, Sergot P and Creton C 1999 Direct observation of cavitation and fibrillation in a probe tack experiment on model acrylic pressure-sensitive-adhesives *J. Adhes.* **69** 307–59

Lange R F M, Van Gurp M and Meijer E W 1999 Hydrogen-bonded supramolecular polymer networks *J. Polym. Sci.* A **37** 3657–70

Lawn B 1993 *Fracture of Brittle Solids* (Cambdridge: Cambridge University Press)

Lefèvre V, Ravi-Chandar K and Lopez-Pamies O 2015 Cavitation in rubber: an elastic instability or a fracture phenomenon? *Int. J. Fract.* **192** 1–23

Léger L, Raphaël E and Hervet H 1999 Surface-anchored polymer chains: their role in adhesion and friction *Adv. Polym. Sci.* **138** 185–225

Lin S B, Durfee L D, Ekeland R A, Mcvie J and Schalau G K 2007 Recent advances in silicone pressure-sensitive adhesives *J. Adhes. Sci. Technol.* **21** 605–23

Lin S B, Durfee L D, Knott A A and Schalau G K 2009 Silicone pressure-sensitive-adhesive *Technology of of Pressure-Sensitive Adhesives and Products* ed I Benedek and M M Feldstein (Boca Raton, FL: CRC Press)

Lin W C, Fan W, Marcellan A, Hourdet D and Creton C 2010 Large strain and fracture properties of poly (dimethyl acrylamide)/ silica hybrid hydrogels *Macromolecules* **43** 2554–63

Lin W C, Marcellan A, Hourdet D and Creton C 2011 Effect of polymer-particle interaction on the fracture toughness of silica filled hydrogels *Soft Matter* **7** 6578–82

Lin Y Y and Hui C Y 2004 Cavity growth from crack-like defects in soft materials *Int. J. Fract.* **126** 205–21

Lin Y Y, Hui C Y and Baney J M 1999 Viscoelastic contact, work of adhesion and the Jkr technique *J. Phys. D: Appl. Phys.* **32** 2250–60

Lindner A, Lestriez B, Mariot S, Brummer R, Maevis T, Lühmann B and Creton C 2006 Adhesive and rheological properties of lightly crosslinked model acrylic networks *J. Adhes.* **82** 267–310

Lindner A, Maevis T, Brummer R, Lühmann B and Creton C 2004 Subcritical failure of soft acrylic adhesives under tensile stress *Langmuir* **20** 9156–69
Long R, Krishnan V R and Hui C-Y 2011 Finite strain analysis of crack tip fields in incompressible hyperelastic solids loaded in plane stress *J. Mech. Phys. Solids* **59** 672–95
Long R, Mayumi K, Creton C, Narita T and Hui C-Y 2014 Time dependent behavior of a dual cross-link self-healing gel: theory and experiments *Macromolecules* **47** 7243–50
Lopez-Pamies O 2009 Onset of cavitation in compressible, isotropic, hyperelastic solids *J. Elast.* **94** 115–45
Lopez-Pamies O, Idiart M I and Nakamura T 2011 Cavitation in elastomeric solids: I—A defect-growth theory *J. Mech. Phys. Solids* **59** 1464–87
Lorenz B, Krick B A, Mulakaluri N, Smolyakova M, Dieluweit S, Sawyer W G and Persson B N J 2013 Adhesion: role of bulk viscoelasticity and surface roughness *J. Phys.: Condens. Matter* **25** 225004
Lorenz B and Persson B N J 2009 Interfacial separation between elastic solids with randomly rough surfaces: comparison of experiment with theory *J. Phys.: Condens. Matter* **21** 015003
Maes F, Montarnal D, Cantournet S, Tournilhac F, Corte L and Leibler L 2012 Activation and deactivation of self-healing in supramolecular rubbers *Soft Matter* **8** 1681–7
Marin G and Derail C 2006 Rheology and adherence of pressure-sensitive adhesives *J. Adhes.* **82** 469–85
Mars W V and Fatemi A 2004 Factors that affect the fatigue life of rubber: a literature survey *Rubber Chem. Technol.* **77** 391–412
Maugis D 1996 On the contact and adhesion of rough surfaces *J. Adhes. Sci. Technol.* **10** 161–75
Maugis D and Barquins M 1978a Adhérence d'une bille de verre sur un massif viscoélastique: étude du recollement *C R. Acad. Sci. Paris II* **287** 49–52
Maugis D and Barquins M 1978b Fracture mechanics and the adherence of viscoelastic bodies *J. Phys. D: Appl. Phys.* **11** 1989–2023
Merkel R, Nassoy P, Leung A, Ritchie K and Evans E 1999 Energy landscapes of receptor-ligand bonds explored with dynamic force spectroscopy *Nature* **397** 50–3
Meyers M A, Chen P-Y, Lin A Y-M and Seki Y 2008 Biological materials: structure and mechanical properties *Prog. Mater. Sci.* **53** 1–206
Miquelard-Garnier G, Hourdet D and Creton C 2009 Large strain behaviour of new hydrophobically modified hydrogels *Polymer* **50** 481–90
Mueller H K and Knauss W G 1971 Crack propagation in a linearly viscoelastic strip *J. Appl. Mech.* **38** 483–8
Münstedt H and Laun H M 1979 Elongational behaviour of a low-density polyethylene melt. II. Transient behaviour in constant stretching rate and tensile creep experiments. Comparison with shear data, temperature dependence of the elongational properties *Rheol. Acta* **18** 492–504
Muralidharan V, Hui C Y, Dollhofer J, Creton C and Lin Y Y 2005 Machine compliance and hardening effects on cavity growth in soft materials *Int. J. Adhes. Adhes.* **26** 117–24
Mzabi S 2010 *Caractérisation et analyse des mécanismes de fracture en fatigue des élastomères chargés PhD Thesis* Université Pierre et Marie Curie, Paris
Mzabi S, Berghezan D, Roux S, Hild F and Creton C 2011 A critical local energy release rate criterion for fatigue fracture of elastomers *J. Polym. Sci.: Polym. Phys.* **49** 1518–24
Nakajima N, Babrowicz R and Harrell E R 1992 Rheology, composition, and peel mechanism of block copolymer-tackifier-based pressure sensitive adhesives *J. Appl. Polym. Sci.* **44** 1437–56
Nakajima T, Fukuda Y, Kurokawa T, Sakai T, Chung U-I and Gong J P 2013a Synthesis and fracture process analysis of double network hydrogels with a well-defined first network *ACS Macro Lett.* **2** 518–21
Nakajima T, Kurokawa T, Ahmed S, Wu W-L and Gong J P 2013b Characterization of internal fracture process of double network hydrogels under uniaxial elongation *Soft Matter* **9** 1955–66
Narita T, Mayumi K, Ducouret G and Hebraud P 2013 Viscoelastic properties of poly(vinyl alcohol) hydrogels having permanent and transient cross-links studied by microrheology, classical rheometry, and dynamic light scattering *Macromolecules* **46** 4174–83
Nase J, Creton C, Ramos O, Sonnenberg L, Yamaguchi T and Lindner A 2010 Measurement of the receding contact angle at the interface between a viscoelastic material and a rigid surface *Soft Matter* **6** 2686–91
Nase J, Lindner A and Creton C 2008 Pattern formation during deformation of a confined viscoelastic layer: from a viscous liquid to a soft elastic solid *Phys. Rev. Lett.* **101** 074503
Nguyen T Q, Liang Q Z and Kausch H H 1997 Kinetics of ultrasonic and transient elongational flow degradation: a comparative study *Polymer* **38** 3783–93
Nziakou Y 2015 Analyse multiéchelle des mécanismes d'endommagement de matériaux composites à morphologie complexe pour l'aéronautique *PhD Thesis* Université Pierre et Marie Curie, Paris
Padding J T, Mohite L V, Auhl D, Briels W J and Bailly C 2011 Mesoscale modeling of the rheology of pressure sensitive adhesives through inclusion of transient forces *Soft Matter* **7** 5036–46
Padding J T, Mohite L V, Auhl D, Schweizer T, Briels W J and Bailly C 2012 Quantitative mesoscale modeling of the oscillatory and transient shear rheology and the extensional rheology of pressure sensitive adhesives *Soft Matter* **8** 7967–81
Papaioannou J., Giannousakis A, Dimakopoulos Y and Tsamopoulos J 2014 Bubble deformation and growth inside viscoelastic filaments undergoing very large extensions *Ind. Eng. Chem. Res.* **53** 7548–69
Pastewka L and Robbins M O 2014 Contact between rough surfaces and a criterion for macroscopic adhesion *Proc. Natl Acad. Sci.* **111** 3298–303
Peppas N A, Bures P, Leobandung W and Ichikawa H 2000 Hydrogels in pharmaceutical formulations *Eur. J. Pharm. Biopharm.* **50** 27–46
Persson B N J 2002 Adhesion between elastic bodies with randomly rough surfaces *Phys. Rev. Lett.* **89** 245502
Persson B N J, Albohr O, Creton C and Peveri V 2004 Contact area between a viscoelastic solid and a hard, randomly rough, substrate *J. Chem. Phys.* **120** 8779–93
Persson B N J, Albohr O, Heinrich G and Ueba H 2005 Crack propagation in rubber-like materials *J. Phys.:Condens. Matter* **17** R1071–142
Persson B N J and Brener E A 2005 Crack propagation in viscoelastic solids *Phys. Rev.* E **71** 036123
Persson B N J, Bucher F and Chiaia B 2002 Elastic contact between randomly rough surfaces: comparison of theory with numerical results *Phys. Rev.* B **65** 184106–7
Persson B N J and Tosatti E 2001 The effect of surface roughness on the adhesion of elastic solids *J. Chem. Phys.* **115** 5597–610
Peykova Y, Lebedeva O V, Diethert A, Müller-Buschbaum P and Willenbacher N 2012 Adhesive properties of acrylate copolymers: Effect of the nature of the substrate and copolymer functionality *Int. J. Adhes. Adhes.* **34** 107–16
Phan-Thien N 1978 A nonlinear network viscoelastic model *J. Rheol.* **22** 259–83
Plazek D J, Choy I C, Kelley F N, Vonmeerwall E and Su L J 1983 Viscoelasticity and tearing energy of fluorinated hydrocarbon elastomers *Rubber Chem. Technol.* **56** 866–82
Plazek D J, Gu G F, Stacer R G, Su L J, Vonmeerwall E D and Kelley F N 1988 Viscoelastic dissipation and the tear energy of urethane cross-linked polybutadiene elastomers *J. Mater. Sci.* **23** 1289–1300

Pocius A V 2002 *Adhesion and Adhesives Technology* (Munich: Hanser)

Poivet S, Nallet F, Gay C and Fabre P 2003 Cavitation-induced force transition in confined viscous liquids under traction *Europhys. Lett.* **62** 244–50

Polignone D A and Horgan C O 1993 Cavitation for incompressible anisotropic nonlinearly elastic spheres *J. Elast.* **33** 27–65

PSTC 2000 *Test Methods for Pressure Sensitive Adhesive Tapes* (Pressure Sensitive Tape Council) (Oakbook Terrace, IL)

Raphaël E and De Gennes P G 1992 Rubber-rubber adhesion with connector molecules *J. Phys. Chem.* **96** 4002–7

Rice J R 1968 A path independent integral and the approximate analysis of strain concentration by notches and cracks *J. Appl. Mech.* **35** 379–86

Rivlin R S and Thomas A G 1953 Rupture of rubber. I. Characteristic energy for tearing *J. Poly. Sci.* **10** 291–318

Roos A and Creton C 2005 Nonlinear Elastic Properies of elastomeric block copolymers *Macromolecules* **38** 7807–18

Roos A, Creton C, Novikov M B and Feldstein M M 2002 Viscoelasticity and tack of poly(vinyl pyrrolidone)-poly(ethylene glycol) blends *J. Polym. Sci.* B **40** 2395–2409

Rose S, Dizeux A, Narita T, Hourdet D and Marcellan A 2013 Time dependence of dissipative and recovery processes in nanohybrid hydrogels *Macromolecules* **46** 4095–104

Rose S, Prevoteau A, Elziere P, Hourdet D, Marcellan A and Leibler L 2014 Nanoparticle solutions as adhesives for gels and biological tissues *Nature* **505** 382–5

Rubinstein M and Colby R H 2003 *Polymer Physics* (Oxford: Oxford University Press)

Rubinstein M and Panyukov S 2002 Elasticity of polymer networks *Macromolecules* **35** 6670–886

Rublon P, Huneau B, Saintier N, Beurrot S, Leygue A, Verron E, Mocuta C, Thiaudière D and Berghezan D 2013 *In situ* synchrotron wide-angle x-ray diffraction investigation of fatigue cracks in natural rubber *J. Synchrotron Radiat.* **20** 105–9

Sakai T 2013 Gelation mechanism and mechanical properties of tetra-peg gel *React. Funct. Polym.* **73** 898–903

Sakai T, Akagi Y, Matsunaga T, Kurakazu M, Chung U and Shibayama M 2010 Highly elastic and deformable hydrogel formed from tetra-arm polymers *Macromol. Rapid Commun.* **31** 1954–9

Satas D 1989 Acrylic adhesives *Handbook of Pressure-Sensitive-Adhesives* 2d edn, ed D Satas (New York: Van Nostrand Reinhold)

Saulnier F, Ondarcuhu T, Aradian A and Raphael E 2004 Adhesion between a viscoelastic material and a solid surface *Macromolecules* **37** 1067–75

Schach R and Creton C 2008 Adhesion at interfaces between highly entangled polymer melts *J. Rheol.* **52** 749–67

Schach R, Tran Y, Menelle A and Creton C 2007 Role of chain interpenetration in the adhesion between immiscible polymer melts *Macromolecules* **40** 6325–32

Schapery R A 1975a Theory of crack initiation and growth in viscoelastic media 1. Theoretical development *Int. J. Fract.* **11** 141–59

Schapery R A 1975b Theory of crack initiation and growth in viscoelastic media 2. Approximate methods of analysis *Int. J. Fract.* **11** 369–88

Schapery R A 1975c Theory of crack initiation and growth in viscoelastic media 3. Analysis of continuous growth *Int. J. Fract.* **11** 549–62

Seitz M E, Martina D, Baumberger T, Krishnan V R, Hui C-Y and Shull K R 2009 Fracture and large strain behavior of self-assembled triblock copolymer gels *Soft Matter* **5** 447–56

Sentmanat M, Wang B N and Mckinley G H 2005 Measuring the transient extensional rheology of polyethylene melts using the Ser universal testing platform *J. Rheol.* **49** 585–606

Sherriff M, Knibbs R W and Langley P G 1973 Mechanism for the action of tackifying resins in pressure-sensitive adhesives *J. Appl. Polym. Sci.* **17** 3423–38

Shull K R 2002 Contacts mechanics and the adhesion of soft solids *Mater. Sci. Eng. R Rep.* **36** 1–45

Shull K R 2006 Fracture and adhesion of elastomers and gels: Large strains at small length scales *J. Polym. Sci.* B **44** 3436–9

Shull K R and Creton C 2004 Deformation behavior of thin compliant layers under tensile loading conditions *J. Polym. Sci.* B **42** 4023–43

Sijbesma R P, Beijer F H, Brunsveld L, Folmer B J B, Hirschberg J H K K, Lange R F M, Lowe J K L and Meijer E W 1997 Reversible polymers formed from self-complementary monomers using quadruple hydrogen bonding *Science* **278** 1601–4

Smith T L 1958 Dependence of the ultimate properties of a Gr-S rubber on strain rate and temperature *J. Polym. Sci.* **32** 99–113

Sobieski L A and Tangney T J 1989 Silicone pressure sensitive adhesives *Handbook of Pressure Sensitive Adhesives* 2nd edn, ed D Satas (New York: Van Nostrand Reinhold)

Spolenak R, Gorb S and Arzt E 2005a Adhesion design maps for bio-inspired attachment systems *Acta Biomater.* **1** 5–13

Spolenak R, Gorb S, Gao H and Arzt E 2005b Effects of contact shape on the scaling of biological attachments *Proc. R. Soc.* A **461** 305–19

Stephenson R 1982 The equilibrium field near the tip of a crack for finite plane strain of incompressible elastic materials *J. Elast.* **12** 65–99

Sun J-Y, Zhao X, Illeperuma W R K, Chaudhuri O, Oh K H, Mooney D J, Vlassak J J and Suo Z 2012 Highly stretchable and tough hydrogels *Nature* **489** 133–6

Tanaka Y 2007 A local damage model for anomalous high toughness of double-network gels *Europhys. Lett.* **78** 56005

Tanaka Y, Kuwabara R, Na Y H, Kurokawa T, Gong J P and Osada Y 2005 Determination of fracture energy of high strength double network hydrogels *J. Phys. Chem.* B **109** 11559–62

Tanguy F, Nicoli M, Lindner A and Creton C 2014 Quantitative analysis of the debonding structure of soft adhesives *Eur. Phys. J.* E **37** 1–12

Teisseire J, Nallet F, Fabre P and Gay C 2007 Understanding cracking versus cavitation in pressure-sensitive adhesives: the role of kinetics *J. Adhes.* **83** 613–77

Thomas A G 1955 Rupture of rubber II the strain concentration at an incision *J. Polym. Sci.* **18** 177–88

Thomas A G and Whittle J M 1970 Tensile rupture of rubber *Rubber Chem. Technol.* **43** 222–8

Tian Y, Pesika N, Zeng H, Rosenberg K, Zhao B, Mcguiggan P, Autumn K and Israelachvili J 2006 Adhesion and friction in gecko toe attachment and detachment *Proc. Natl Acad. Sci.* **103** 19320–5

Tobing S, Klein A, Sperlinh L-H and Petrasko B 2001 Effect of network morphology on adhesive performance in emulsion blends of acrylic pressure sensitive adhesives *J. Appl. Polym. Sci.* **81** 2109–117

Trabelsi S, Albouy P-A and Rault J 2002 Stress-induced crystallization around a crack tip in natural rubber *Macromolecules* **35** 10054–61

Treloar L R G 1958 *The Physics of Rubber Elasticity* (Oxford: Oxford University Press)

Treloar L R G 1973 The elasticity and related properties of rubbers *Rep. Prog. Phys.* **36** 755–826

Tuncaboylu D C, Argun A, Algi M P and Okay O 2013 Autonomic self-healing in covalently crosslinked hydrogels containing hydrophobic domains *Polymer* **54** 6381–8

Tuncaboylu D C, Sari M, Oppermann W and Okay O 2011 Tough and self-healing hydrogels formed via hydrophobic interactions *Macromolecules* **44** 4997–5005

Urahama Y 1989 Effect of peel load on stringiness phenomena and peel speed of pressure-sensitive adhesive tape *J. Adhes.* **31** 47–58

Verdier C, Piau J M and Benyahia L 1998 Peeling of acrylic pressure-sensitive-adhesives: cross-linked versus uncross-linked adhesives *J. Adhes.* **68** 93–116
Villey R, Creton C, Cortet P-P, Dalbe M-J, Jet T, Saintyves B, Santucci S, Vanel L, Yarusso D J and Ciccotti M 2015 Rate-dependent elastic hysteresis during the peeling of pressure sensitive adhesives *Soft Matter* **11** 3480–91
Volokh K Y 2007 Softening hyperelasticity for modeling material failure: analysis of cavitation in hydrostatic tension *Int. J. Solids Struct.* **44** 5043–55
Wang Y Y, Boukany P Y, Wang S Q and Wang X R 2007 From elastic extension to elongational flow of entangled melts *Phys. Rev. Lett.* **99** 237801
Webber R E, Creton C, Brown H R and Gong J P 2007 Large strain hysteresis and mullins effect of tough double-network hydrogels *Macromolecules* **40** 2919–27
Williams J A and Kauzlarich J J 2005 The influence of peel angle on the mechanics of peeling flexible adherends with arbitrary load–extension characteristics *Tribol. Int.* **38** 951–8
Williams J G 1984 *Fracture Mechanics of Polymers* (Chichester: Ellis Horwood)
Williams J G 1993 Root rotation and plastic work effects in the peel test *J. Adhes.* **41** 225–39
Williams M L, Landel R F and Ferry J D 1955 The temperature dependence of relaxation mechanisms in amorphous polymers and other glass-forming liquids *J. Am. Chem. Soc.* **77** 3701–7
Williams M L and Schapery R A 1965 Spherical flaw instability in hydrostatic tension *Int. J. Fract. Mech.* **1** 64–71
Xu D B, Hui C Y and Kramer E J 1992 Interface fracture and viscoelastic deformation in finite size specimens *J. Appl. Phys.* **72** 3305–16
Yamaguchi T and Doi M 2006 Debonding dynamics of pressure-sensitive adhesives: 3D block model *Eur. Phys. J.* E **21** 331–9
Yamaguchi T, Koike K and Doi M 2007 *In situ* observation of stereoscopic shapes of cavities in soft adhesives *Europhys. Lett.* **77** 64002
Yamaguchi T, Morita H and Doi M 2006 Modeling on debonding dynamics of pressure-sensitive-adhesives *Eur. Phys. J.* E **20** 7–17
Yang S Y, Carlson A, Cheng H Y, Yu Q M, Ahmed N, Wu J, Kim S, Sitti M, Ferreira P M, Huang Y G and Rogers J A 2012 Elastomer surfaces with directionally dependent adhesion strength and their use in transfer printing with continuous roll-to-roll applications *Adv. Mater.* **24** 2117–22
Yao X, Hu Y, Grinthal A, Wong T-S, Mahadevan L and Aizenberg J 2013 Adaptive fluid-infused porous films with tunable transparency and wettability *Nat. Mater.* **12** 529–34
Yarusso D J 1999 Quantifying the relationship between peel and rheology for pressure sensitive adhesives *J. Adhes.* **70** 299–320
Yerzley F L 1939 Adhesion of neoprene to metal *Ind. Eng. Chem.* **31** 950–6
Yu Q M, Tanaka Y, Furukawa H, Kurokawa T and Gong J P 2009 Direct Observation of damage zone around crack tips in double-network gels *Macromolecules* **42** 3852–5
Yurdumakan B, Raravikar N R, Ajayan P M and Dhinojwala A 2005 Synthetic gecko foot-hairs from multiwalled carbon nanotubes *Chem. Commun.* 3799–801
Zhang H, Chen Y J, Lin Y J, Fang X L, Xu Y Z, Ruan Y H and Weng W G 2014 Spiropyran as a mechanochromic probe in dual cross-linked elastomers *Macromolecules* **47** 6783–90
Zhang H, Scholz A K, De Crevoisier J, Berghezan D, Narayanan T, Kramer E J and Creton C 2015 Nanocavitation around a crack tip in a soft nanocomposite: A scanning microbeam small angle x-ray scattering study *J. Polym. Sci. B Polym. Phys.* **53** 422–9
Zhang H, Scholz A K, De Crevoisier J, Vion-Loisel F, Besnard G, Hexemer A, Brown H R, Kramer E J and Creton C 2012 Nanocavitation in carbon black filled styrene–butadiene rubber under tension detected by real time small angle x-ray scattering *Macromolecules* **45** 1529–43
Zhang H, Scholz A K, Vion-Loisel F, Merckel Y, Brieu M, Brown H, Roux S P, Kramer E J and Creton C 2013 Opening and closing of nanocavities under cyclic loading in a soft nanocomposite probed by real-time small-angle x-ray scattering *Macromolecules* **46** 901–13
Zhang Newby B-M, Chaudhury M K and Brown H R 1995 Macroscopic evidence of the effect of interfacial slippage on adhesion *Science* **269** 1407–9
Zhang Newby B M and Chaudhury M K 1997 Effect of interfacial slippage on viscoelastic adhesion *Langmuir* **13** 1805–9
Zhou Y, Robinson A, Steiner U and Federle W 2014 Insect adhesion on rough surfaces: analysis of adhesive contact of smooth and hairy pads on transparent microstructured substrates *Journal of the Royal Society Interface* **11** 20140499
Zosel A 1985 Adhesion and tack of polymers: influence of mechanical properties and surface tensions *Colloid Polym. Sci.* **263** 541–53
Zosel A 1989 Adhesive failure and deformation behaviour of polymers *J. Adhes.* **30** 135–49
Zosel A 1991 Effect of Cross-Linking on tack and peel strength of polymers *J. Adhes.* **34** 201–9
Zosel A 1992 Fracture energy and tack of pressure sensitive adhesives *Advances in Pressure Sensitive Adhesive Technology* ed D Satas (Warwick, RI: Satas & Associates)
Zosel A 1997 The effect of bond formation on the tack of polymers *J. Adhes. Sci. Technol.* **11** 1447–57
Zosel A 1998 The effect of fibrillation on the tack of pressure-sensitive-adhesives *Int. J. Adhes. Adhes.* **18** 265–71
Zülle B, Linster J J, Meissner J and Hürlimann H P 1987 Deformation Hardening and thinning in both elongation and shear of a low density polyethylene melt *J. Rheol.* **31** 583–98